Eionet Report - ETC/ATNI 2020/10

European air quality maps for 2018

PM_{10}, $PM_{2.5}$, Ozone, NO_2 and NO_x
Spatial estimates and their uncertainties

November 2020

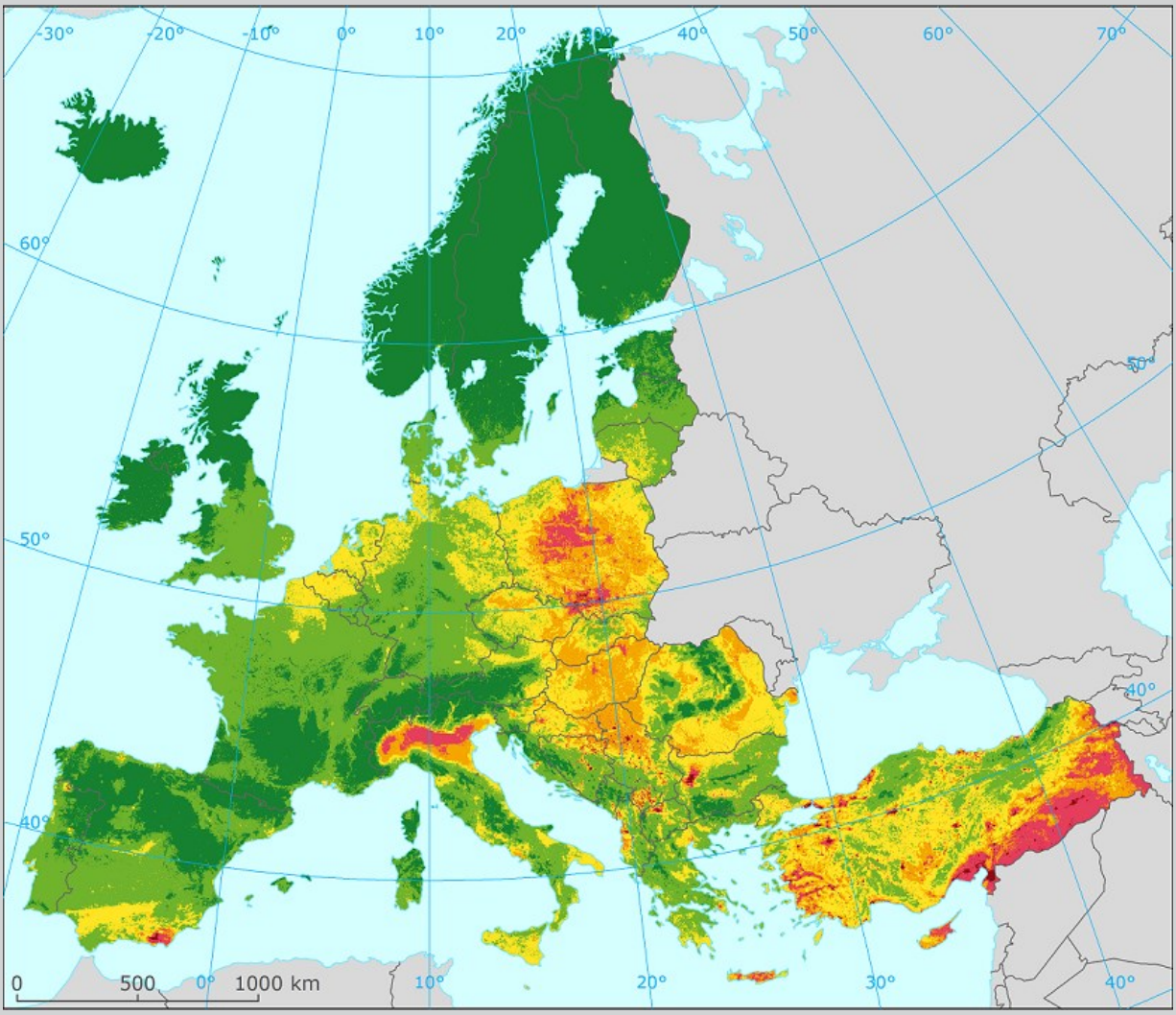

Authors:

Jan Horálek (CHMI), Markéta Schreiberová (CHMI), Leona Vlasáková (CHMI), Jana Marková (CHMI), Frédéric Tognet (INERIS), Philipp Schneider (NILU), Pavel Kurfürst (CHMI), Jana Schovánková (CHMI)

ETC/ATNI consortium partners:
NILU – Norwegian Institute for Air Research, Aether Limited, Czech Hydrometeorological Institute (CHMI), EMISIA SA, Institut National de l'Environnement Industriel et des risques (INERIS), Universitat Autònoma de Barcelona (UAB), Umweltbundesamt GmbH (UBA-V), 4sfera Innova, Transport & Mobility Leuven NV (TML)

European Environment Agency
European Topic Centre on Air pollution, transport, noise and industrial pollution

Cover picture: Concentration map of PM_{10} indicator 90.4 percentile of daily means for 2018. Units: $\mu g \cdot m^{-3}$. (Map 2.2 of this report.)

The withdrawal of the United Kingdom from the European Union did not affect the production of the report.
Data reported by the United Kingdom are included in all analyses and assessments contained herein, unless otherwise indicated.

Author(s)
Jan Horálek, Markéta Schreiberová, Leona Vlasáková, Jana Marková, Pavel Kurfürst, Jana Schovánková: Czech Hydrometeorological Institute (CHMI, CZ)
Philipp Schneider: Norwegian Institute for Air Research (NILU, NO)
Frédéric Tognet: National Institute for Industrial Environment and Risk (INERIS, FR)

ETC/ATNI c/o NILU
ISBN 978-82-93752-20-2

European Topic Centre on Air pollution,
transport, noise and industrial pollution
c/o NILU – Norwegian Institute for Air Research
P.O. Box 100, NO-2027 Kjeller, Norway
Tel.: +47 63 89 80 00
Email: etc.atni@nilu.no
Web : https://www.eionet.europa.eu/etcs/etc-atni

Contents

Summary

European air quality concentrations maps have been prepared for the year 2018. The maps are based on air quality data as reported under the air quality directive by EEA member and cooperating countries and voluntary reporting countries. Concentration maps have been produced to assess the situation with respect to the most stringent air quality limit values and the indicators most relevant for the assessment of impacts on human health and vegetation.

The mapping method follows the methodology developed earlier (Horálek et al, 2020a, and references cited therein); it combines the monitoring data with supplementary data (such as the results from a chemical transport model, land cover, meteorological and geographical data). The method ('Regression – Interpolation – Merging Mapping') is based on a linear regression model followed by kriging of the residuals produced from that model (residual kriging). This methodology has been applied in an overall consistent way during the past 14 years, although it has been subject to continuous improvement. This enables the evaluation of changes in exposure over time. Next to this, maps of Phytotoxic Ozone Dose (POD) indicators are presented for the first time in this regular mapping report, based on methodology described in CLRTAP (2017) according to Emberson et al. (2000). These maps are prepared based on hourly ozone rural maps (created similarly like other air quality maps), hourly meteorological data and soil hydraulic properties data.

Population exposure

Concentrations of particulate matter continued to exceed the EU and WHO standards in large parts of Europe. 4.5 % of the European population (excluding Turkey in the case of $PM_{2.5}$) is exposed to levels above the EU $PM_{2.5}$ limit value of 25 $\mu g \cdot m^{-3}$; 76 % of the European population is exposed to levels above the WHO $PM_{2.5}$ Air Quality Guideline of 10 $\mu g \cdot m^{-3}$ (Table 3.1). 9 % of the European population is exposed to levels above the EU PM_{10} limit value of 40 $\mu g \cdot m^{-3}$; 49 % of the European population is exposed to levels above the WHO PM_{10} Air Quality Guideline of 20 $\mu g \cdot m^{-3}$. Table 2.2 shows that 21 % of the population is exposed to concentrations above the PM_{10} daily limit value in more than 35 days per year. Figure ES.1 shows that the countries with the highest values of annual average PM_{10} are located in the eastern parts of Europe as well. The concentrations of $PM_{2.5}$ and PM_{10} are often highly correlated, with the highest $PM_{2.5}$ exposures also found in the eastern parts of Europe.

Figure ES.1 PM_{10} annual concentrations to which the population per country was exposed in 2018. The annual limit value (40 µg·m^{-3}) is marked by the red line.

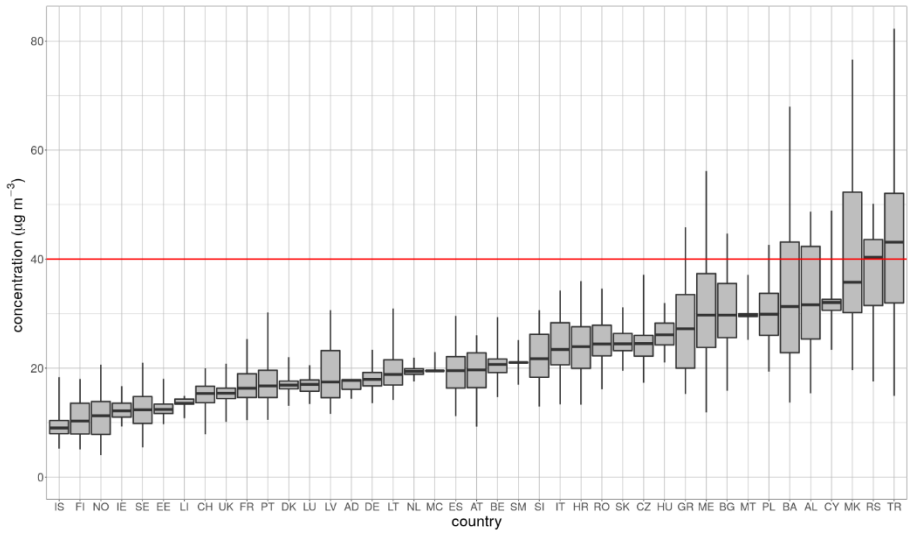

Note: For each country, the box plot shows the concentration to which a percentage of the population was exposed. The black marker corresponds to 50%, the box's edges to 25% and 75%, and the whiskers' edges to 2% and 98% of the population exposed.

The NO_2 annual mean concentration map shows a different spatial distribution than the PM maps. Table 5.1 indicates that in 18 countries a limited fraction of the European population (4 % in total) is exposed to concentrations above the annual limit value of 40 µg·m^{-3}. Figure ES.2 shows that in all countries, the majority of population lived well below the limit value in 2018, according to the presented assessment. High exposures are observed in the larger urban areas (e.g. greater London, the Benelux-Ruhr area, Po Valley, Rome, Naples, Paris, Madrid, Barcelona and Istanbul).

Figure ES.2 NO_2 annual concentrations to which the population per country was exposed in 2018.The annual limit value (40 µg·m^{-3}) is marked by the red line.

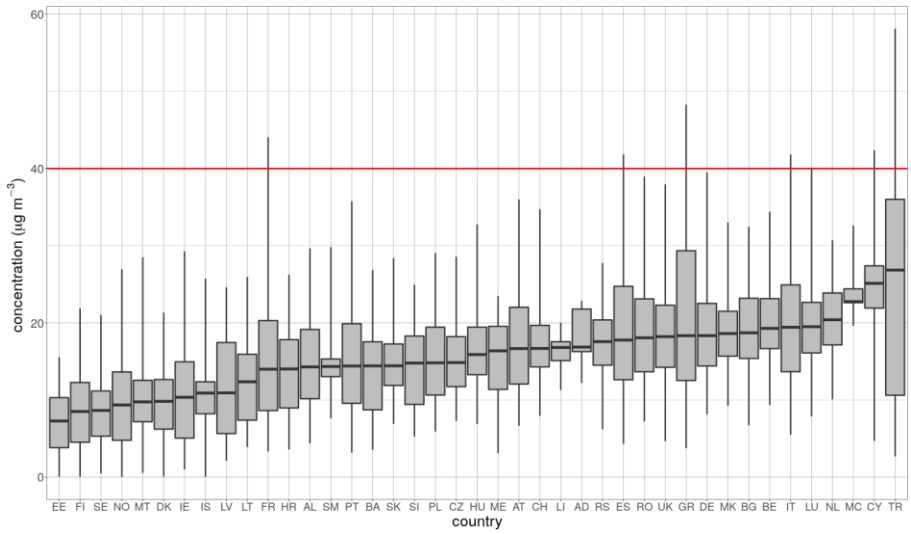

Note: For each country, the box plot shows the concentration to which a percentage of the population was exposed. The black marker corresponds to 50%, the box's edges to 25% and 75%, and the whiskers' edges to 2% and 98% of the population exposed.

Exposure to ozone concentrations above the EU target value (TV) threshold (a maximum daily 8-hour average value of 120 µg·m^{-3} not to be exceeded on more than 25 days per year) occurs in 2018 in large

parts of Central, Western, Eastern and Southern Europe. 35 % of the Europeans live in areas where the ozone TV is exceeded (Table 4.1). Figure ES.3 shows that the countries with the highest values of SOMO35 are located in the southern parts of Europe.

Figure ES.3 Ozone concentrations (expressed as the indicator SOMO35) to which the population per country was exposed in 2018

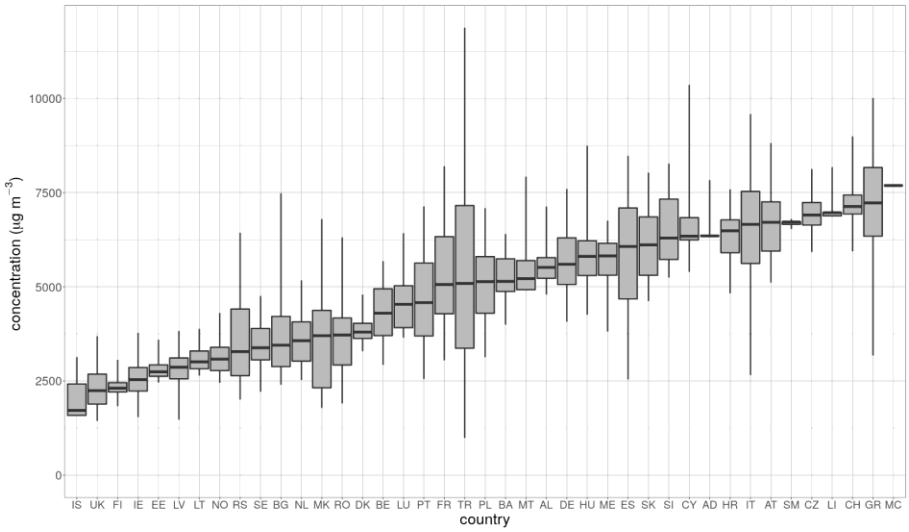

Note: For each country, the box plot shows the concentration to which a percentage of the population was exposed. The black marker corresponds to 50%, the box's edges to 25% and 75%, and the whiskers' edges to 2% and 98% of the population exposed.

Accumulated risks

Although the spatial distributions of PM, NO_2 and ozone concentrations differ widely, the possibility of an accumulation of risk resulting from high exposures to all three pollutants cannot be excluded. Combining the maps of the three most frequently exceeded standards (PM_{10} daily limit value, NO_2 annual limit value and ozone target value) shows that out of the total population of 621 million in the model area, 7.4% (46.2 million) lived in areas where 2 or 3 air quality standards were exceeded; 4.5 million people lived in areas where all three standards were exceeded. The worst situation was observed in Turkey, where 4.2 % of the population live in areas where all three standards are exceeded; this is followed by Italy (in particular the Po Valley), where it is also the case for 1.8 % of the population.

Vegetation exposure

Standards for the protection of vegetation have been set, among others, for NO_x and ozone. In a limited number of cases, the NO_x critical level has been exceeded, though this is relevant only if there is vegetation in those areas. A larger impact on vegetation can be expected from the direct exposure to ozone. The target value for the protection of vegetation (AOT40) is exceeded in about 45 % of the agricultural areas. The long-term objective is exceeded in 96 % of the agricultural areas. The critical level for the protection of forests (AOT40) is exceeded in about 88 % of the forested areas.

Critical levels of Phytotoxic Ozone Dose (POD) for wheat (both for grain yield and protein yield of wheat) has been exceeded in large parts of central, western and southern Europe. In the most of Europe, critical levels for tuber yield of potato (in terms of POD for potato) have been exceeded, with the highest values of POD for potato in central Europe and Denmark.

Changes over time

Since 2005, the maps have been prepared in an overall consistent way, although the mapping methodology has been subject to continuous improvement. This enables an analysis of changes in exposure over time. For changes in population-weighted concentrations, see Figure ES.4. The population-weighted concentration is calculated for the area of all countries considered in the report, except Turkey, for comparability reasons, because the area of Turkey has not been mapped until 2016.

While PM_{10} and ozone maps have been prepared for the whole period, $PM_{2.5}$ have been routinely constructed since 2010 map and NO_2 since 2014 map, with few maps for older years available. Thus, $PM_{2.5}$ maps are available for the whole period apart from 2006, while for NO_2 the years 2006, 2008 and 2011-2012 are missing.

Throughout the years, some methodology changes have been applied. Apart from minor changes, a major change was introduced for PM_{10} and $PM_{2.5}$ since 2017 maps, taking into account air quality in urban traffic areas, as for the NO_2 maps. For comparability reasons, also the maps based on the old methodology have been included in Figure ES.4 and in the trend analysis performed in Chapter 6. The PM concentrations show a steady decrease of about 0.7 $\mu g \cdot m^{-3}$ per year for PM_{10} annual average and 0.4 $\mu g \cdot m^{-3}$ per year for $PM_{2.5}$ annual average. For the ozone concentration (expressed as SOMO35) no trend is observed, next to the year-to-year variability. The NO_2 concentration (in terms of annual average) shows a decrease of about 0.5 $\mu g \cdot m^{-3}$ per year.

For changes in agricultural-weighted concentrations, see Figure ES.5. Again, the agricultural-weighted concentration is calculated for the area of all countries considered in the report, except Turkey. The agricultural-weighted concentration tends to decrease by about 320 $\mu g \cdot m^{-3} \cdot h$ per year over the period 2005-2018, in terms of AOT40 for vegetation.

Figure ES.4 Changes in population-weighted concentrations of PM_{10} (annual mean), $PM_{2.5}$ (annual mean), ozone (SOMO35), and NO_2 (annual mean) in 2005-2018. For PM_{10} and $PM_{2.5}$, results based on both the old (blue dots) and the updated (red dots) mapping methodology are presented, where available.

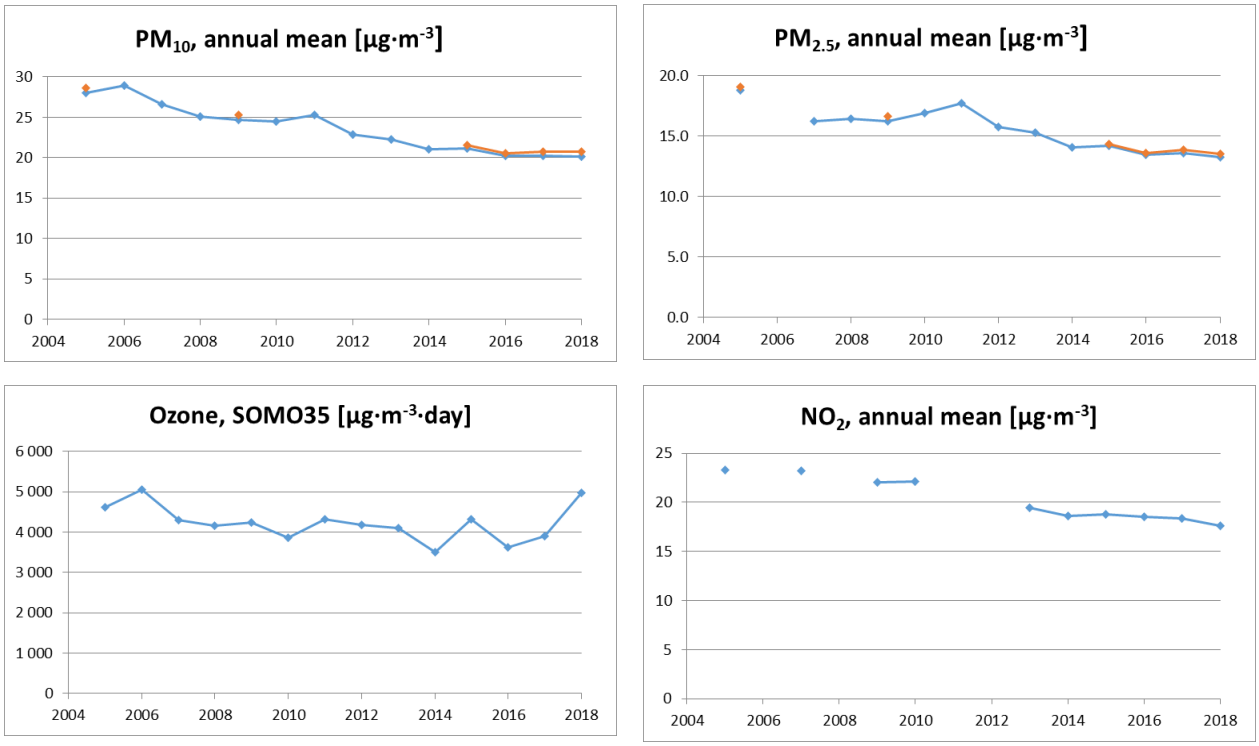

Figure ES.5 Changes in agricultural-weighted concentrations of ozone indicator AOT40 for vegetation.

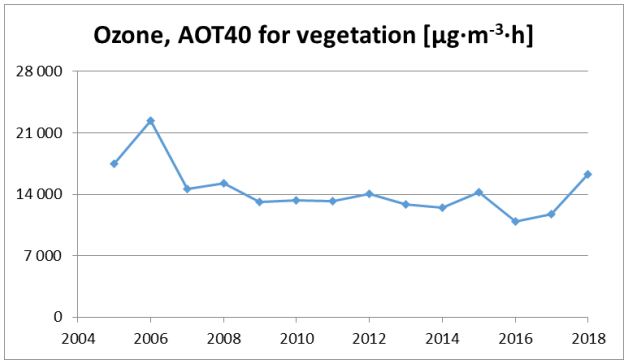

Acknowledgements

The EEA task manager was Alberto González Ortiz.

We are grateful to Håkan Pleijel (University of Gothenburg, Sweden) and Ignacio González-Fernández (CIEMAT, Spain) from ICP Vegetation (UNECE Convention on Long-Range Transboundary Air Pollution) for providing their advice on the choice of crops for Phytotoxic Ozone Dose calculation.

1 Introduction

This report provides an update of European air quality concentration maps, population exposure and vegetation exposure estimates for 2018. It builds on the previous reports (Horálek et al., 2020a, and references cited therein). The analysis is based on interpolation of annual statistics of validated monitoring data from 2018, reported by the EEA member and cooperating countries (and the voluntary reporting country of Andorra) in 2019. The paper presents mapping results and includes an uncertainty analysis of the interpolated maps, adopting the latest methodological developments, see Horálek et al. (2020a) and references cited therein. The mapping area covers all of Europe apart from Belarus, Moldova, Ukraine and the European parts of Russia and Kazakhstan. Turkey (including both European and Asian areas) is included in the mapping area for all pollutants except $PM_{2.5}$, due to the lack of rural stations in Turkey for $PM_{2.5}$ for 2018 in the AQ e-reporting database (EEA, 2020a).

We consider in this report PM_{10}, $PM_{2.5}$, ozone, NO_2 and NO_x for 2018, being the most relevant pollutants for annual updating due to their potential impacts on health or ecosystems. The analysis method applied is similar to that of previous years. Another potentially relevant pollutant, benzo[a]pyrene (BaP), is not presented, as the station coverage is not dense enough for enabling the regular mapping. The current status of mapping the BaP concentrations in Europe was discussed by Horálek et al. (2017a).

The mapping is based primarily on air quality measurements. It combines monitoring data, chemical transport model results and other supplementary data (such as altitude and meteorology). The method is a linear regression model followed by kriging of the residuals produced from that model ('residual kriging'). It should be noted that this methodology does not allow for formal compliance checking with limit or target values as set by the air quality directive (EC, 2008).

The maps of health-related indicators of ozone are created for the rural and urban (including suburban) background areas separately on a grid at 10x10 km^2 resolution. Subsequently, the rural and urban background maps are merged into one final combined air quality indicator map using a 1x1 km^2 population density grid, following a weighting criterion applied per grid cell. This fine resolution takes into account the smaller settlements in Europe that are not resolved at the 10x10 km^2 grid resolution. The maps of health related indicators of PM_{10}, $PM_{2.5}$, and NO_2 are constructed by improved methodology developed in Horálek et al. (2017b, 2018, 2019): next to the rural and urban background map layers, the urban traffic map layer is constructed and incorporated into the final merged map using the road data. All individual map layers are created at 1x1 km^2 resolution and land cover and road data are included in the mapping process as supplementary data. The maps of ozone and NO_x vegetation-related indicators are at a grid resolution of 2x2 km^2 and based on rural background measurements; in the case of ozone they serve as input to the EEA's core set indicator CSI005 (EEA, 2020d).

Among the ozone vegetation-related indicators, for the first time in this regular mapping report we present maps of Phytotoxic Ozone Dose (POD) indicators, following the conclusions of Colette et al. (2018). These indicators take into account the plant physiology, not only the ozone concentrations in the ambient air (as in the AOT40 indicators), and reflect ozone actually absorbed by the vegetation. Ozone enters plant tissue by diffusion through stomata that are opened during the photosynthetic process; therefore, vegetation is the most sensitive to injury during the hours for which the stomata are opened. Stomata respond to environmental conditions such as temperature, light, air humidity and soil moisture. It is widely acknowledged that the impact of ozone on vegetation is more closely related to the ozone flux absorbed through the stomata than to the exposure to ozone in the atmosphere (Musselman and Massman, 1998; Nussbaum et al., 2003). The ozone flux through the stomata of leaves above a specific threshold accumulated during a specified time is called POD; it is calculated based on methodology described in CLRTAP (2017) according to Emberson et al. (2000) based on Jarvis (1976). The POD annual maps are calculated based on hourly ozone rural maps (created similarly like the annual ozone maps), hourly meteorological data and the soil hydraulic properties

data. In the report, two POD maps are presented, namely the maps of POD for wheat and potato, in agreement with CLRTAP (2017). Wheat and potato (together with tomato) are considered as representative species of crops in Europe.

Next to the annual indicator maps, we present in tables the population exposure to PM_{10}, $PM_{2.5}$, O_3, and NO_2, and the exposure of vegetation to ozone in terms of AOT40 indicators. Tables of population exposure are prepared using the final combined maps and the population density map of 1x1 km^2 grid resolution. For PM_{10}, $PM_{2.5}$ and NO_2, the population exposure in each grid cell is calculated separately for urban areas directly influenced by traffic and for the background (both rural and urban) areas, in order to better reflect the population exposed to traffic emissions. The tables of the vegetation exposure are prepared with a 2x2 km^2 grid resolution based on the Corine Land Cover 2018 dataset.

Chapters 2, 3, 4 and 5 present the concentration maps and exposure estimates for PM_{10}, $PM_{2.5}$, ozone and NO_2, respectively. Chapter 5 presents the concentration map for NO_x; exceedances of the critical level for the protection of vegetation occur in very limited areas and, as such, it is considered not to provide relevant information from the European scale perspective. Chapter 6 summarizes the trends in exposure estimates in the period 2005-2018.

Annex 1 describes briefly the different methodological aspects. Annex 2 documents the input data applied in the 2018 mapping and exposure analysis. Annex 3 presents the technical details of the maps and their uncertainty analysis including the cross-validation results. Annex 4 shows the inter-annual changes including the inter-annual difference maps between 2017 and 2018. Annex 5 presents the concentration maps including the station points, in order to provide more complete information of the air quality in 2018 across Europe.

2 PM_{10}

The Ambient Air Quality Directive (EC, 2008) sets limit values for long-term and for short-term PM_{10} concentrations. The long-term annual PM_{10} limit value is set at 40 $\mu g \cdot m^{-3}$. The Air Quality Guideline recommended by the World Health Organization (WHO, 2005) for the PM_{10} annual average is 20 $\mu g \cdot m^{-3}$. The short-term limit value indicates that the daily average PM_{10} concentration should not exceed 50 $\mu g \cdot m^{-3}$ during more than 35 days per year. It corresponds to the 90.4 percentile of daily PM_{10} concentrations in one year. This daily limit value is the most frequently exceeded air quality limit value in Europe. The Air Quality Guideline recommended by the World Health Organization (WHO, 2005) for the short-term limit value indicates that the 99 percentile of the daily average PM_{10} concentrations should not exceed 50 $\mu g \cdot m^{-3}$ (meaning, three days of exceedance are allowed).

This chapter presents the 2018 updates of two PM_{10} indicators: the annual average and the 90.4 percentile of the daily averages. The latter is a more relevant indicator in the context of the AQ Directive (EC, 2008) than the formerly used 36th highest daily mean (Horálek et al., 2016b).

The maps of PM_{10} are based on the improved mapping methodology developed and tested in Horálek et al. (2019). The map layers are created for the rural, urban background and urban traffic areas separately on a grid at 1x1 km^2 resolution. Subsequently, the urban background and urban traffic map layers are merged together using the gridded road data into one urban map layer. This urban map layer is further combined with the rural map layer into the final PM_{10} map using a population density grid at 1x1 km^2 resolution. For both PM_{10} indicators, we present this final combined map in this 1x1 km^2 grid resolution.

The population exposure tables are calculated based on these maps, according to the methodology described in Horálek et al. (2019), i.e. they are calculated separately for urban areas directly influenced by traffic and for the background (both rural and urban) areas, in order to better reflect the population exposed to traffic. For details, see Annex 1, Equation A1.6.

2.1 PM_{10} annual average

2.1.1 Concentration map

Map 2.1 presents the final combined concentration map for the 2018 PM_{10} annual average as the result of interpolation and merging of the separate map layers as described in Annex 1 (for a more detailed description, see Horálek et al., 2007, 2019). Red and purple areas indicate exceedances of the limit value (LV) of 40 $\mu g \cdot m^{-3}$.

The final combined concentration map presented in Map 2.1 is constructed on a 1x1 km^2 grid resolution (Annex 1). The station points are not presented in the map, in order to better visualise the urban areas. However, concentration values from measurements at the station points used in the kriging interpolation methodology (Annex 3) are considered to provide relevant information. In Map A5.1 of Annex 5 these point values are presented on top of Map 2.1 and illustrate the smoothing effect the interpolation methodology can have on the gridded concentration fields.

Map 2.1 shows annual LV exceedances in southern Spain near Almeria, in urban areas of Southern and Eastern Europe states (Albania, Bulgaria, North Macedonia, Montenegro and Serbia), in parts of Turkey and in southern Poland in the region around Katowice. The spatial extent of the exceedance area near Almeria has decreased in 2018 compared to 2017. Concerning the estimated exceedances in the Almeria area, it should be noted that they are primarily based on high concentration values indicated in this area by the chemical transport modelling, and not on measurements (which are not available in this area with the minimum data coverage required to be taken into account).

The uncertainty of the concentration map can be expressed in relative terms of the absolute Root Mean Square Error (RMSE) uncertainty related to the mean air pollution indicator value for all stations (see Annex 1). This *relative mean uncertainty* (RRMSE) of the final combined map of PM_{10} annual average is 17 % for rural areas and 19 % for urban background areas without Turkish stations (i.e. quite similar to the last years), and respectively 18 % for rural areas and 26 % for urban background areas including Turkish stations (Annex 3). The main reason for presenting the results without Turkish stations is to enable the comparison with previous years.

Map 2.1 Concentration map of PM_{10} annual average, 2018

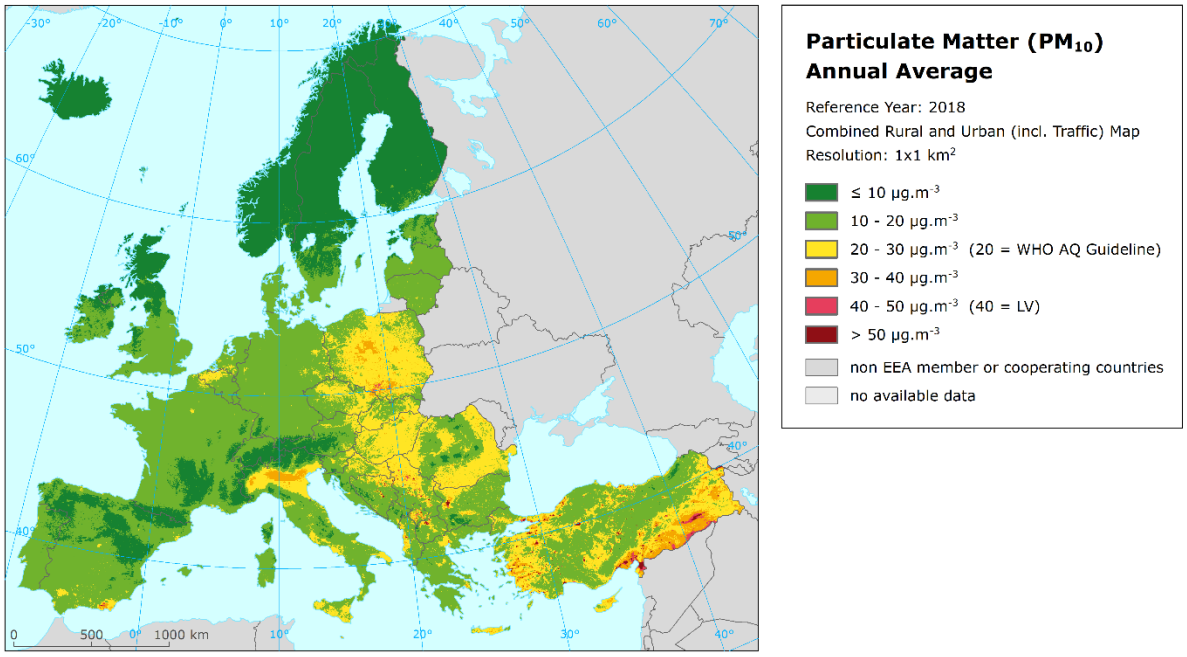

2.1.2 Population exposure

Table 2.1 gives the population frequency distribution for a limited number of exposure classes, as well as the population-weighted concentration for individual countries and for Europe as a whole according to Equation A1.7.

The human exposure to PM10 has been calculated based on the improved methodology as developed in Horálek et al. (2019), i.e. similarly as for NO2. The population exposure is calculated according to Equation A1.6 of Annex 1, i.e. it is calculated separately for urban areas directly influenced by traffic and for the background (both rural and urban) areas, in order to better reflect the population exposed to traffic. Based on this, the different concentration levels in urban background and traffic areas inside the 1x1 km2 grid cells are taken into account.

About 49 % of the European population and 42 % of the EU-28 population has been exposed to annual average concentrations above the Air Quality Guideline of 20 µg·m-3 recommended by the World Health Organization (WHO, 2005). CSI004 (EEA, 2020c) estimates that about 48 % of the population in urban agglomerations in the EU-28 was exposed in 2018 to levels above the WHO guideline. The latter estimate accounts only for the urban population of the EU-28. It therefore represents areas where, in general, somewhat higher PM10 concentrations occur. The estimates in Table 2.1 account for the total European and EU-28 population, including the population in rural areas, smaller cities and villages that are in general exposed to lower levels of PM10. Next to this, it should be mentioned that CSI004 refers to the population in cities for which PM10 data is available.

Table 2.1: Population exposure and population-weighted concentration, PM_{10} annual average, 2018

Country	ISO	Population [inhbs·1000]	PM_{10} – annual average, exposed population, 2018 [%]						PM_{10} ann. avg.
			< 10	10 - 20	20 - 30	30 - 40	40 - 50	> 50	Pop. weighted
Albania	AL	2 870	0.0	10.5	32.1	30.0	26.1	1.3	32.4
Andorra	AD	75	0.7	99.3					16.9
Austria	AT	8 822	2.8	50.1	47.1				19.1
Belgium	BE	11 399		40.4	59.6				20.7
Bosnia & Herzegovina	BA	3 500	0.0	13.9	30.1	22.7	21.4	11.8	34.1
Bulgaria	BG	7 050	0.0	9.0	41.6	39.1	9.5	0.7	30.9
Croatia	HR	4 105	0.0	25.2	63.1	11.7	0.1		23.9
Cyprus	CY	1 226		0.1	20.7	70.8	8.3	0.1	32.5
Czechia	CZ	10 610	0.0	10.6	79.5	9.4	0.6		24.8
Denmark (incl. Faroe Islands)	DK	5 781	0.2	96.9	2.9				16.9
Estonia	EE	1 319	3.0	96.5	0.5				12.8
Finland	FI	5 513	45.6	53.7	0.8				10.8
France (metropolitan)	FR	64 738	1.4	80.5	17.4	0.6			17.0
Germany	DE	82 792	0.1	84.9	15.0				18.1
Greece	GR	10 741		25.0	33.3	32.9	7.4	1.4	28.0
Hungary	HU	9 778		0.6	94.8	4.6			26.2
Iceland	IS	348	60.0	40.0					9.4
Ireland	IE	4 830	6.7	93.3					12.5
Italy	IT	60 484	0.3	20.1	61.9	17.6			24.1
Latvia	LV	1 934	0.1	67.4	22.7	9.7			19.2
Liechtenstein	LI	38	1.0	99.0					13.7
Lithuania	LT	2 809		61.9	34.5	3.6			19.5
Luxembourg	LU	602		94.0	6.0				16.9
Malta	MT	476		0.1	76.6	23.3			30.2
Monaco	MC	38		78.5	21.5				20.2
Montenegro	ME	622	0.2	18.0	32.4	46.2	0.2	3.0	29.2
Netherlands	NL	17 181		81.0	19.0				19.4
North Macedonia	MK	2 075	0.0	2.2	22.1	36.7	12.2	26.8	42.1
Norway	NO	5 296	41.4	53.2	5.4				11.3
Poland	PL	37 977		2.8	48.2	39.7	9.4		30.3
Portugal (excl. Azores, Madeira)	PT	9 793	0.8	75.1	21.2	2.9			17.4
Romania	RO	19 531	0.0	11.6	78.0	10.2	0.2		24.9
San Marino	SM	34		14.2	85.8				20.8
Serbia (incl. Kosovo*)	RS	8 800	0.0	3.8	17.7	27.0	48.6	2.8	37.8
Slovakia	SK	5 443		2.6	93.5	3.9			24.9

Slovenia	SI	2 067	0.0	36.2	57.9	5.9			22.1
Spain (excl. Canarias)	ES	44 481	0.8	53.2	44.6	1.2	0.1	0.0	19.5
Sweden	SE	10 120	26.2	69.5	4.3				12.4
Switzerland	CH	8 484	6.5	91.6	1.9				15.0
Turkey	TR	80 811	0.0	9.2	13.2	20.2	28.6	28.7	43.2
United Kingdom (& Crown dep.)	UK	66 525	1.8	95.6	2.6				15.3
Total		**621 122**	**1.8** / **51.1**	**49.3**	**30.2**	**9.7**	**5.3** / **9.0**	**3.7**	**23.4**
Total without Turkey		**540 312**	**2.1** / **56.8**	**54.7**	**32.5**	**8.3**	**2.2** / **2.5**	**0.3**	**20.8**
EU-28		**507 878**	**1.7** / **57.6**	**55.9**	**33.6**	**7.8**	**1.1** / **1.1**	**0.0**	**20.4**
Kosovo*	KS	1 799	0.0	3.4	14.7	24.1	48.7	9.1	39.1
Serbia (excl. Kosovo*)	RS	7 001		3.9	18.4	27.7	48.6	1.3	37.4

(*) under the UN Security Council Resolution 1244/99

Note: The percentage value "0.0" indicates that an exposed population exists, but it is small and estimated to be less than 0.05 %. Empty cells mean no population in exposure.

Approximately 9 % of population of the European area (including Turkey[1]) has been exposed to concentrations exceeding the EU annual limit value (ALV) of 40 µg·m^{-3}; the same is the case for 2.5 % for the European population excluding Turkey and for 1 % of the EU-28 population. In Bosnia & Herzegovina, North Macedonia, Serbia including Kosovo[2] and Turkey, more than 30 % of the population has been exposed to concentrations above the ALV. A limited fraction of the population (3-27 %) has been exposed to concentrations above the ALV in Albania, Bulgaria, Cyprus, Greece, Montenegro and Poland. However, as the current mapping methodology tends to underestimate high values (see Annex 3, Section A3.1), the exceedance percentage will most likely be underestimated. Additional population exposure above the ALV could therefore be expected in countries like Bulgaria, Cyprus, Montenegro or Poland where a relatively large fraction of the population lives in areas with concentration levels above 30 µg·m^{-3}.

The European-wide population-weighted concentration of the annual average for 2018 is estimated to be about 23 µg·m^{-3} including Turkey, 21 µg·m^{-3} without Turkey, and 20 µg·m^{-3} for the EU-28 only.

Figure 2.1 shows, for the whole mapped area (that is, all Europe including Turkey), the population frequency distribution for exposure classes of 1 µg·m^{-3}. One can see the highest population frequency for classes between 16 and 20 µg·m^{-3}. A quite continuous decline of population frequency is visible for classes between 20 and 35 µg·m^{-3} and beyond 40 µg·m^{-3}.

[1] The whole Turkish population, both European and Asian.

[2] In this paper, references to Kosovo shall be understood to be in the context of UN Security Council Resolution 1244/99.

Figure 2.1 Population frequency distribution, PM_{10} annual average, 2018

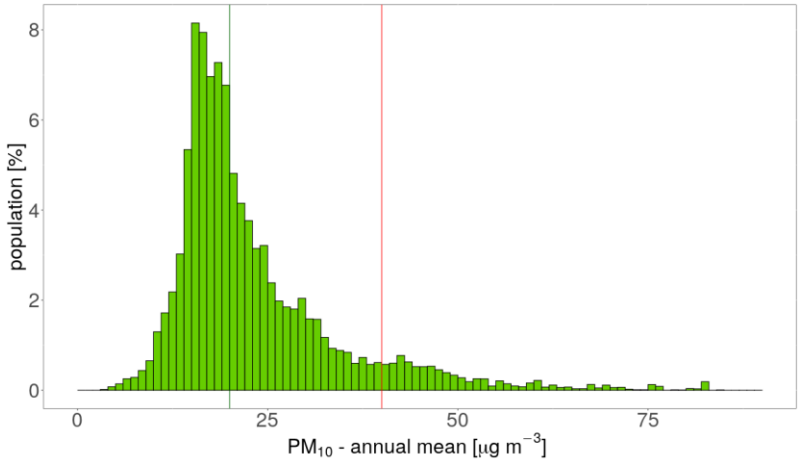

Note: Apart from the population distribution shown in graph, it was estimated that 0.08 % of population lived in areas with PM_{10} annual average concentration in between 90 and 310 µg·m^{-3}.

2.2 PM_{10} – 90.4 percentile of daily means

The AQ Directive (EC, 2008) describes the PM_{10} daily limit value (DLV) as "a daily average of 50 µg·m^{-3} not to be exceeded more than 35 times a calendar year". This requirement can be evaluated by the indicator 36th highest daily mean, which is in principle equivalent to the indicator 90.4 percentile of daily means. However, for measurement data these two indicators are equivalent only if no data is missing, which is in general not the case. As shown in de Leeuw (2012), the additional uncertainty related to incomplete time series is substantially smaller when using percentile values instead of the x-th highest value. Furthermore, the AQ Directive requires the use of the 90.4 percentile when random measurements are used to assess the requirements of the PM_{10} DLV. As in the previous reports since the maps for 2014, we express the PM_{10} daily means as the 90.4 percentile instead of the formerly used 36th highest daily mean.

2.2.1 Concentration map

Map 2.2 presents the final combined map, where red and purple marked areas indicate values of the 90.4 percentile of daily means above 50 µg·m^{-3} (i.e. exceedances of the DLV of 50 µg·m^{-3} on more than 35 measurement days). The similar mapping procedure as in the case of the annual average is used. The mapping details and the uncertainty analysis are presented in Annex 3. Large areas above the DLV are observed in northern Italy (i.e. the Po Valley), in the region with the agglomerations Ostrava (CZ) – Katowice (PL) – Krakow (PL) and in eastern parts of Turkey. Urban areas with concentrations above the DLV are observed in Albania, Bosnia & Herzegovina, Bulgaria, Croatia, Greece, Hungary, Montenegro, North Macedonia, Poland, Romania, Serbia including Kosovo, Slovenia, and Turkey . In general, the central and the eastern parts of Europe appear with higher concentrations than the western and the northern parts. As for the PM_{10} annual averages, the estimated exceedances in the Almeria area are based on the chemical transport modelling, not on measurements.

The relative mean uncertainty (relative RMSE) of the final combined map of the 90.4 percentile of PM_{10} daily means is 18 % for rural areas and 21 % for urban background areas without Turkish stations, resp. 19 % for rural areas and 28 % for urban background areas including Turkish stations (Annex 3).

The final combined map *including* the indicator 90.4 percentile of daily means based on the actual measurement data at station points is presented in Map A5.2 of Annex 5.

Map 2.2 Concentration map of PM_{10} indicator 90.4 percentile of daily means, 2018

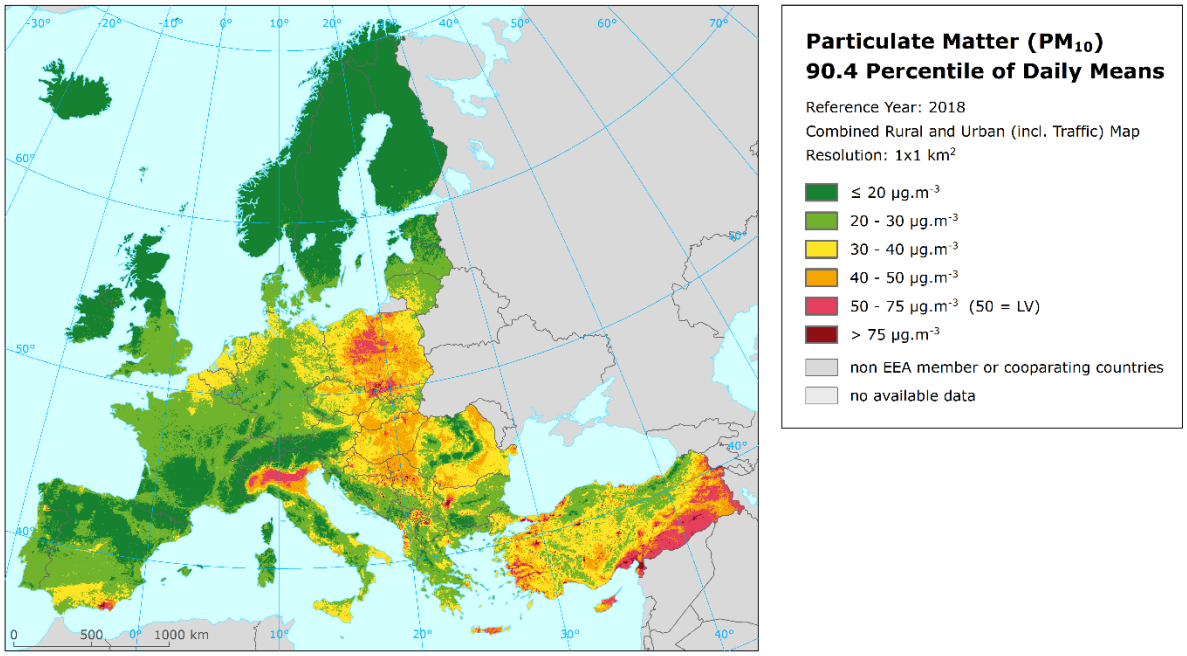

2.2.2 Population exposure

Table 2.2 gives the population frequency distribution for a limited number of exposure classes calculated at 1x1 km^2 grid resolution, as well as the population-weighted concentration for individual countries and for Europe as a whole.

Table 2.2: Population exposure and population-weighted concentrations, PM_{10} indicator 90.4 percentile of daily means, 2018

Country	ISO	Population [inhbs·1000]	PM_{10} - perc90.4, exposed population, 2018 [%]						PM_{10} - perc90.4
			< 20	20 - 30	30 - 40	40 - 50	50 - 75	> 75	Pop. weighted
Albania	AL	2 870	0.0	5.3	12.7	17.2	36.0	28.8	58.6
Andorra	AD	75	1.8	98.2					26.1
Austria	AT	8 822	5.6	30.9	38.0	25.5	0.0		33.0
Belgium	BE	11 399	0.0	7.9	84.0	8.2			35.1
Bosnia & Herzegovina	BA	3 500	0.1	6.3	11.8	16.1	26.7	38.9	67.4
Bulgaria	BG	7 050	0.2	5.6	10.3	28.3	52.4	3.1	52.7
Croatia	HR	4 105	0.2	10.4	30.1	19.6	39.0	0.6	45.2
Cyprus	CY	1 226			0.2	13.0	80.0	6.8	54.3
Czechia	CZ	10 610	0.0	2.5	27.9	56.2	12.2	1.3	43.5
Denmark (incl. Faroe Islands)	DK	5 781	0.6	77.1	22.1	0.2			28.8
Estonia	EE	1 319	10.0	83.9	6.1	0.0			23.0
Finland	FI	5 513	54.2	41.0	4.8	0.0	0.0		20.0
France (metropolitan)	FR	64 738	5.4	62.8	29.2	2.5	0.0		27.8
Germany	DE	82 792	0.5	59.1	38.8	1.6	0.1		29.5
Greece	GR	10 741	0.0	13.1	26.0	27.6	31.1	2.2	45.0
Hungary	HU	9 778		0.0	6.9	67.0	26.1		46.7
Iceland	IS	348	92.0	1.8	6.1	0.1			16.6
Ireland	IE	4 830	35.2	63.9	0.9				21.5
Italy	IT	60 484	0.9	12.1	43.8	20.8	22.4		40.4
Latvia	LV	1 934	1.0	47.3	25.7	18.3	7.6		33.0
Liechtenstein	LI	38	2.1	97.9					24.9
Lithuania	LT	2 809		20.7	65.3	10.3	3.8		34.8
Luxembourg	LU	602	0.0	93.4	6.6				26.8
Malta	MT	476		0.0	2.3	87.5	10.2		46.0
Monaco	MC	38			100.0				31.7
Montenegro	ME	622	0.9	12.1	8.3	19.7	51.7	7.4	57.1
Netherlands	NL	17 181		3.9	96.1				32.3
North Macedonia	MK	2 075	0.0	1.1	2.8	12.4	42.0	41.8	81.5
Norway	NO	5 296	48.2	40.1	11.5	0.1			20.3
Poland	PL	37 977		0.3	8.4	26.2	54.9	10.2	55.4
Portugal (excl. Azores, Madeira)	PT	9 793	5.8	58.3	29.0	6.8	0.0		29.1
Romania	RO	19 531	0.1	4.8	38.4	48.4	8.3		41.5
San Marino	SM	34		6.1	89.3	4.5			34.8
Serbia (incl. Kosovo*)	RS	8 800	0.0	1.8	5.4	10.5	29.6	52.8	70.3
Slovakia	SK	5 443	0.0	0.4	18.2	66.3	15.0	0.2	44.5

Country	ISO	Population [inhbs·1000]	PM_{10} - perc90.4, exposed population, 2018 [%]						PM_{10} - perc90.4
			< 20	20 - 30	30 - 40	40 - 50	50 - 75	> 75	Pop. weighted
Slovenia	SI	2 067	0.1	16.4	36.6	35.3	11.6		39.2
Spain (excl. Canarias)	ES	44 481	2.5	37.3	53.2	5.9	0.9	0.2	31.7
Sweden	SE	10 120	38.2	50.1	10.8	0.8	0.0		22.2
Switzerland	CH	8 484	8.4	81.7	9.3	0.7			25.7
Turkey	TR	80 811	0.2	3.6	9.6	7.2	32.1	47.2	74.7
United Kingdom (& Crown dep.)	UK	66 525	8.0	84.5	7.5	0.0			25.9
Total		**621 122**	**3.9**	**34.4**	**28.5**	**12.1**	**13.4**	**7.7**	**40.1**
			38.3				**21.1**		
Total without Turkey		**540 312**	**4.4**	**38.6**	**31.0**	**12.8**	**10.8**	**2.4**	**35.4**
			43.0				**13.2**		
EU-28		**507 878**	**4.0**	**39.2**	**32.4**	**13.1**	**10.3**	**0.9**	**34.5**
			43.2				**11.2**		
Kosovo*	KS	1 799	0.0	1.5	5.1	6.7	20.7	66.0	77.4
Serbia (excl. Kosovo*)	RS	7 001	0.0	1.9	5.4	11.4	31.7	49.6	68.6

(*) under the UN Security Council Resolution 1244/99

Note: The percentage value "0.0" indicates that an exposed population exists, but it is small and estimated to be less than 0.05 %. Empty cells mean no population in exposure.

We estimate that in 2018 about 21 % of the European population lived in areas where the 90.4 percentile of the PM_{10} daily means exceeded the EU limit value of 50 µg·m^{-3}. In Albania, Bosnia & Herzegovina, Bulgaria, Cyprus, Montenegro, North Macedonia, Poland, Serbia (including Kosovo) and Turkey, more than half of the population was exposed to concentrations exceeding the DLV. In Croatia, Czechia, Greece, Hungary, Italy, Malta, Slovakia and Slovenia the portion of the population living in areas with concentrations above the DLV was between 10 and 50 percent.

For the EU-28 around 11 % of the total population lived in areas where the 90.4 percentile of the PM_{10} daily mean exceeded the EU limit value of 50 µg·m^{-3}. According to CSI004 (EEA, 2020c), in 2018 about 15 % of the urban population in the EU-28 was exposed to PM_{10} above this limit value. The slight difference between the two estimates is influenced by the fact that the EEA accounts for the urban population only, while Table 2.2 provides estimates also including inhabitants in rural areas, smaller cities and villages.

The European-wide population-weighted concentration of the 90.4 percentile of PM_{10} daily means is estimated for 2018 at about 40 µg·m^{-3} (including Turkey), resp. 35 µg·m^{-3} (without Turkey), and 34.5 µg·m^{-3} for the EU-28.

Figure 2.2 shows, for the whole mapped area, the population frequency distribution for exposure classes of 2 µg·m^{-3}. One can see the highest population frequency for classes between ca. 24 and 32 µg·m^{-3}, continuous decline of population frequency for classes between ca. 34 and 50 µg·m^{-3} and continuous mild decline of population frequency for classes between ca. 50 and 100 µg·m^{-3}.

As in previous years, the daily limit value was more widely exceeded than the annual limit value in 2018.

Figure 2.2: Population frequency distribution, PM_{10} indicator 90.4 percentile of daily means, 2018

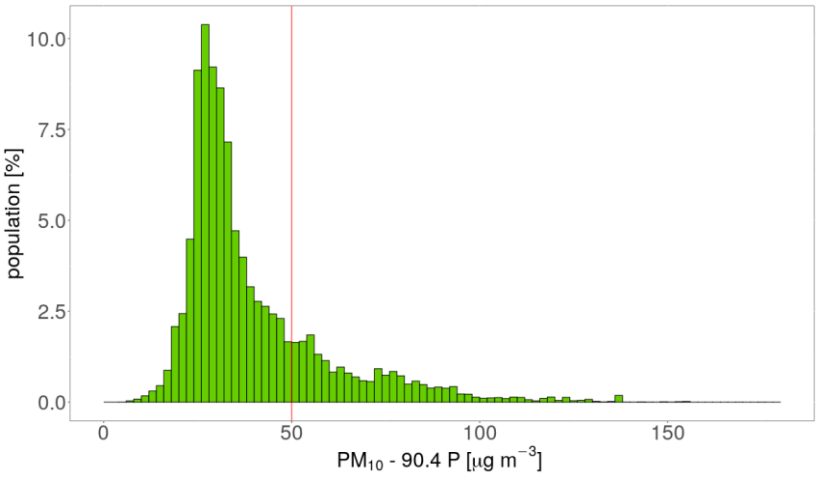

Note: Apart from the population distribution shown in graph, it was estimated that 0.07 % of population lived in areas with values of PM_{10} indicator 90.4 percentile of daily means in between 180 and 610 $\mu g \cdot m^{-3}$.

3 $PM_{2.5}$

In the Ambient Air Quality Directive (EC, 2008), the limit value (LV) for the annual average $PM_{2.5}$ concentrations was set at 25 µg·m^{-3}. In the AQ directive there is also an indicative limit value (ILV) of 20 µg·m^{-3} defined as Stage 2, in place since 2020. The Air Quality Guideline recommended by the World Health Organization (WHO, 2005) for the $PM_{2.5}$ annual average is 10 µg·m^{-3}.

The current number of $PM_{2.5}$ measurement stations is still somewhat limited and its spatial distribution is irregular over Europe. Therefore, in this paper the mapping of the health-related indicator $PM_{2.5}$ annual average is based on a mapping methodology developed in Denby et al. (2011a, 2011b). This methodology derives additional *pseudo* $PM_{2.5}$ annual mean concentrations from PM_{10} annual mean measurement concentrations. As such, it increases the number and spatial coverage of $PM_{2.5}$ 'data points' and these data are used to derive a European wide map of annual mean $PM_{2.5}$. Pseudo $PM_{2.5}$ stations data are estimated using PM_{10} measurement data, surface solar radiation, latitude and longitude.

Like for PM_{10}, the map of $PM_{2.5}$ is based on the improved mapping methodology developed in Horálek et al. (2019). The map layers are created for the rural, urban background and urban traffic areas separately on a grid at 1x1 km^2 resolution. Subsequently, the urban background and urban traffic map layers are merged together using the gridded road data into one urban map layer. This urban map layer is further combined with the rural map layer into the final PM_{10} map using a population density grid at 1x1 km^2 resolution. We present this final combined map at this 1x1 km^2 grid resolution.

Annex 3 provides details on the regression and kriging parameters applied for deriving the $PM_{2.5}$ annual average map, as well as the uncertainty analysis of the map. Annex 4 discusses briefly the inter-annual changes observed in the concentration maps and the relevant population exposure.

3.1 $PM_{2.5}$ annual average

3.1.1 Concentration map

Map 3.1 presents the final combined map for the 2018 $PM_{2.5}$ annual average as a result of the interpolation and merging of the separate rural and urban map layers. The dark red areas exceed the ALV of 25 µg·m^{-3}. Red areas show exceedances of the indicative LV of 20 µg·m^{-3} defined as Stage 2 (ILV_{2020}).

Due to the lack of rural $PM_{2.5}$ stations in Turkey, no proper interpolation results could be estimated for this country in a rural map. Therefore, we do not present the estimated $PM_{2.5}$ values for Turkey in the final map.

According to Map 3.1, the areas with the highest $PM_{2.5}$ concentrations appear to be the Po Valley in northern Italy, the areas around the Balkan cities of Athens, Sofia, Tirana, Skopje and Belgrade, the Krakow – Katowice (PL) – Ostrava (CZ) industrial region and the area around Warsaw. Different other cities in Bulgaria, Greece, Serbia, Kosovo, North Macedonia, Bosnia & Herzegovina and Poland also show elevated $PM_{2.5}$ annual average concentrations. Like in the case of PM_{10}, the central and the eastern parts of Europe show higher concentrations than the western and the northern parts.

The relative mean uncertainty of the 2018 map of $PM_{2.5}$ annual average is 20 % for rural areas and 18 % for urban background areas and determined exclusively on the actual $PM_{2.5}$ measurement data points, i.e. not on the pseudo stations (Annex 3).

Map 3.1 Concentration map of $PM_{2.5}$ annual average, 2018

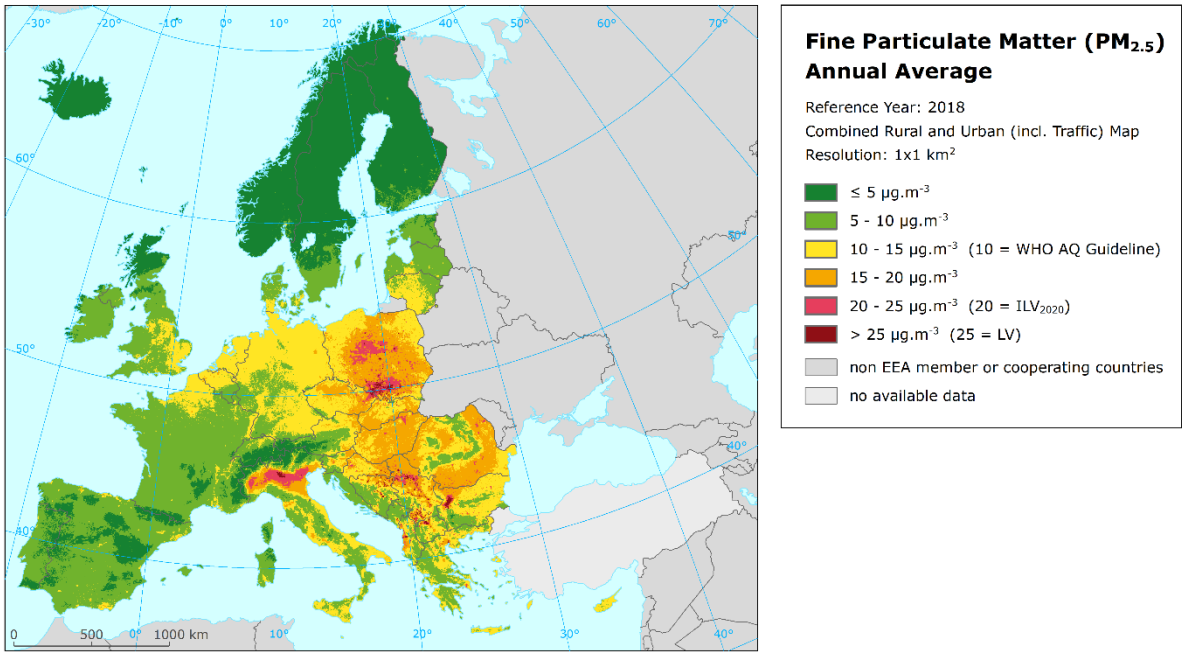

In order to provide more complete information of the air quality across Europe, the final combined map including the measurement data at station points is presented in Map A5.3 of Annex 5.

3.1.2 Population exposure

Table 3.1 gives the population frequency distribution for a limited number of exposure classes calculated on a grid of 1x1 km^2 resolution, as well as the population-weighted concentration for individual countries and for Europe as a whole according to Equation A1.7 of Annex 1.

The population exposure has been calculated according to Equation A1.6 of Annex 1, i.e. it has been calculated separately for urban areas directly influenced by traffic and for the background (both rural and urban) areas, in order to better reflect the population exposed to traffic.

In 2018, 76 % of the European (excluding Turkey) and 77 % of the EU-28 population has been exposed to $PM_{2.5}$ annual mean concentrations above the Air Quality Guideline of 10 µg·m^{-3} as defined by the World Health Organization (WHO, 2005). The European wide, resp. EU-28, population exposure exceeding the EU limit value (LV) of 25 µg·m^{-3} has been 4.5 %, resp. 3 %. In Albania, Bosnia & Herzegovina, Montenegro, North Macedonia and Serbia (including Kosovo), more than 25 % of the population suffers from exposures above this limit value; in Bulgaria, Croatia, Czechia, Greece and Poland, it has been between 5 to 25 %. The Stage 2 indicative limit value (ILV_{2020}) of 20 µg·m^{-3} has been exceeded for about 13 % (European wide) resp. 11 % (EU-28) of the population. In Albania, Bosnia & Herzegovina, Bulgaria, Montenegro, North Macedonia, Poland and Serbia (including Kosovo), a half or more of the population has been exposed to concentrations above the ILV_{2020}. As the current mapping methodology tends to underestimate high values (Annex 3), the exceedance percentages and/or the number of countries with population exposed to concentrations above both the current ALV and the indicative ILV_{2020} will most likely be higher.

Table 3.1 Population exposure and population-weighted concentration, $PM_{2.5}$ annual average 2018

Country	ISO	Population [inhbs·1000]	$PM_{2.5}$ – annual average, exposed population, 2018 [%]						$PM_{2.5}$ ann. avg.
			< 5	5 - 10	10 - 15	15 - 20	20 - 25	> 25	Pop. weighted
Albania	AL	2 870		1.7	14.6	26.5	25.5	31.8	21.6
Andorra	AD	75	0.8	99.2					8.5
Austria	AT	8 822	0.6	13.2	49.0	37.3			13.6
Belgium	BE	11 399		6.8	81.2	12.0			12.7
Bosnia & Herzegovina	BA	3 500		3.1	11.8	19.6	14.0	51.4	26.4
Bulgaria	BG	7 050		1.2	12.2	33.7	35.3	17.7	21.0
Croatia	HR	4 105		7.9	21.1	27.1	39.1	4.8	18.0
Cyprus	CY	1 226		0.3	91.3	0.0	7.6	0.9	14.5
Czechia	CZ	10 610		0.2	14.3	66.3	11.7	7.5	18.3
Denmark (incl. Faroe Islands)	DK	5 781	0.6	22.2	77.2				10.5
Estonia	EE	1 319	0.6	98.3	1.1				7.0
Finland	FI	5 513	33.3	66.7					5.9
France (metropolitan)	FR	64 738	0.2	45.4	49.1	5.4			10.6
Germany	DE	82 792	0.0	5.2	89.5	5.3	0.1		12.3
Greece	GR	10 741		3.3	37.2	22.5	25.3	11.8	18.3
Hungary	HU	9 778			2.8	82.5	14.7		18.3
Iceland	IS	348	58.6	41.4					4.7
Ireland	IE	4 830	1.4	89.9	8.8				7.8
Italy	IT	60 484	0.2	7.4	48.1	22.8	19.8	1.8	15.5
Latvia	LV	1 934		35.1	43.2	20.7	1.0		12.1
Liechtenstein	LI	38	0.1	99.4	0.5				8.6
Lithuania	LT	2 809		5.6	82.7	11.8			12.8
Luxembourg	LU	602		55.1	44.9				10.0
Malta	MT	476		0.6	89.2	10.2			12.5
Monaco	MC	38			100.0				12.6
Montenegro	ME	622		8.4	13.3	27.0	20.2	31.1	20.5
Netherlands	NL	17 181		0.2	99.8				12.0
North Macedonia	MK	2 075		0.3	2.4	5.8	32.0	59.5	30.7
Norway	NO	5 296	32.1	56.7	11.2				6.4
Poland	PL	37 977		0.0	5.7	30.8	41.8	21.7	21.7
Portugal (excl. Azores, Madeira)	PT	9 793	1.9	77.2	15.2	5.6			8.4
Romania	RO	19 531		0.5	15.0	65.0	18.6	0.9	17.6
San Marino	SM	34			95.7	4.3			13.3
Serbia (incl. Kosovo*)	RS	8 800		0.5	3.3	16.3	12.6	67.3	26.6
Slovakia	SK	5 443		0.0	3.0	82.2	11.2	3.5	18.2
Slovenia	SI	2 067		4.7	35.7	46.1	13.5		15.8
Spain (excl. Canarias)	ES	44 481	0.6	48.5	46.6	4.3			10.2
Sweden	SE	10 120	33.4	65.9	0.7				6.1
Switzerland	CH	8 484	1.9	43.4	54.1	0.5			9.8
United Kingdom (& Crown dep.)	UK	66 525	0.5	36.8	62.7				10.0
Total (no Turkey)		**540 312**	**1.5**	**22.1**	**47.6**	**15.8**	**8.6**	**4.5**	**13.5**
			23.6				**13.1**		
EU-28		**507 878**	**1.2**	**22.1**	**49.4**	**16.1**	**8.5**	**2.7**	**13.2**
			23.3				**11.2**		
Kosovo*	KS	1 799		0.1	3.8	9.5	12.0	74.5	28.2
Serbia (excl. Kosovo*)	RS	7 001		0.6	3.2	18.0	12.8	65.5	26.3

(*) under the UN Security Council Resolution 1244/99

Note 1: Turkey not included due to the lack of the rural stations.

Note 2: The percentage value "0.0" indicates that an exposed population exists, but it is small and estimated to be less than 0.05 %. Empty cells mean no population in exposure.

According to EEA CSI004 (EEA, 2020c), about 4 % of the urban population in the EU-28 was exposed to $PM_{2.5}$ concentrations above the LV in 2018. The slight difference with the estimated 3 % in Table 3.1 is because the EEA accounts for the urban population only. Whereas, Table 3.1 provides estimates for the total population, including the population in rural areas, smaller cities and villages. When it comes to the WHO AQ guideline, the EU-28 urban population exposed to concentrations above its recommended value (10 µg·m^{-3}) in 2018 was estimated at 74 % by CSI004, which is quite similar to the EU-28 total population estimation of 77 % as presented in Table 3.1.

The European-wide population-weighted concentration of the $PM_{2.5}$ annual means has been estimated for 2018 at about 14 µg·m^{-3} for Europe as a whole and about 13 µg·m^{-3} for the EU-28. being the lowest value in the time series 2005-2018 (see Section 3.2).

Figure 3.1 shows, for the whole mapped area, the population frequency distribution for exposure classes of 1 µg·m^{-3}. The highest population frequency is found for classes between 11 and 13 µg·m^{-3}.

Figure 3.1 Population frequency distribution, $PM_{2.5}$ annual average, 2018

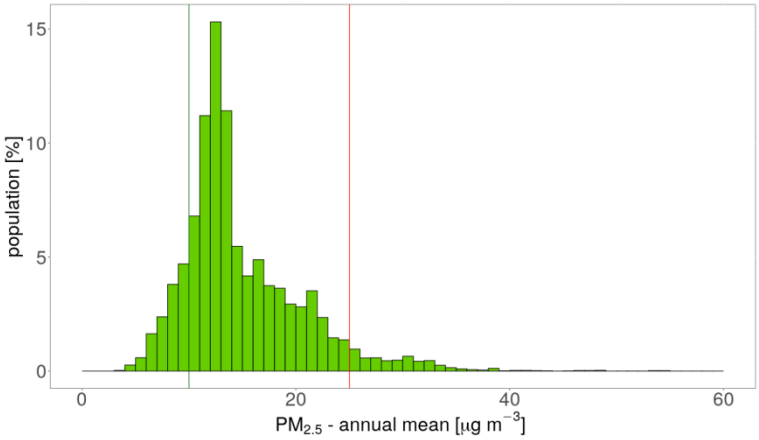

Note: Next to the population distribution shown in graph, it was estimated that 0.005 % of population lived in areas with $PM_{2.5}$ annual average concentration in between 60 and 220 µg·m^{-3}.

4 Ozone

For ozone, three health-related indicators, i.e., *93.2 percentile of maximum daily 8-hour means* (see below), *SOMO35* and *SOMO10*, and four vegetation-related indicators, i.e., *AOT40 for vegetation, AOT40 for forests*, POD_6 *for wheat* and POD_6 *for potato* are considered. For the definition of the SOMO35, SOMO10 and AOT40 and POD indicators, see following sections and Annex 2.

The separate rural and urban background health-related indicator fields are calculated at a resolution of 10x10 km^2. Subsequently, the final health-related indicator maps are created by combining rural and urban areas based on the 1x1 km^2 gridded population density map. We present these maps on this 1x1 km^2 grid resolution. The population exposure tables are calculated on the basis of these health-related indicator maps.

The vegetation-related indicator maps are calculated from observations at rural background stations and are representative for rural areas only (assuming urban areas do not cover vegetation). The maps have a resolution of 2x2 km^2. This resolution serves the needs of the EEA Core Set Indicator 005 (EEA, 2020d) on ecosystem exposure to ozone.

Annex 3 provides details on the regression and kriging parameters applied for deriving the maps of the ozone indicators, as well as the uncertainty analysis of the maps. Annex 4 discusses briefly the inter-annual changes observed in the concentration maps and the relevant population and vegetation exposure.

4.1 Ozone – 93.2 percentile of maximum daily 8-hour means

The AQ Directive (EC, 2008) describes the ozone target value (TV) for the protection of human health as "a maximum daily 8-hour mean of 120 $\mu g \cdot m^{-3}$ not to be exceeded on more than 25 times a calendar year, averaged over three years". On an annual basis, it can be evaluated by the indicator 26th highest maximum daily 8-hour mean, which is in principle equivalent to the indicator 93.2 percentile of maximum daily 8-hour means. However, for measurement data these two indicators are equivalent only if no data is missing, which is in general not the case. As shown in de Leeuw (2012), the additional uncertainty related to incomplete time series is substantially smaller when using percentile values instead of the x-th highest value. As in the previous reports since 2014 maps, we express this ozone indicator as the 93.2 percentile of maximum daily 8-hour means instead of the formerly used 26th highest maximum daily 8-hour mean.

4.1.1 Concentration map

Map 4.1 presents the final combined map for 93.2 percentile of maximum daily 8-hour means as a result of combining the separate rural and urban interpolated maps following the procedures as described in Annex 1 (for a more detailed description, see Horálek et al., 2007, 2010). The supplementary data used are EMEP model output, altitude and surface solar radiation for rural areas and EMEP model output, wind speed and surface solar radiation for urban areas (Annex 3).

In the final combined map the red and dark red areas show values of the 93.2 percentile of maximum daily 8-hour means above 120 $\mu g \cdot m^{-3}$ in 2018, i.e. above the TV threshold of 120 $\mu g \cdot m^{-3}$ on more than 25 days in 2018. Note that in the AQ Directive (EC, 2008) the TV is actually defined as 120 $\mu g \cdot m^{-3}$ not to be exceeded on more than 25 days per calendar year *averaged over three years*. Here only 2018 data are presented, and no three-year average has been calculated.

The map shows that in 2018 percentile values above 120 $\mu g \cdot m^{-3}$ occur in a large area of Europe, namely in Germany, Switzerland, Austria, Czechia, parts of Slovakia, Poland, Hungary, Greece, Italy, Spain,

Portugal, France and Turkey. Percentile values above 120 µg·m^{-3} occur also in Northern Europe, at high mountain altitudes in Norway. In general, in former years the southern parts of Europe show higher ozone concentrations than the northern parts, which is caused mainly by higher solar radiation and temperature in these areas. Furthermore, in general, higher levels of ozone do also occur more frequently in mountainous areas than in lowlands. The situation in 2018 was different, as 2018 was the third warmest year on record in Europe and temperatures in central and northern Europe during late spring and summer were 4 to 8 °C above the 10-year mean 2008-2017 (Copernicus, 2019). As already mentioned, concentrations above the TV occurred in 2018 in Central and Western Europe, and even in part of Northern Europe. On the other hand, concentrations under the TV occurred in 2018 in parts of southern Italy including Sicilia and Sardinia, in parts of Spain and parts of the Balkan area. For the comparison with 2017 values, see Annex 4.

The relative mean uncertainty of the 2018 map of the 93.2 percentile of maximum daily 8-h ozone means is about 8 % for rural and 9 % for urban areas (Annex 3).

In order to provide more complete information of the air quality across Europe, the final combined map including the measurement data at station points is presented in Map A5.4 of Annex 5.

Map 4.1 Concentration map of ozone indicator 93.2 percentile of maximum daily 8-hour means, 2018

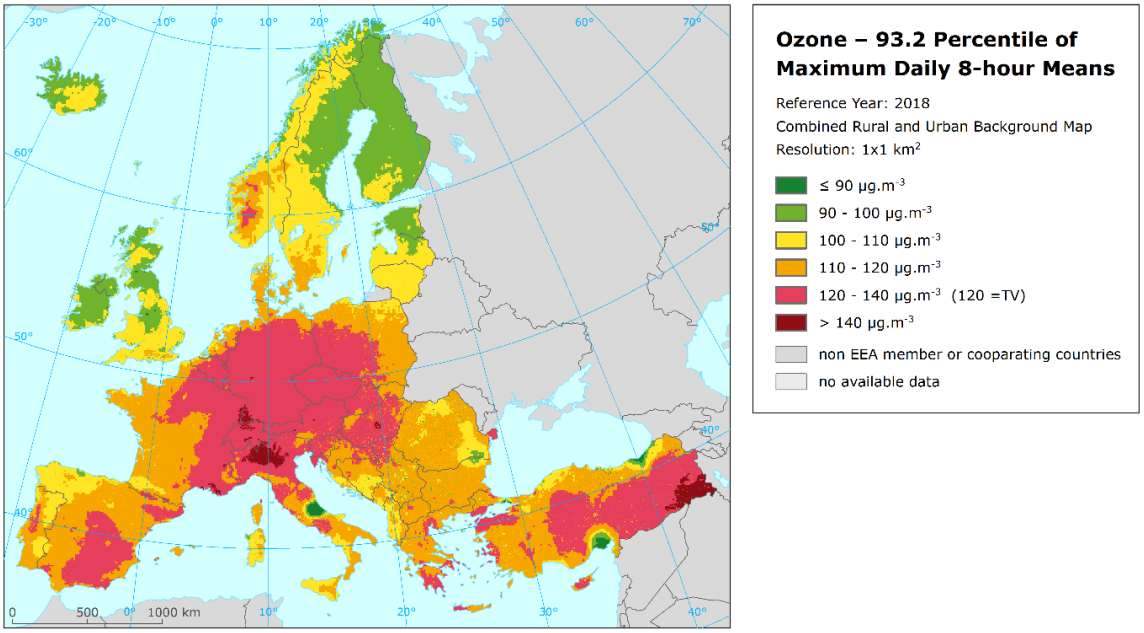

4.1.2 Population exposure

Table 4.1 gives, for the 93.2 percentile of maximum daily 8-hour means, the population frequency distribution for a limited number of exposure classes, as well as the population-weighted concentration for individual countries and for Europe as a whole.

It has been estimated that in 2018 about 35 % of the European population including Turkey (37 % excluding Turkey) and 38 % of the EU-28 population lived in areas where the ozone concentration exceeded the health related target value threshold (TV of 120 µg·m^{-3}). According to CSI004 (EEA, 2020c), about 34 % of the urban population in the EU-28 was exposed to ozone above the TV threshold

in 2018. It should be mentioned that the CSI004 refers only to the population in cities for which ozone measurement data is available and does not take into account population in rural areas, where ozone concentrations tend to be higher.

Table 4.1 Population exposure and population-weighted concentrations, ozone indicator 93.2 percentile of maximum daily 8-hour means, 2018

Country	ISO	Population [inhbs·1000]	Ozone - perc93.2, exposed population, 2018 [%]						Ozone - perc93.2
			< 90	90 - 100	100 - 110	110 - 120	120 - 140	> 140	Pop. weighted
Albania	AL	2 870		1.1	88.2	10.8			106.4
Andorra	AD	75				99.1	0.9		112.4
Austria	AT	8 822			1.0	15.3	83.7	0.0	124.3
Belgium	BE	11 399		0.2	4.0	27.2	68.6	0.0	123.8
Bosnia & Herzegovina	BA	3 500		19.3	40.3	37.6	2.8		108.1
Bulgaria	BG	7 050	1.1	55.9	31.8	11.3	0.1		100.4
Croatia	HR	4 105		0.9	22.5	57.8	18.8		115.0
Cyprus	CY	1 226		5.2	70.2	16.6	7.9		108.2
Czechia	CZ	10 610				0.7	99.3		127.5
Denmark (incl. Faroe Islands)	DK	5 781		0.5	58.8	40.7	0.0		109.2
Estonia	EE	1 319		92.9	7.1	0.0			98.1
Finland	FI	5 513		92.0	8.0	0.0			96.0
France (metropolitan)	FR	64 738		0.3	14.2	37.1	48.2	0.2	119.2
Germany	DE	82 792			0.4	9.5	89.9	0.2	126.0
Greece	GR	10 741	0.7	10.1	43.2	33.7	12.2		110.8
Hungary	HU	9 778		0.1	19.7	64.6	15.4	0.1	116.0
Iceland	IS	348	64.4	35.4	0.2				88.6
Ireland	IE	4 830	6.8	85.0	8.2	0.0			95.8
Italy	IT	60 484	2.0	5.2	17.7	27.4	31.2	16.6	122.1
Latvia	LV	1 934	18.7	19.3	62.0	0.0			98.7
Liechtenstein	LI	38					100.0		132.1
Lithuania	LT	2 809		1.5	98.5	0.1			102.9
Luxembourg	LU	602				53.9	46.1		120.1
Malta	MT	476		40.9	45.6	13.1	0.4		103.0
Monaco	MC	38					100.0		126.4
Montenegro	ME	622		14.4	75.3	10.3			105.9
Netherlands	NL	17 181		0.2	25.2	51.1	23.4		115.0
North Macedonia	MK	2 075	24.5	44.1	25.3	6.0	0.2		96.9
Norway	NO	5 296		35.7	61.4	2.8	0.0		102.5
Poland	PL	37 977		0.9	16.3	53.2	29.6		116.2
Portugal (excl. Azores, Madeira)	PT	9 793		9.0	56.8	32.4	1.9		107.6
Romania	RO	19 531	3.4	32.7	51.6	12.2	0.1		101.7
San Marino	SM	34					100.0		123.9
Serbia (incl. Kosovo*)	RS	8 800	4.4	53.5	28.0	12.8	1.3		100.3
Slovakia	SK	5 443			2.5	59.2	38.3		118.5
Slovenia	SI	2 067				66.1	33.9		118.1
Spain (excl. Canarias)	ES	44 481	0.3	9.7	21.9	44.2	24.0		113.2
Sweden	SE	10 120		16.5	75.5	8.0	0.0		104.1
Switzerland	CH	8 484				2.1	93.1	4.9	133.0
Turkey	TR	80 811	18.7	21.4	24.2	17.8	17.0	1.0	104.2
United Kingdom (& Crown dep.)	UK	66 525	5.6	58.9	35.1	0.4			97.7
Total		**621 122**	**3.5**	**15.6**	**22.1**	**23.9**	**33.0**	**1.9**	
			19.1				**34.9**		**113.2**
Total without Turkey		**540 312**	**1.4**	**14.9**	**21.9**	**24.7**	**35.2**	**2.0**	
			16.3				**37.2**		**114.4**
EU-28		**507 878**	**1.3**	**14.1**	**21.1**	**25.6**	**35.9**	**2.0**	
			15.4				**37.9**		**114.7**
Kosovo*	KS	1 799		64.9	24.0	11.1			100.4
Serbia (excl. Kosovo*)	RS	7 001	5.4	50.8	29.0	13.2	1.6		100.2

(*) under the UN Security Council Resolution 1244/99

Note: The percentage value "0.0" indicates that an exposed population exists, but it is small and estimated to be less than 0.05 %. Empty cells mean no population in exposure.

In the following countries (apart from the microstates) at least 30 % of the population suffered exposures above the TV threshold: Austria, Belgium, Czechia, France, Germany, Italy, Luxembourg, Poland, Slovakia, Slovenia and Switzerland. As the current mapping methodology tends to underestimate high values due to interpolation smoothing (Annex 3), the exceedance percentage is most likely somewhat underestimated; additional population exposure above the TV threshold might be expected in additional countries: Croatia, Denmark, Greece, Hungary, the Netherlands, Spain and Turkey. The reason is that in these countries the estimated percentage population exposed to the concentrations above 110 µg·m^{-3} is considerable.

The overall European and EU-28 population-weighted ozone concentrations in terms of the 93.2 percentile of maximum daily 8-hour means has been estimated for 2018 as being 113 µg·m^{-3} and 115 µg·m^{-3}, respectively, while for the area without Turkey it has been 114 µg·m^{-3}, which is the second highest value of the fourteen year period 2005-2018 (Section 6.3).

Figure 4.1 shows, for the whole mapped area, the population frequency distribution for exposure classes of 2 µg·m^{-3}. The highest population frequency is found for classes between 110 and 130 µg·m^{-3}.

Figure 4.1 Population frequency distribution, O_3 indicator 93.2 percentile of maximum daily 8-hour means, 2018

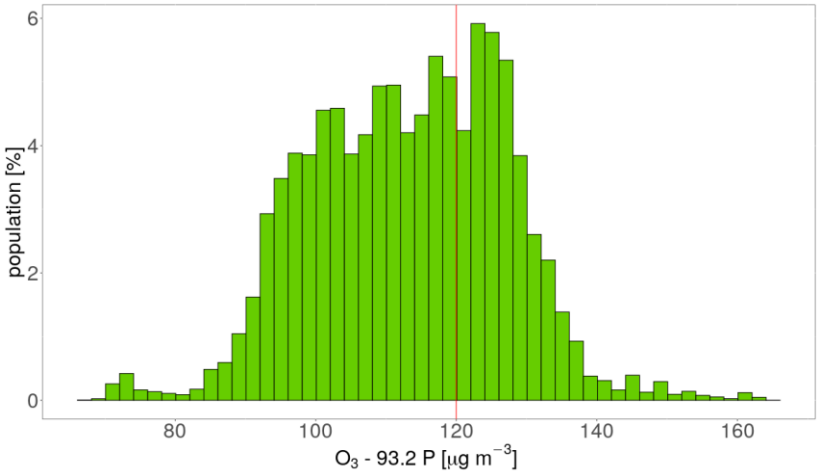

4.2 Ozone – SOMO35 and SOMO10

SOMO35 is the annually accumulated ozone maximum daily 8-hourly means in excess of 35 ppb (i.e. 70 µg·m^{-3}). It is not subject to any of the EU air quality directives and there are no limit or target values defined. Comparing the 93.2 percentile of maximum daily 8-hour means versus the SOMO35 for all background stations shows no simple relationship between the two indicators. However, it seems that the TV of the 93.2 percentile of maximum daily 8-hour means (being 120 µg·m^{-3}) is related approximately with a SOMO35 value in the range of 6 000 - 8 000 µg·m^{-3}·d. This comparison motivates a somewhat arbitrarily chosen threshold of 6 000 µg·m^{-3}·d, in order to facilitate the discussion of the observed distributions of SOMO35 levels in their spatial and temporal context. This threshold is used in this and previous papers (Horálek et al., 2020a, and the references cited therein) when dealing with the population exposure estimates.

SOMO10 is the annually accumulated ozone maximum daily 8-hourly means in excess of 10 ppb (i.e. 20 µg·m^{-3}). We have introduced this indicator for the second time, due to its link to the health impact assessment. Be it noted that the WHO recommends to use the SOMO10 as an alternative to the SOMO35 when estimating the health impact of ozone (WHO, 2013).

4.2.1 Concentration maps

Map 4.2 presents the final combined map for SOMO35 as a result of combining the separate rural and urban interpolated maps following the same procedure as for 93.2 percentile of the maximum daily 8-hour means. The mapping details and the uncertainty analysis are presented in Annex 3. In the final combined map the red and dark red areas show values above 8 000 µg·m^{-3}·d, while the orange areas show values above 6 000 µg·m^{-3}·d.

Like in the case of the 93.2 percentile of the maximum daily 8-hour means, generally the southern parts of Europe show higher ozone SOMO35 concentrations than the northern parts. Higher levels of ozone also occur more frequently in mountainous areas south of 50 degrees latitude than in lowlands. The relative mean uncertainty of the 2018 map of the SOMO35 is about 27 % for rural and 29 % for urban areas (see Annex 3).

Compared to 2017, most of northern, north-western and central Europe show a quite high increase in 2018, due to the exceptional hot summer in 2018 in central and north Europe see Annex 4, Section A4.3.

Map 4.2 Concentration map of ozone indicator SOMO35, 2018

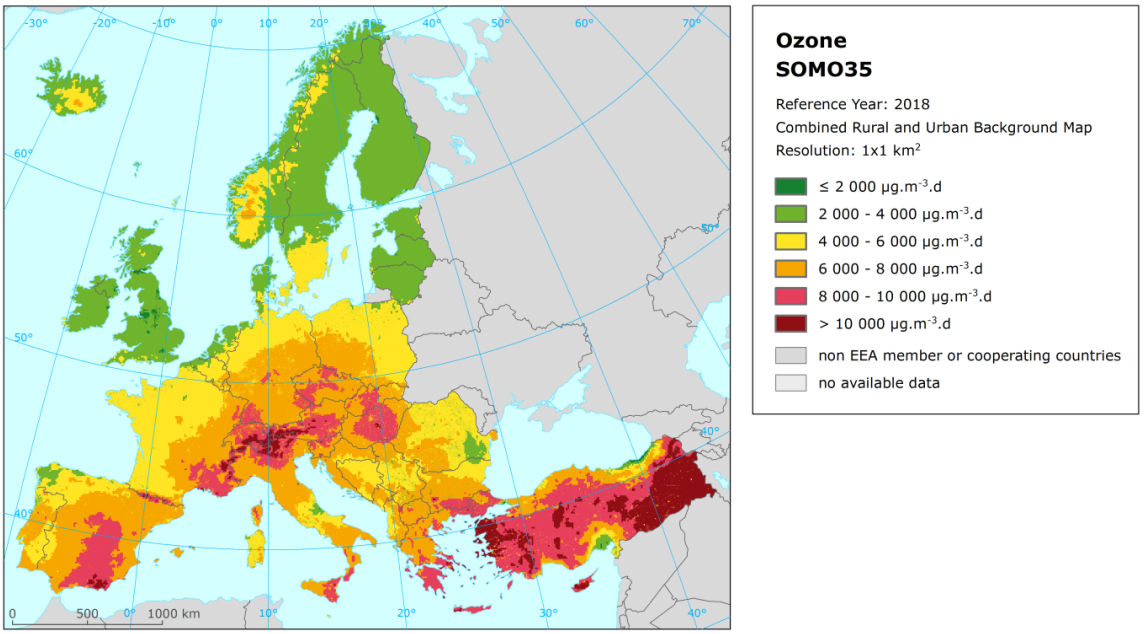

Map 4.3 presents the final combined map for SOMO10, as a results of the similar mapping procedure as in the cases of other ozone health-related indicators. The boundaries of concentration classes have been chosen quite arbitrary, in order to reflect the concentration distribution of this indicator. In the final combined map the red and dark red areas show values above 24 000 µg·m^{-3}·d.

The spatial distribution of the SOMO10 concentrations are quite similar like in the case of the SOMO35, i.e. higher values in the southern parts of Europe compared to its northern parts, and also in the mountainous areas compared to the lowlands. The relative mean uncertainty of the 2018 map of the SOMO10 is about 13 % for rural areas and about 14 % for urban areas (see Annex 3).

In order to provide more complete information of the air quality across Europe, the final combined maps including the ozone indicators SOMO35 and SOMO10 values at station points, based on the measurement data are presented in Maps A5.5 and A5.6, respectively, of Annex 5.

Map 4.3 Concentration map of ozone indicator SOMO10, 2018

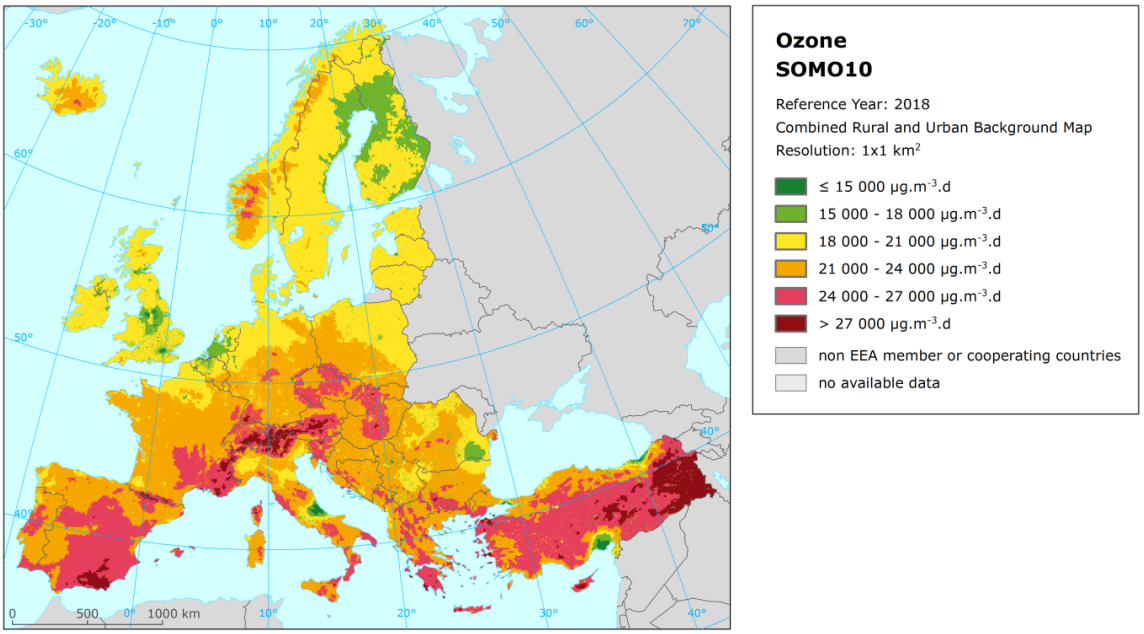

4.2.2 Population exposure

Table 4.2 gives for SOMO35 the population frequency distribution for a limited number of exposure classes, as well as the population-weighted concentration for individual countries and for Europe as a whole.

It has been estimated that in 2018 about 32 % of the European population (including Turkey), resp. about 31 % of European population without Turkey and of the EU-28 population, lived in areas with SOMO35 values above 6 000 µg·m^{-3}·d (see above on the motivation of this criterion).

In 2018, like in the previous several years, the northern and north-western European countries have had almost no inhabitants exposed to SOMO35 concentrations above 6 000 µg·m^{-3}·d. In Iceland and Norway there have been areas with SOMO35 above 6 000 µg·m^{-3}·d (see map 4.2), but they mostly correspond to non-populated areas. Most of the countries in Southern and Central and Eastern Europe have shown exposures above or well above 6 000 µg·m^{-3}·d, most notably (at least 50 % of population) Liechtenstein, Switzerland, Czechia, Greece, Cyprus, Austria, Croatia, Italy, Slovenia, Spain and Slovakia. This can also be observed in Map 4.2.

In 2018, both the total European and the EU-28, population-weighted ozone concentrations, in terms of SOMO35, were estimated to be around 5 000 µg·m^{-3}·d. For Europe without Turkey, it was also almost 5 000 µg·m^{-3}·d, which is the second highest in the fourteen years period 2005-2018 (Table 6.3). Compared to 2017, notably higher values have occurred in central Europe (Annex 4).

The total European, resp. the EU-28, population-weighted ozone concentrations, in terms of SOMO10, were estimated to be about 19 400 µg·m^{-3}·d, resp. 19 500 µg·m^{-3}·d. For Europe without Turkey, it was also 19 500 µg·m^{-3}·d.

Table 4.2 Population exposure and population-weighted concentrations, ozone indicator SOMO35, 2018

Country	ISO	Population [inhbs·1000]	Ozone - SOMO35, exposed population, 2018 [%]						Ozone - SOMO35
			< 2000	4000	6000	8000	10000	> 10000	Pop, weighted
Albania	AL	2 870		0.2	83.4	16.3	0.1		5 601
Andorra	AD	75				98.3	1.4	0.3	6 593
Austria	AT	8 822			26.7	63.9	9.2	0.3	6 731
Belgium	BE	11 399		37.5	61.7	0.8			4 298
Bosnia & Herzegovina	BA	3 500		2.5	90.0	7.5			5 218
Bulgaria	BG	7 050		67.5	24.7	6.6	1.2	0.0	3 765
Croatia	HR	4 105			29.9	69.5	0.5		6 342
Cyprus	CY	1 226			22.8	60.5	13.1	3.6	6 844
Czechia	CZ	10 610			5.6	90.4	3.9		6 946
Denmark (incl. Faroe Islands)	DK	5 781		72.6	27.3	0.0			3 866
Estonia	EE	1 319		99.7	0.3				2 793
Finland	FI	5 513	7.8	92.2	0.0				2 351
France (metropolitan)	FR	64 738		18.7	51.3	27.4	2.5	0.1	5 274
Germany	DE	82 792		1.3	64.3	33.6	0.7	0.0	5 674
Greece	GR	10 741		8.1	13.1	46.3	30.5	2.0	7 157
Hungary	HU	9 778		1.1	62.8	31.6	4.4	0.1	5 892
Iceland	IS	348	61.7	38.2	0.0				1 999
Ireland	IE	4 830	8.7	90.4	0.9				2 556
Italy	IT	60 484	0.3	5.6	26.8	53.4	13.6	0.3	6 490
Latvia	LV	1 934	18.7	80.7	0.7				2 732
Liechtenstein	LI	38				96.1	3.9		7 045
Lithuania	LT	2 809		99.4	0.6				3 096
Luxembourg	LU	602		28.2	64.5	7.3			4 604
Malta	MT	476			85.3	12.9	1.3	0.5	5 498
Monaco	MC	38				100.0			7 686
Montenegro	ME	622		8.8	56.7	34.5	0.0		5 630
Netherlands	NL	17 181		70.6	29.4				3 620
North Macedonia	MK	2 075	14.0	48.1	31.5	6.3	0.0		3 533
Norway	NO	5 296		96.3	3.7	0.0			3 128
Poland	PL	37 977		14.9	66.3	18.7	0.1		5 095
Portugal (excl. Azores, Madeira)	PT	9 793		37.7	46.3	16.0	0.1		4 672
Romania	RO	19 531	3.3	68.0	25.3	3.4	0.0		3 683
San Marino	SM	34				100.0			6 700
Serbia (incl. Kosovo*)	RS	8 800	1.8	64.5	29.3	4.2	0.1		3 583
Slovakia	SK	5 443			47.8	50.1	2.1		6 129
Slovenia	SI	2 067			42.3	51.1	6.5	0.0	6 494
Spain (excl. Canarias)	ES	44 481	0.3	16.9	29.0	48.8	4.9	0.0	5 841
Sweden	SE	10 120		80.6	19.4	0.0			3 465
Switzerland	CH	8 484			3.4	85.8	10.4	0.4	7 214
Turkey	TR	80 811	11.5	21.9	27.7	19.1	12.0	7.9	5 504
United Kingdom (& Crown dep.)	UK	66 525	34.2	65.0	0.8	0.0			2 314
Total		**621 122**	**5.4**	**27.3**	**35.1**	**26.6**	**4.5**	**1.0**	**5 027**
			32.7				**32.1**		
Total without Turkey		**540 312**	**4.6**	**28.0**	**36.1**	**27.6**	**3.5**	**0.1**	**4 962**
			32.6				**31.2**		
EU-28		**507 878**	**4.8**	**27.4**	**36.4**	**27.7**	**3.6**	**0.1**	**4 970**
			32.2				**31.4**		
Kosovo*	KS	1 799		63.4	29.9	6.7	0.0		3 922
Serbia (excl. Kosovo*)	RS	7 001	2.3	64.8	29.2	3.6	0.1		3 500

(*) under the UN Security Council Resolution 1244/99

Note: The percentage value "0.0" indicates that an exposed population exists, but it is small and estimated to be less than 0.05 %. Empty cells mean no population in exposure.

Table 4.3 Population exposure and population-weighted concentrations, ozone indicator SOMO10, 2018

Country	ISO	Population [inhbs·1000]	Ozone – SOMO10, exposed population, 2018 [%]						Ozone – SOMO10
			< 15000	18000	21000	24000	27000	> 27000	Pop, weighted
Albania	AL	2 870		0.3	57.8	40.7	1.1		20 980
Andorra	AD	75			76.8	21.3	1.4	0.5	20 618
Austria	AT	8 822			36.1	54.9	8.4	0.6	21 481
Belgium	BE	11 399	0.2	61.7	36.4	1.7			17 689
Bosnia & Herzegovina	BA	3 500		22.5	52.4	24.9	0.2		19 449
Bulgaria	BG	7 050	0.6	63.9	26.1	8.4	0.9	0.0	17 679
Croatia	HR	4 105			59.2	38.8	1.9	0.0	21 002
Cyprus	CY	1 210		6.5	73.8	6.2	12.3	1.2	20 042
Czechia	CZ	10 610			11.4	81.0	7.6		22 084
Denmark (incl. Faroe Islands)	DK	5 781		0.4	98.5	1.1			19 523
Estonia	EE	1 319		73.5	26.5				17 625
Finland	FI	5 513		84.8	15.2				17 276
France (metropolitan)	FR	64 738		11.3	47.9	35.7	5.0	0.1	20 509
Germany	DE	82 792		3.3	81.5	14.5	0.6	0.0	19 874
Greece	GR	10 741	0.1	10.3	23.1	53.2	12.9	0.4	21 685
Hungary	HU	9 778		4.8	69.9	22.5	2.8	0.1	20 124
Iceland	IS	348		91.0	8.9	0.0			16 593
Ireland	IE	4 830		57.2	42.4	0.3			17 966
Italy	IT	60 484	1.8	6.6	46.8	38.9	5.8	0.1	20 793
Latvia	LV	1 934	18.7	49.5	31.8	0.0			17 310
Liechtenstein	LI	38				99.9	0.1		21 454
Lithuania	LT	2 809		71.3	28.6	0.0			17 694
Luxembourg	LU	602		21.9	67.7	10.5			19 011
Malta	MT	476				86.3	13.2	0.5	23 185
Monaco	MC	38				100.0			23 313
Montenegro	ME	622		13.1	42.9	42.5	1.5		20 646
Netherlands	NL	17 181	0.2	67.9	31.8				17 331
North Macedonia	MK	2 075	22.7	43.4	26.8	6.7	0.4		17 214
Norway	NO	5 296		27.6	70.7	1.7	0.0		18 569
Poland	PL	37 977		18.3	62.5	18.8	0.3		19 612
Portugal (excl. Azores, Madeira)	PT	9 793		7.9	44.5	40.8	6.8	0.0	20 823
Romania	RO	19 531	6.4	62.3	25.5	5.8	0.0		17 557
San Marino	SM	34			32.1	67.9			21 121
Serbia (incl. Kosovo*)	RS	8 800	21.0	49.6	20.4	9.0	0.1		16 999
Slovakia	SK	5 443			54.5	42.1	3.4	0.0	20 940
Slovenia	SI	2 067			50.3	36.4	13.2	0.1	21 481
Spain (excl. Canarias)	ES	44 481		4.0	35.5	41.4	18.9	0.1	21 732
Sweden	SE	10 120		13.2	85.9	0.9			18 940
Switzerland	CH	8 484			13.9	79.2	6.5	0.4	21 770
Turkey	TR	80 811	28.9	23.4	21.8	9.2	13.2	3.4	18 194
United Kingdom (& Crown dep.)	UK	66 525	20.1	71.5	8.2	0.1			16 089
Total		**621 106**	**6.4**	**23.7**	**42.4**	**21.9**	**5.0**	**0.5**	
			30.1				**5.5**		**19 360**
Total without Turkey		**540 295**	**3.4**	**23.8**	**45.2**	**23.6**	**3.9**	**0.1**	
			27.2				**4.0**		**19 519**
EU-28		**515 135**	**3.1**	**23.7**	**45.9**	**23.1**	**4.1**	**0.1**	
			26.8				**4.2**		**19 539**
Kosovo*	KS	1 799		71.67	18.07	10.13	0.13		17 687
Serbia (excl. Kosovo*)	RS	7 001	26.17	44.16	20.91	8.72	0.05		16 831

(*) under the UN Security Council Resolution 1244/99

Note: The percentage value "0.0" indicates that an exposed population exists, but it is small and estimated to be less than 0.05 %. Empty cells mean no population in exposure.

Figure 4.2 shows, for the whole mapped area, the frequency distribution of SOMO35 for population exposure classes of 250 µg·m^{-3}·d. The highest frequencies are found for classes between 1 500 and 5 000 µg·m^{-3}·d. One can see a steep decline of population frequency for exposure classes between 7 000 and 9000 µg·m^{-3} and a continuous mild decline of population frequency for classes above 9 000 µg·m^{-3}·d.

Figure 4.2 Population frequency distribution, ozone indicator SOMO35, 2018

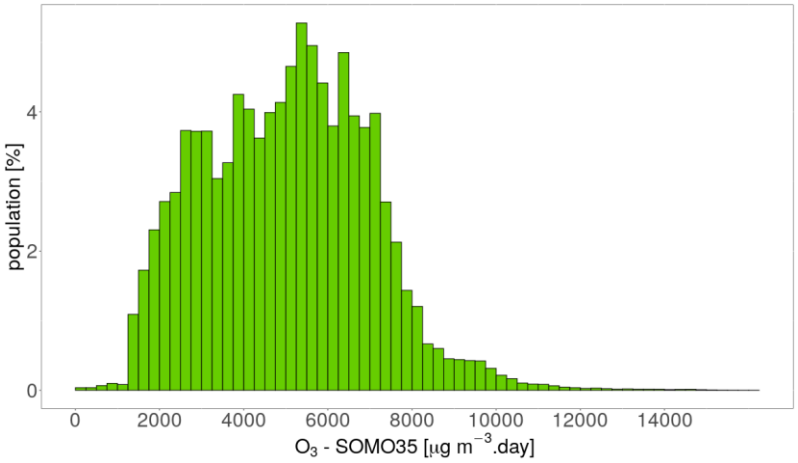

Figure 4.3 shows the population frequency distribution of SOMO10 for population exposure classes of 500 µg·m^{-3}·d. The graph shows the highest frequencies for classes between 18 000 and 23 000 µg·m^{-3}·d.

Figure 4.3 Population frequency distribution, ozone indicator SOMO10, 2018

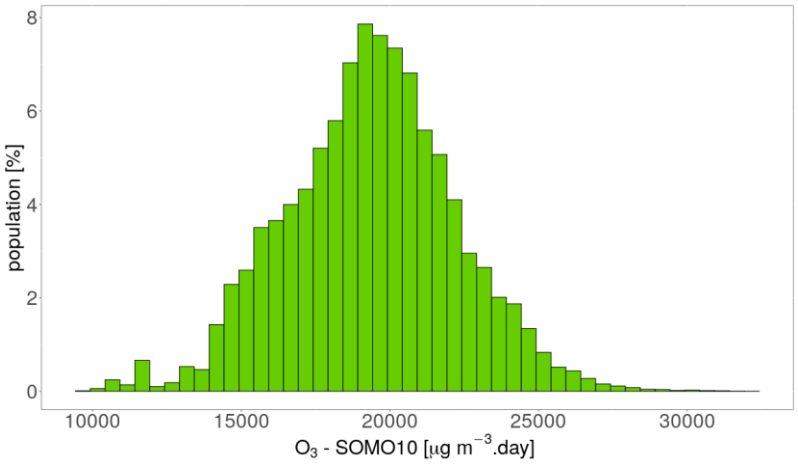

4.3 Ozone – AOT40 vegetation and AOT40 forests

In the Ambient Air Quality Directive (EC, 2008) a target value (TV) and a long-term objective (LTO) for the *protection of vegetation* from high ozone concentrations accumulated during the growing season have been defined. TV and LTO are specified using "accumulated ozone exposure over a threshold of 40 parts per billion" (AOT40). This is calculated as a sum of the difference between hourly concentrations greater than 80 $\mu g \cdot m^{-3}$ (i.e. 40 parts per billion) and 80 $\mu g \cdot m^{-3}$, using only observations between 08:00 and 20:00 Central European Time (CET) each day, calculated over three months from 1 May to 31 July. The TV is 18 000 $\mu g \cdot m^{-3} \cdot h$ (averaged over five years) and the LTO is 6 000 $\mu g \cdot m^{-3} \cdot h$.

Note that the term *vegetation* as used in the AQ Directive (EC, 2008) is not further defined. Nevertheless, the TV used in the directive is the same as the critical level used in the Mapping Manual (CLRTAP, 2017) for "agricultural crops", so we have interpreted the term *vegetation* in the AQ directive as primarily agricultural crops. Therefore, the exposure of *agricultural crops* has been evaluated here based on the AOT40 for vegetation as defined in the AQ directive and the agricultural areas, defined as the CORINE Land Cover level-1 class *2 Agricultural areas* (encompassing the level-2 classes *2.1 Arable land, 2.2 Permanent crops, 2.3 Pastures* and *2.4 Heterogeneous agricultural areas)*, see Section 4.3.2. Note that in addition to these agricultural areas there are several other CLC classes that could be considered "vegetation", namely level-2 classes *1.4 Artificial, non-agricultural vegetated areas* (encompassing the level-3 classes *1.4.1 Green urban areas* and *1.4.2 Sport and leisure facilities*), *3.1 Forests* (see below) and 3.*2 Scrub and/or herbaceous vegetation associations*.

Next to the AOT40 for vegetation protection, the AQ Directive (EC, 2008) defines also the AOT40 for *forest protection*, which is calculated similarly as the AOT40 for vegetation, but is summed over six months from 1 April to 30 September. For AOT40 for forests there is no TV defined. However, there is a critical level (CL) established by CLRTAP (2017). This critical level is set at 10 000 $\mu g \cdot m^{-3} \cdot h$.

For the exposure of forests evaluation, the CLC level-2 class *3.1 Forests* has been used.

The ecosystem based accumulative ozone indicators described in this section are specifically prepared for calculation of the EEA Core Set Indicator 005 (EEA, 2020d). For the estimation of the vegetation and forested area exposure to accumulated ozone, the maps in this section are created on a grid of 2x2 km^2 resolution. The exposure frequency distribution outcomes are based on the overlay with the 100x100 m^2 grid resolution of the CLC2016 land cover classes.

4.3.1 Concentration maps

The interpolated maps of AOT40 for vegetation and AOT40 for forests are created for rural areas only, as urban areas are considered not to represent agricultural or forested areas. These maps are therefore applicable to rural areas only, and as such they are based on AOT40 data derived from rural background station observations only. These AOT40 monitoring data are combined in the mapping with the supplementary data sources EMEP model output, altitude and surface solar radiation. These supplementary data sources are the same as those selected at the human health related ozone indicators.

Map 4.4 presents the final map of AOT40 for *vegetation* in 2018. Note that in the AQ Directive (EC, 2008) the TV is actually defined as 18 000 $\mu g \cdot m^{-3} \cdot h$ *averaged over five years*. Here only 2018 data are presented, and no five-year average has been calculated.

The areas in the map with concentrations above the TV threshold of 18 000 $\mu g \cdot m^{-3} \cdot h$ are marked in red and dark red. The areas below the long term objective (LTO) are marked in green. The high and very high AOT40 levels for vegetation do occur specifically in southern, south-western and south-eastern regions of Europe; they also occurred in central regions of Europe in 2018. Highest levels (dark red) were measured in the south of Greece and Spain, in the south-west and south-east of Turkey, in the

north of Italy, in the middle of Czechia and in other smaller parts in Germany, Austria, Switzerland and France. The relative mean uncertainty of the 2018 map of the AOT40 for vegetation is about 30 % (Annex 3).

Map 4.5 presents the final map of AOT40 for *forests* in 2018. The areas in the map with concentrations above the critical level (CL) defined by CLRTAP (2017) are marked in yellow, orange, red and dark red. One can see large European forested areas exceeding this level.

Like for the AOT40 for vegetation indicator, the highest levels of the AOT40 for forests are found in the south-western, southern and south-eastern European region. Like for the AOT40 for vegetation indicator, in 2018 highest levels occur also in Central Europe. Nevertheless, in 2018 values above the CL are found everywhere in Europe except the Atlantic areas in the north of Spain, parts of the United Kingdom, Ireland and parts of Northern Europe. The relative mean uncertainty of the 2018 map of the AOT40 for forests is about 30 % (Annex 3).

Map 4.4 Concentration map of O_3 indicator AOT40 for vegetation, rural map, 2018

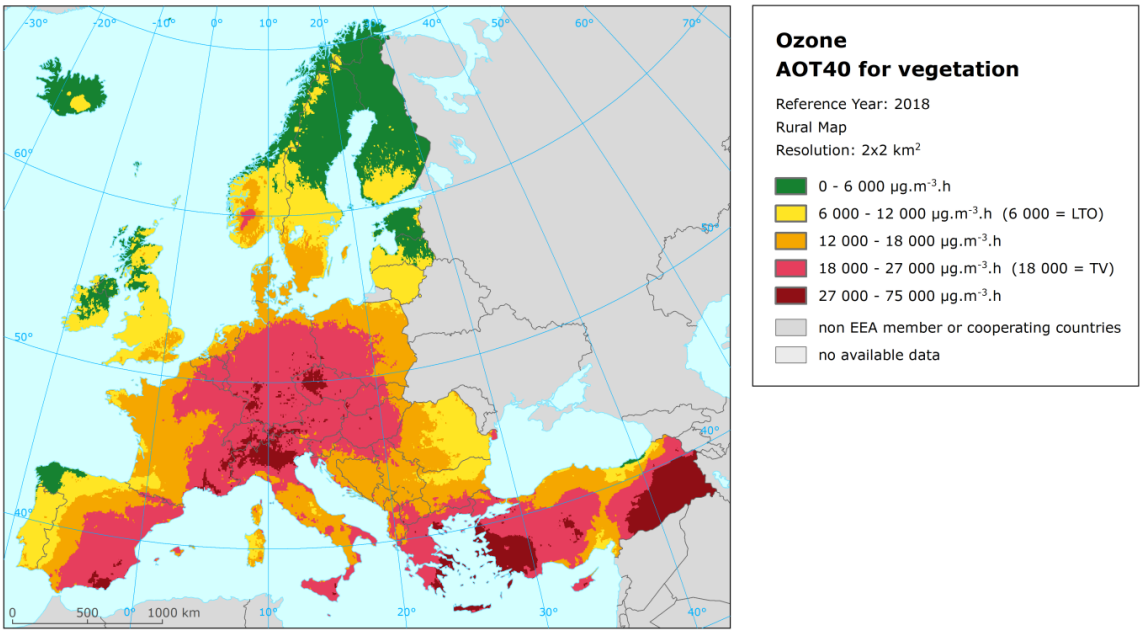

In order to provide more complete information of the air quality across Europe, the AOT40 maps including the AOT40 values based on the actual rural background measurement data at station points are presented in Maps A5.7 and A5.8 of Annex 5.

Map 4.5 Concentration map of ozone indicator AOT40 for forests, rural map, 2018

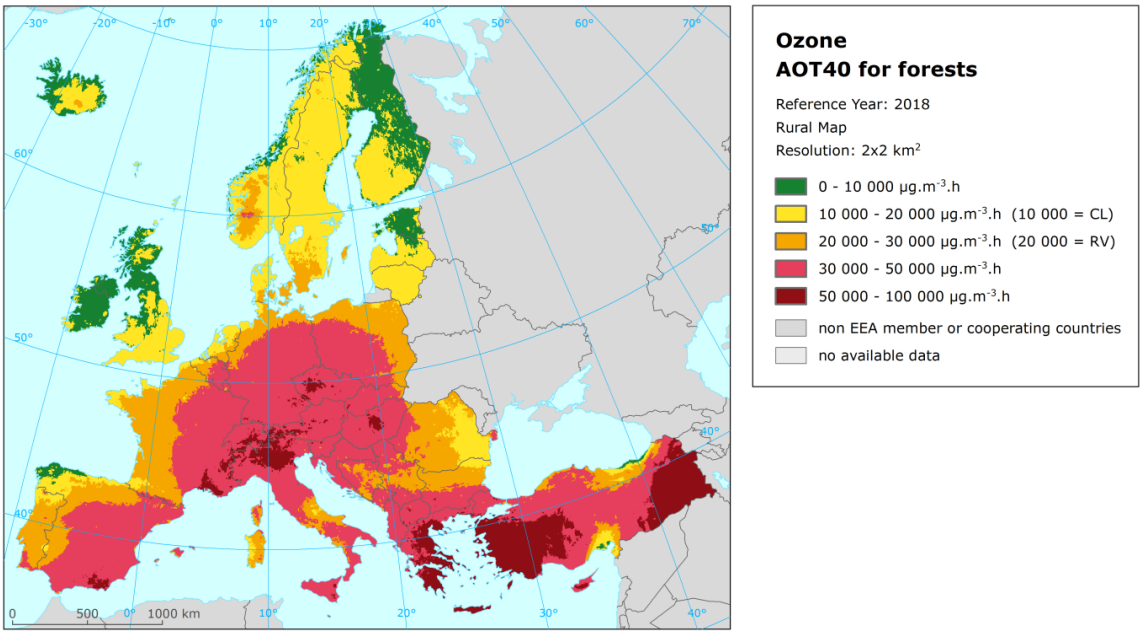

4.3.2 Vegetation exposure

Agricultural crops

The rural map with the ozone indicator AOT40 for vegetation has been combined with the land cover CLC2012 map. Following a similar procedure as described in Horálek et al. (2007), the exposure of agricultural areas (as defined above) has been calculated at the country-level.

Table 4.4 gives the absolute and relative agricultural area for each country and for four European regions where the ozone target value (TV) threshold and long-term objective (LTO) for protection of vegetation as defined in the AQ Directive (EC, 2008) are exceeded. The frequency distribution of the agricultural area over some exposure classes per country is presented as well. The table presents the country grouping of the following regions: 1) *Northern Europe*: Denmark, Estonia, Finland, Latvia, Lithuania, Norway, and Sweden, 2) *North-western Europe*: Belgium, France north of 45 degrees latitude, Ireland, Iceland, Luxembourg, the Netherlands, and United Kingdom, 3) *Central and Eastern Europe*: Austria, Bulgaria, Czechia, Germany, Hungary, Liechtenstein, Poland, Romania, Slovakia and Switzerland, and 4) *Southern Europe*: Albania, Bosnia-Herzegovina, Croatia, Cyprus, France south of 45 degrees latitude, Greece, Italy, Malta, Monaco, Montenegro, North Macedonia, Portugal, San Marino, Serbia (including Kosovo under the UN Security Council Resolution 1244/99), Slovenia, Spain and Turkey. Table 4.4 illustrates that in 2018, about 45 % of all European agricultural land has been exposed to ozone exceeding the TV of 18 000 µg·m^{-3}·h. For the areas excluding Turkey and for the EU-28, it has been about 40 %, which is the third highest percentage of the fourteen-year period 2005-2018, see Table 6.4.

Considering the LTO of 6 000 µg·m^{-3}·h, the total European area in excess has been about 96 %. For the areas excluding Turkey and for the EU-28, it has been 95 %. In 2018, values of the AOT40 for vegetation above the LTO have occurred in all countries with the exception of Iceland. On the other hand, in the most of countries there has been an area about or higher than 90 % with ozone levels being in excess of the TV. In almost half (19 from 40) and a quarter of the countries more than 50 % and 90 % of their agricultural area experienced exposures above the TV threshold in 2018, respectively.

Table 4.4 Agricultural area exposure and exceedance and agricultural-weighted concentrations, ozone indicator AOT40 for vegetation, 2018

Country	Agricultural area, 2018					Percentage of agricultural area, 2018 [%]					Agricult.-weighted conc.
	Total area	> LTO (6 000 µg·m^{-3}·h)		> TV (18 000 µg·m^{-3}·h)		< 6 000	6 000 - 12 000	12 000 - 18 000	18 000 - 27 000	> 27 000	
	[km^2]	[km^2]	[%]	[km^2]	[%]	µg·m^{-3}·h	µg·m^{-3}·h	µg·m^{-3}·h	µg·m^{-3}·h	µg·m^{-3}·h	[µg·m^{-3}·h]
Albania	8 017	8 017	100.0	4 320	53.9			46.1	53.9		18 065.7
Austria	26 827	26 827	100.0	26 585	99.1			0.9	98.2	0.9	23 228.7
Belgium	17 473	17 473	100.0	12 906	73.9		1.3	24.8	73.9		19 676.1
Bosnia-Herzegovina	17 023	17 023	100.0	674	4.0		0.1	96.0	4.0		14 696.4
Bulgaria	57 390	57 390	100.0	3 912	6.8		47.2	46.0	6.8	0.0	12 974.9
Croatia	22 168	22 168	100.0	13 232	59.7			40.3	59.5	0.1	18 229.7
Cyprus	4 291	4 291	100.0	3 915	91.2			8.8	88.3	2.9	21 728.3
Czechia	44 784	44 784	100.0	44 784	100.0				76.4	23.6	25 633.3
Denmark (incl. Faroe Is.)	31 235	31 193	99.9	117	0.4	0.1	6.6	92.9	0.4		14 030.5
Estonia	14 252	761	5.3			94.7	5.3	0.0			5 227.1
Finland	27 505	10 844	39.4			60.6	39.4				5 601.0
France (metropolitan)	323 377	323 377	100.0	103 679	32.1		6.7	61.3	31.2	0.9	16 492.2
Germany	204 463	204 463	100.0	168 623	82.5		0.3	17.3	80.3	2.2	22 105.5
Greece	50 052	50 052	100.0	49 407	98.7			1.3	73.1	25.6	24 830.7
Hungary	60 390	60 390	100.0	53 896	89.2			10.8	89.2	0.1	20 965.7
Iceland	2 518					100.0					3 049.4
Ireland	46 756	26 581	56.9			43.1	56.9				6 257.9
Italy	155 718	155 712	100.0	95 086	61.1	0.0	5.2	33.8	46.4	14.6	20 595.0
Latvia	25 532	14 619	57.3			42.7	57.3				6 320.0
Liechtenstein	37	37	100.0	37	100.0				100.0		25 831.9
Lithuania	38 155	38 138	100.0			0.0	99.9	0.0			8 632.3
Luxembourg	1 351	1 351	100.0	1 299	96.1			3.9	96.1		22 250.5
Malta	125	125	100.0	125	100.0				88.6	11.4	21 267.2
Monaco	0										
Montenegro	2 231	2 231	100.0	2 197	98.5			1.5	82.3	16.2	14 373.0
Netherlands	23 644	23 644	100.0	2 763	11.7		19.8	68.5	11.7		14 534.4
North Macedonia	9 146	9 146	100.0	4 365	47.7			52.3	47.7	0.0	17 956.2
Norway	15 637	10 717	68.5	7	0.0	31.5	62.7	5.8	0.0		7 724.4
Poland	183 268	183 268	100.0	72 880	39.8		4.2	56.0	39.7	0.0	17 258.7
Portugal (excl. Az., Mad.)	42 566	42 313	99.4	2	0.0	0.6	94.8	4.6	0.0		9 591.1
Romania	135 279	135 279	100.0	6 809	5.0		56.5	38.5	5.0		11 816.7
San Marino	42	42	100.0	42	100.0				100.0		20 596.3
Serbia (incl. Kosovo*)	46 768	46 768	100.0	13 395	28.6		1.2	70.1	28.6		16 011.0
Slovakia	23 100	23 100	100.0	17 812	77.1			22.9	76.7	0.5	20 543.4
Slovenia	6 986	6 986	100.0	6 108	87.4			12.6	87.4	0.1	19 640.6
Spain (excl. Canarias)	236 224	224 059	94.9	109 137	46.2	5.1	20.6	28.1	44.9	1.3	17 573.2
Sweden	39 035	34 958	89.6	26	0.1	10.4	50.1	39.4	0.1		11 035.4
Switzerland	11 359	11 359	100.0	11 335	99.8			0.2	93.8	5.9	23 960.6
Turkey	339 984	337 804	99.4	260 659	76.7	0.6	3.9	18.8	47.6	29.1	23 757.9
United Kingdom (& dep.)	135 760	118 156	87.0	2	0.0	13.0	72.6	14.4	0.0		9 140.4
Total	**2 430 470**	**2 325 449**	**95.7**	**1 090 133**	**44.9**	**4.3**	**19.3**	**31.5**	**38.4**	**6.5**	17 349.8
Total without Turkey	**2 090 486**	**1 987 645**	**95.1**	**829 474**	**39.7**	**4.9**	**21.9**	**33.5**	**36.9**	**2.8**	16311.3
EU-28	**1 977 169**	**1 881 807**	**95.2**	**793 103**	**40.1**	**4.8**	**22.6**	**32.5**	**37.2**	**2.9**	16 361.9
France over 45N	256 784	256 784	100.0	87 256	34.0		3.4	62.6	33.9	0.0	16 671.8
France bellow 45N	66 594	66 594	100.0	16 423	24.7		19.3	56.0	20.7	4.0	15 799.5
Kosovo	4 167	4 167	100.0	215	5.1			94.9	5.1		15 328.9
Serbia (without Kosovo*)	42 601	42 601	100.0	13 180	30.9		1.3	67.7	30.9		16 077.7
Northern	191 351	141 231	73.8	150	0.1	26.2	50.0	23.7	0.1		8931.7
North-western	484 287	443 991	91.7	104 226	21.5	8.3	28.7	41.5	21.5	0.0	13504.0
Central & eastern	746 898	746 898	100.0	406 672	54.4		15.0	30.6	52.3	2.2	18491.0
Southern	1 007 934	993 330	98.6	579 085	57.5	1.4	12.3	28.8	43.5	14.0	19930.9

(*) under the UN Security Council Resolution 1244/99

Note 1: Country not included due to the lack of land cover data: Andorra.

Note 2: The percentage value "0.0" indicates that an agricultural area exists, but it is small and estimated to be less than 0.05 %. Empty cells mean no agriculture area in exposure.

Forests

The rural map with ozone indicator AOT40 for forests was combined with the land cover CLC2012 map. Following a similar procedure as described in Horálek et al. (2007), the exposure of forest areas (as defined above) has been calculated for each country, for the same four European regions as for crops and for Europe as a whole. Table 4.5 gives the absolute and relative forest area where the Critical Level (CL) as defined in CLRTAP (2017) and the value 20 000 $\mu g \cdot m^{-3} \cdot h$ (which is equal to the earlier used Reporting Value, RV, as was defined in the repealed ozone directive 2002/3/EC) are exceeded. Next to the forest area in exceedance, the table presents the frequency distribution of the forest area over some exposure classes.

Table 4.5 Forested area exposure and exceedance and forest-weighted concentrations, ozone indicator AOT40 for forests, 2018

Country	Forested area, 2018					Percentage of forested area, 2018 [%]					Forest - weighted conc.
	Total area	> CL (10 000 µg·m^{-3}·h)		> RV (20 000 µg·m^{-3}·h)		< 10 000	10 000 - 20 000	20 000 - 30 000	30 000 - 50 000	> 50 000	
	[km^2]	[km^2]	[%]	[km^2]	[%]	µg·m^{-3}·h	µg·m^{-3}·h	µg·m^{-3}·h	µg·m^{-3}·h	µg·m^{-3}·h	[µg·m^{-3}·h]
Albania	7 104	7 104	100.0	7 104	100.0			0.0	99.7	0.3	41 304.9
Austria	36 667	36 667	100.0	36 667	100.0			0.1	96.0	3.9	42 710.9
Belgium	6 085	6 045	99.3			0.7	99.3				32 648.5
Bosnia-Herzegovina	23 911	23 911	100.0	23 911	100.0			46.6	53.4		30 406.1
Bulgaria	34 675	34 675	100.0	33 196	95.7		4.3	41.4	54.4	0.0	31 769.1
Croatia	19 734	19 734	100.0	19 734	100.0			1.9	98.1	0.0	35 895.8
Cyprus	1 458	1 458	100.0	1 458	100.0			2.0	35.7	62.4	50 035.9
Czech Republic	25 867	25 867	100.0	25 867	100.0				84.6	15.4	47 430.1
Denmark (incl. Faroe Is.)	3 747	3 747	100.0	1 527	40.8		59.2	40.7	0.0		19 729.1
Estonia	21 080	4 038	19.2			80.8	19.2				9 597.1
Finland	211 668	82 417	38.9			61.1	38.9				9 886.7
France (metropolitan)	143 376	143 376	100.0	140 009	97.7		2.3	32.7	62.3	2.7	33 417.8
Germany	108 031	108 031	100.0	107 770	99.8		0.2	7.7	90.7	1.3	40 839.9
Greece	26 122	26 122	100.0	26 122	100.0				48.6	51.4	51 402.4
Hungary	17 407	17 407	100.0	17 407	100.0			0.7	91.4	7.9	42 978.5
Iceland	537	50	9.3			90.7	9.3				7 192.6
Ireland	4 510	662	14.7			85.3	14.7				8 498.6
Italy	79 052	79 052	100.0	77 933	98.6		1.4	16.1	69.3	13.2	38 222.6
Latvia	24 261	21 085	86.9	2	0.0	13.1	86.9	0.0			11 307.4
Liechtenstein	79	79	100.0	79	100.0				89.5	10.5	47 001.6
Lithuania	19 455	19 455	100.0	192	1.0		99.0	1.0			15 381.9
Luxembourg	937	937	100.0	937	100.0			9.3	90.7		35 173.1
Malta	2	2	100.0	2	100.0				86.9	13.1	46 970.6
Monaco	1	1	100.0	1	100.0				100.0		42 321.2
Montenegro	5 777	5 777	100.0	5 777	100.0			13.2	86.8		33 269.2
Netherlands	3 118	3 114	99.9	1 959	62.8	0.1	37.0	59.7	3.1		21 644.6
North Macedonia	8 144	8 144	100.0	8 144	100.0			0.0	97.1	2.9	43 135.7
Norway	103 494	78 112	75.5	6 861	6.6	24.5	68.8	6.6	0.0		13 255.7
Poland	96 966	96 966	100.0	96 168	99.2		0.8	46.6	52.6		31 543.8
Portugal (excl. Az., Mad.)	16 512	16 512	100.0	14 701	89.0		11.0	79.4	9.6		23 837.9
Romania	71 273	71 273	100.0	56 613	79.4		20.6	69.3	10.2		24 042.3
San Marino	6	6	100.0	6	100.0				100.0		40 144.3
Serbia (incl. Kosovo)	27 120	27 120	100.0	27 120	100.0			5.5	94.5	0.0	31 060.3
Slovakia	20 484	20 484	100.0	20 484	100.0			9.8	88.8	1.3	39 112.2
Slovenia	11 441	11 441	100.0	11 441	100.0			0.3	98.9	0.8	39 654.9
Spain (excl. Canarias)	107 927	100 844	93.4	86 452	80.1	6.6	13.3	18.6	60.4	1.1	30 411.7
Sweden	261 757	248 876	95.1	20 223	7.7	4.9	87.4	7.7	0.0		13 986.5
Switzerland	11 850	11 850	100.0	11 850	100.0				89.5	10.5	45 472.0
Turkey	114 886	113 838	99.1	106 418	92.6	0.9	6.5	16.3	43.4	33.0	41 955.4
United Kingdom (& dep.)	20 247	8 838	43.7	5	0.0	56.3	43.6	0.0			10 323.7
Total	**1 696 767**	**1 485 119**	**87.5**	**994 141**	**58.6**	**12.5**	**28.9**	**16.2**	**37.8**	**4.6**	**26 516.5**
Total without Turkey	**1 581 881**	**1 371 281**	**86.7**	**887 723**	**56.1**	**13.3**	**30.6**	**16.2**	**37.4**	**2.5**	**25 396.5**
EU-28	**1 393 819**	**1 209 120**	**86.7**	**796 866**	**57.2**	**13.3**	**29.6**	**17.0**	**37.4**	**2.7**	**25 719.2**
France over 45N	90 007	90 007	100.0	88 348	98.2		1.8	28.6	69.1	0.5	32 838.4
France bellow 45N	53 369	53 369	100.0	51 660	96.8		3.2	39.6	50.8	6.4	34 395.1
Kosovo	4 316	4 316	100.0	4 316	100.0			1.3	98.7	0.0	35 937.7
Serbia (without Kosovo)	22 804	22 804	100.0	22 804	100.0			6.3	93.7		30 141.1
Northern	645 460	457 730	70.9	28 806	4.5	29.1	66.5	4.5	0.0		12356.2
North-western	125 440	109 654	87.4	91 249	72.7	12.6	14.7	22.1	50.3	0.3	27950.1
Central & eastern	423 300	423 300	100.0	406 102	95.9		4.1	28.2	65.4	2.3	35839.0
Southern	502 566	494 435	98.4	467 984	93.1	1.6	5.3	19.8	59.9	13.4	36459.1

(*) under the UN Security Council Resolution 1244/99

Note 1: Country not included due to the lack of land cover data: Andorra.

Note 2: The percentage value "0.0" indicates that a forested area exists, but it is small and estimated to be less than 0.05 %. Empty cells mean: no forested area in exposure.

The Critical Level was exceeded in 2018 at about 88 % of all European forested area. For the area excluding Turkey and for the EU-28 it was exceeded at about 87 %, which is the second highest exceedance observed for the fourteen-year period 2005-2018 (Table 6.4). As in previous years, most countries continue to have in 2018 considerable forest areas in excess to the CL, with specifically almost all forest area in southern and central, eastern and western European countries. In 2018, areas in excess to the CL occurred also in Northern Europe with the exception of parts of Iceland, United Kingdom, Ireland, Finland, Norway, Sweden, Latvia and Estonia.

In this context, it should be mentioned that the AOT40 indicator is probably not the best proxy for vegetation damage assessment. AOT40 does not take into account plant physiological control of ozone absorbed doses, which is taken into account in the POD (i.e. Phytotoxic Ozone Dose) indicators, as discussed in Section 4.4 for main crops. POD indicators are known to be more related with ozone effects on plant growth than ambient air ozone concentrations alone. The AOT40 does not take into account either the influence of meteorological conditions on growing season timing. Growing season start and end dates can change across Europe, and between years for a given site, depending on factors such as air temperature, solar radiation, photoperiod or rainfall. High temperature and dry weather favouring ozone pollution cause a reduction of ozone absorbed doses by plants due to plant physiological response to drought (i.e., the vegetation closes its stomata protecting itself from the exposure to ozone). However, plants may still be sensitive to ozone in such weather conditions, as illustrated by foliar injury records in Aleppo pine stands growing in southern France UNECE (2016) or controlled experimental results (e.g. Alonso et al., 2014).

4.4 Ozone – Phytotoxic Ozone Dose (POD)

Ozone is generally recognized to be the most relevant pollutant for plants. Visible injury, reduction in growth, changes in biomass partitioning, or a higher susceptibility to pathogen attack can be the effect of ozone influence (Krupa et al., 2000). Scientific evidence suggests that observed effects of ozone on vegetation are more strongly related to the uptake of ozone through the stomatal leaf pores (stomatal flux) than to the concentration in the atmosphere around the plants (Mills et al., 2011). It is generally accepted that the most severe ozone effects on plants are caused by ozone that is taken up through the stomata into the leaf interior (Reich, 1987; Ashmore et al., 2004).

Ozone flux through the stomata of leaves found at the top of the canopy has been calculated using a multiplicative algorithm based on the methodology described by CLRTAP (2017) according to Emberson et al. (2000) based on Jarvis (1976).

The cumulative stomatal ozone fluxes (F_{sto}) are calculated over the course of the growing season based on ambient ozone concentration and stomatal conductance (g_{sto}) to ozone. The stomatal conductance has been calculated using a multiplicative stomatal conductance model (Emberson et al., 2000) based on Jarvis (1976) as a function of species-specific maximum g_{sto} (expressed on a single leaf-area basis), phenology, and prevailing environmental conditions (photosynthetic photon flux density, PPFD), air temperature, vapour pressure deficit (VPD), and soil moisture.

POD_Y (Phytotoxic Ozone Dose) is the accumulated plant uptake (flux) of ozone above a threshold of Y during a specified time or growth period. The flux-based POD_Y metrics are preferred in risk assessment over the concentration-based AOT40 exposure index. AOT40 accounts for the atmospheric ozone concentration above the leaf surface and is therefore biologically less relevant for ozone impact assessment than POD_Y as it does not take into account how ozone uptake is affected by climate, soil and plant factors.

Several POD_Y indicators are described in CLRTAP (2017). POD_YSPEC is a species or group of species-specific POD_Y that requires comprehensive input data and is suitable for detailed risk assessment.

POD_YIAM is a vegetation-type specific POD_Y that requires less input data and is suitable for large-scale modelling, including integrated assessment modelling. POD_YSPEC is further used in this report.

For the wheat as for other crop species including potato and tomato, the Y value is taken equal to 6 nmol m^{-2} PLA s^{-1} (i.e. per unit projected leaf area). For the details of POD_Y (and specifically POD_6SPEC as used in this report) calculation, see Annex 1, Section A1.3.

The species-specific flux models and associated response functions and critical levels for ozone-sensitive crops and cultivars can be used to quantify the potential negative impacts of O_3 on the security of food supplies at the local and regional scale. They can be used to estimate yield losses, including economic losses. A flux-threshold Y of 6 (POD_6SPEC) provides the strongest flux-effect relationships for crops (Pleijel et al., 2007). O_3 effects proved to be significant at a 5% reduction of the effect parameter (Mills et al., 2011), hence Critical Levels (CL) were determined for this 5% reduction of the effect parameter (i.e. yield, weight or quality of grain, tuber or fruit), based on the slope of the relationship. The POD_6SPEC Critical Levels (CL) for crops were determined based on this reduction of relevant yield or weight, as shown in Table 4.5.

Table 4.6 POD6SPEC Critical Levels for crops as determined by CLRTAP

Crop	Effect parameter	POD_6SPEC Critical Level
Wheat	grain yield	1.3 mmol.m^{-2} PLA
Wheat	1000-grain weight	1.5 mmol.m^{-2} PLA
Wheat	protein yield	2.0 mmol.m^{-2} PLA
Potato	tuber yield	3.8 mmol.m^{-2} PLA
Tomato	fruit yield	2 mmol.m^{-2} PLA
Tomato	fruit quality	3.8 mmol.m^{-2} PLA

Source: CLRTAP, 2017

Wheat, potato and tomato are considered as representative species of crops in Europe (tomato can be regarded as representative horticultural crop for the Mediterranean and Black Sea regions, while potato for other regions). Therefore, POD_6SPEC for these crops (labelled further simply as POD_6 for wheat, potato and tomato, respectively) are recommended for regular map construction. This report presents maps of POD_6 for wheat and potato. (We limit wheat to the bread wheat.) In near future, we intend to include the POD_6 for tomato in the mapped indicators.

4.4.1 Phytotoxic Ozone Dose maps

The POD maps have been calculated based on the hourly ozone maps, together with the meteorological and soil hydraulic properties data, based on the methodology described in Annex 1, Section A1.3. The calculation has been executed in 0.1° x 0.1° resolution. The hourly ozone maps are created for rural areas only, based on rural background stations. The POD maps are therefore applicable to rural areas only. Next to this, it should be noted that in the POD calculations, all growing areas are considered rain-fed (i.e. without irrigation), see Colette et al. (2018). Thus, the maps are directly applicable only for areas without irrigation. If applied for irrigated areas, the POD values might be somewhat underestimated.

The hourly ozone maps needed for POD calculation have been calculated at the 2x2 km^2 resolution, based on rural background measurements. The maps for each hour of the year 2018 have been

constructed using the same methodology like the annual maps, i.e. the multiple linear regression followed by the kriging of its residuals (see Annex 1, Section A1.1) based on the measurement data, EMEP model output, altitude and the surface solar radiation. For details, see Annex 3, Section A3.3.

Map 4.6 presents the final map of Phytotoxic Ozone Dose (POD_6) for wheat in 2018. The areas in the map with POD_6 values above the Critical Level (CL) for protein yield of wheat (i.e. 2 $mmol.m^{-2}$ PLA) are marked in orange, red and dark red. The areas with POD_6 values below the CL for grain yield of wheat (i.e. 1.3 $mmol.m^{-2}$ PLA) are marked in green and dark green. The areas with POD_6 values in between CLs for grain yield and grain weight and in between CLs for grain weight and protein yield are marked in yellow and dark yellow, respectively. All these CLs were exceeded in large areas of central, western and southern Europe.

The highest levels of the POD_6 for wheat in 2018 are found in the south-western, western, southern and south-eastern European region. Nevertheless, high values of the POD_6 for wheat can be found even in other European areas (e.g. central Europe, namely Czechia and Hungary) since the POD_6 is dependent not only on ozone levels but also on the environmental conditions. On the other hand, the lowest levels of the POD_6 for wheat generally occur in areas with lower ozone concentrations (e.g. northern European regions) and/or where environmental conditions limit the ozone stomatal conductance (dry and warm areas, including parts of the southern, south-western and south-eastern Europe). Low values of POD_6 for wheat in some areas in the south of Europe (i.e. with high ozone values, but limited ozone stomatal conductance) are in agreement with findings of Colette et al. (2018).

Map 4.6 Phytotoxic Ozone Dose (POD_6) rural map for wheat, 2018

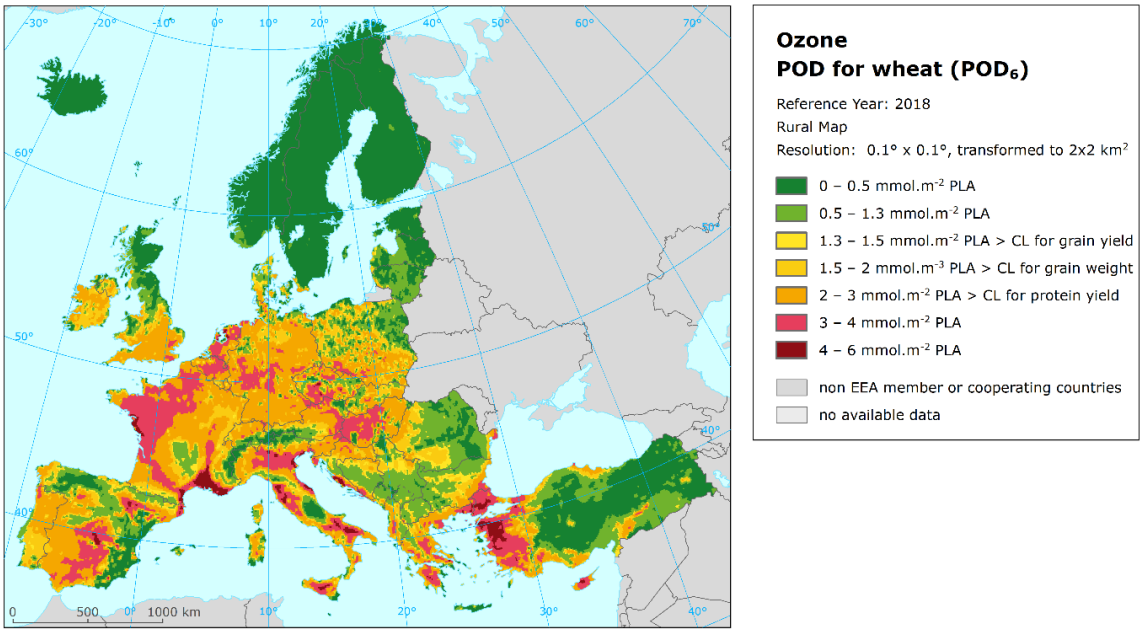

Map 4.7 presents the final map of Phytotoxic Ozone Dose (POD_6) for potato in 2018. The areas with POD_6 values above the Critical Level (CL) for tuber yield of potato (i.e. 3.8 $mmol.m^{-2}$ PLA) are marked in yellow, dark yellow, orange, red and dark red. The most of Europe showed values of POD_6 for potato above this CL in 2018. The highest POD_6 levels are found in the central European region and in Denmark. Nevertheless, smaller areas with high POD_6 values are also located in the south-western,

western, southern and south-eastern European region. On the other hand, the lowest levels of the POD_6 for potato in 2018 are found in northern, southern, south-western and south-eastern European regions.

Map 4.7 Phytotoxic Ozone Dose (POD_6) rural map for potato, 2018

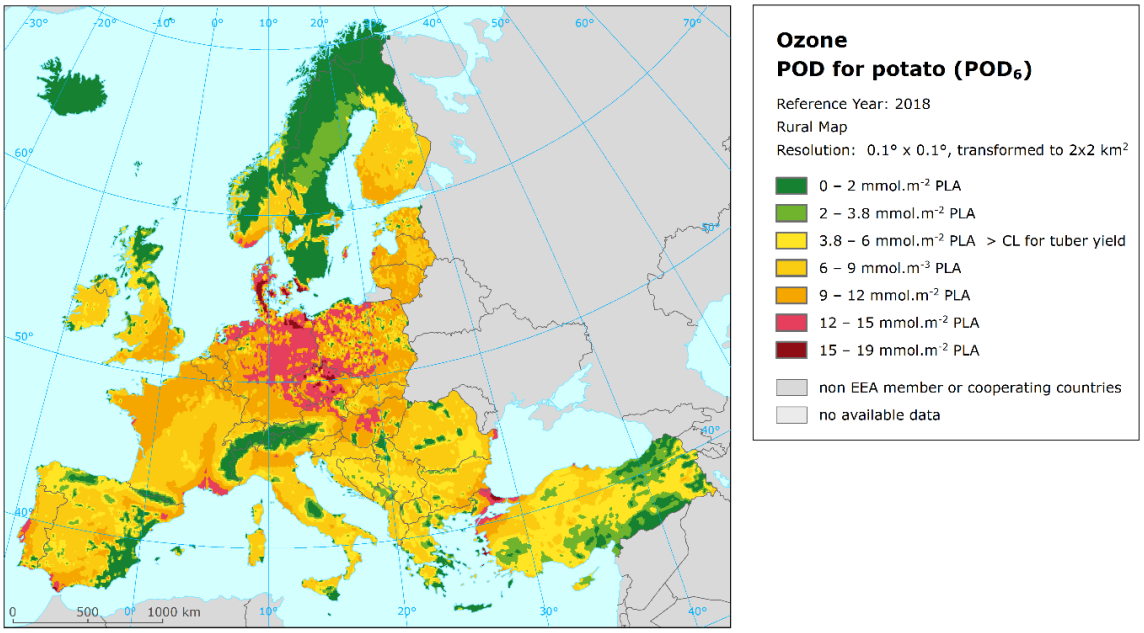

5 NO_2 and NO_x

Annual average maps for NO_2 (related to protection of human health) and for NO_x (related to protection of vegetation) have been produced and presented in the regular mapping report since the maps for year 2014.

The methodology for creating the concentration maps follows the same principle as for the rest of pollutants: a linear regression model on the basis of European wide station measurement data, followed by kriging of the residuals produced from that regression model (residual kriging).

The map on NO_2 is based on an improved mapping methodology developed in Horálek et al. (2017b, 2018). The map layers are created for the rural, urban background and urban traffic areas separately on a grid at 1x1 km^2 resolution. Subsequently, the urban background and urban traffic map layers are merged using the gridded road data into one urban map layer. This urban map layer is further combined with the rural map layer into the final NO_2 map using a population density grid at 1x1 km^2 resolution. We present this final combined map in this 1x1 km^2 grid resolution.

The map of the vegetation-related indicator NO_x annual average is created on a grid at 2x2 km^2 resolution, based on rural background measurements only, as vegetation is considered not to be extensively present at urban and suburban areas. Hence, this map is applicable to rural areas only. The resolution is chosen equally to the one of the vegetation indicator for ozone.

Annex 3 provides details on the regression and kriging parameters applied for deriving the maps, as well as the uncertainty analysis of the maps.

5.1 NO_2 – Annual mean

5.1.1 Concentration maps

The AQ Directive (EC, 2008) sets two limit values (LV) for NO_2 for the human health protection. The first one is an annual LV (ALV) at the level of 40 $\mu g \cdot m^{-3}$. This is the same concentration level as recommended by the World Health Organization for the NO_2 annual average as the Air Quality Guideline (WHO, 2005). The second one is an hourly LV (HLV, 200 $\mu g \cdot m^{-3}$ not to be exceeded on more than 18 hours per year). The HLV has been exceeded in 2018 at only 0.5 % of all the reporting stations, mostly at urban stations, in five countries, with only Turkey presenting more than two exceeding stations in (EEA, 2020b). In view of this low number of exceedances, the short-term LV has not been included in the mapping procedures.

Map 5.1 presents the final combined concentration 1x1 km^2 gridded map for the 2018 NO_2 annual average as the result of interpolation and merging of the separate maps as described in Annex 1.

Supplementary data used in the linear regression are in principle the same as described in Horálek et al. (2017b). For rural areas they consist of EMEP model output, altitude, OMI satellite data, wind speed, population density and land cover indicators; for urban background areas these are EMEP model output, altitude, OMI satellite data, wind speed, population density and land cover indicators; for traffic areas the EMEP model output, altitude, and OMI satellite data are used (Annex 3).

According to Map 5.1, the areas where the ALV of 40 $\mu g \cdot m^{-3}$ was exceeded include urbanized parts of some large cities, particularly Milan, Naples, Rome, Turin, Paris, Barcelona, Madrid, London, Athens, Ankara, Istanbul, and some other smaller cities in Turkey. Some other cities show NO_2 levels above 30 $\mu g \cdot m^{-3}$, e.g. in Germany, Italy, the Netherlands, Belgium, United Kingdom, Turkey. Most of the European area shows NO_2 levels below 20 $\mu g \cdot m^{-3}$, with most of the rural areas below 10 $\mu g \cdot m^{-3}$. Some larger areas above 20 $\mu g \cdot m^{-3}$ can be found in the Po Valley, the Benelux, the German Ruhr region, in central and southern England, in the Île de France region and around Rome.

It should be noted that the interpolated map is created at 1x1 km^2 only and as such refers to the rural and urban *background* situations only, while the exceedances of the NO_2 limit values occur mostly at local *hotspots* such as dense traffic locations and densely urbanised and industrialised areas. Although the urban traffic map layer is used in the map creation, the traffic locations are smoothed in the 1x1 km^2 resolution. The relative mean uncertainty of the NO_2 annual average map is 29 % for rural and 26 % for urban background areas (Annex 3).

In order to provide more complete information of the air quality across Europe, the final combined map including the measurement data at station points is presented in Map A5.9 of Annex 5.

Map 5.1 Concentration map of NO_2 annual average, 2018

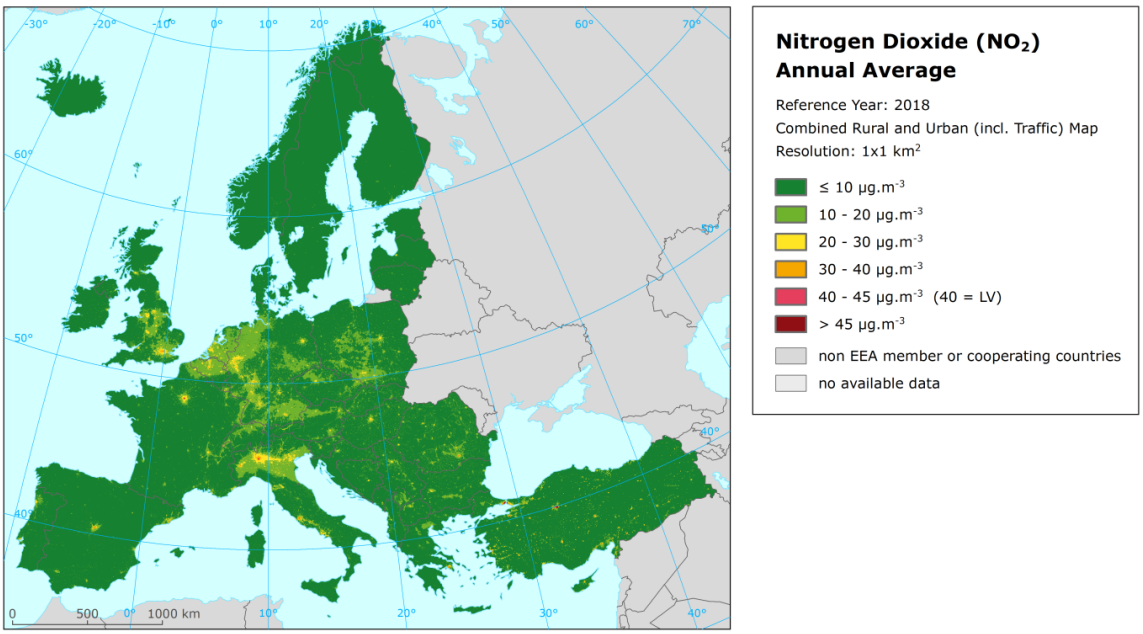

5.1.2 Population exposure

Table 5.1 gives the population frequency distribution for a limited number of exposure classes calculated on a grid of 1x1 km^2 resolution, as well as the population-weighted concentration for individual countries and for Europe as a whole according to Equation A1.7 of Annex 1.

The human exposure to NO_2 has been calculated based on the improved methodology as developed in Horálek et al. (2017b). The population exposure has been calculated according to Equation A1.6 of Annex 1, i.e. it has been calculated separately for urban areas directly influenced by traffic and for the background (both rural and urban) areas, in order to better reflect the population exposed to traffic. Based on this, the different concentration levels in urban background and traffic areas inside the 1x1 km^2 grid cells are taken into account.

Table 5.1 Population exposure and population-weighted concentration, NO_2 annual average 2018

Country	ISO	Population [inhbs·1000]	NO_2 – annual average, exposed population, 2018 [%]						NO_2 ann. avg.
			< 10	10 - 20	20 - 30	30 - 40	40 - 45	> 45	Pop. weighted
Albania	AL	2 870	24.4	53.9	20.1	1.6			14.7
Andorra	AD	75	1.8	67.5	30.7				18.1
Austria	AT	8 822	14.2	52.3	27.8	4.3	1.1	0.3	17.7
Belgium	BE	11 399	2.6	54.3	33.8	8.7	0.7		20.4
Bosnia & Herzegovina	BA	3 500	29.2	57.4	13.0	0.4			13.9
Bulgaria	BG	7 050	10.5	49.1	36.9	3.4			19.0
Croatia	HR	4 105	30.0	55.7	13.2	1.1			13.8
Cyprus	CY	1 226	12.2	9.3	69.9	4.1	4.5		23.5
Czechia	CZ	10 610	14.3	68.2	15.8	1.7	0.0		15.5
Denmark (incl. Faroe Islands)	DK	5 781	51.3	44.5	3.8	0.3			9.8
Estonia	EE	1 319	69.6	30.4					7.1
Finland	FI	5 513	61.6	35.7	2.7				8.6
France (metropolitan)	FR	64 738	31.4	42.9	17.1	4.8	2.2	1.6	15.9
Germany	DE	82 792	6.0	55.4	32.0	4.8	1.2	0.7	19.1
Greece	GR	10 741	17.0	38.0	22.2	17.2	3.0	2.6	21.0
Hungary	HU	9 778	11.6	65.2	19.2	3.5	0.4		17.0
Iceland	IS	348	34.5	59.6	5.9				10.4
Ireland	IE	4 830	48.3	41.0	9.0	1.7			11.0
Italy	IT	60 484	11.6	40.9	35.0	9.7	1.8	0.9	20.1
Latvia	LV	1 934	44.9	35.7	19.4				11.9
Liechtenstein	LI	38	1.3	97.4	0.2	1.1			16.5
Lithuania	LT	2 809	34.2	60.3	4.4	1.1			12.3
Luxembourg	LU	602	6.8	47.6	34.6	8.5	2.4		20.2
Malta	MT	476	52.0	38.4	9.6				10.4
Monaco	MC	38		3.4	75.1	21.5			25.0
Montenegro	ME	622	22.6	59.7	17.8				15.0
Netherlands	NL	17 181	1.9	45.0	50.5	2.6			20.4
North Macedonia	MK	2 075	3.0	59.6	34.8	2.6			19.0
Norway	NO	5 296	54.3	36.7	7.7	1.2			10.0
Poland	PL	37 977	20.6	56.5	21.3	1.1	0.4	0.1	15.6
Portugal (excl. Az., Mad.)	PT	9 793	26.5	49.0	19.2	4.2	0.9	0.3	15.4
Romania	RO	19 531	11.4	50.8	26.8	9.2	0.7	1.0	19.3
San Marino	SM	34	6.1	89.3	3.5	1.0			14.4
Serbia	RS	8 800	12.0	60.2	26.5	1.3	0.0		17.2
Slovakia	SK	5 443	13.3	77.3	8.5	0.9			14.8
Slovenia	SI	2 067	28.5	53.4	18.0	0.2			14.5
Spain (excl. Canarias)	ES	44 481	13.4	46.1	26.2	10.9	2.7	0.7	19.4
Sweden	SE	10 120	64.4	33.2	2.0	0.4			8.7
Switzerland	CH	8 484	5.8	71.4	17.5	5.1	0.3		17.6
Turkey	TR	80 811	24.2	9.8	26.2	21.6	6.6	11.6	25.9

Country	ISO	Population [inhbs·1000]	NO_2 – annual average, exposed population, 2018 [%]						NO_2 ann. avg.
			< 10	10 - 20	20 - 30	30 - 40	40 - 45	> 45	Pop. weighted
United Kingdom (& Cr. dep.)	UK	66 525	9.3	53.1	30.5	5.5	0.7	0.9	18.8
Total		**621 122**	**17.8**	**45.2**			**1.8**	**2.0**	
				63.0	**25.8**	**7.4**		**3.8**	**19.2**
Total without Turkey		**540 312**	**17.0**	**49.9**			**1.1**	**0.7**	
				66.9	**25.8**	**5.5**		**1.8**	**17.6**
EU-28		**507 878**	**16.7**	**49.4**			**1.2**	**0.7**	
				66.2	**26.2**	**5.7**		**1.9**	**17.8**
Kosovo*	KS	1 799	8.7	64.2	27.1				17.0
Serbia (excl. Kosovo*)	RS	7 001	12.8	59.2	26.4	1.6	0.0		17.3

(*) under the UN Security Council Resolution 1244/99

Note: The percentage value "0.0" indicates that an exposed population exists, but it is small and estimated to be less than 0.05 %. Empty cells mean no population in exposure.

Thus – like for PM_{10} and $PM_{2.5}$ – the population exposure refers not only to the rural and urban *background* areas, but to the urban *traffic* locations as well. However, it should be mentioned that only population density data at 1x1 km^2 resolution has been used. This means that contrary to the concentration levels, the population density is constant within each 1x1 km^2 grid cell. This shortcoming can increase the uncertainty of the population exposure results.

It has been estimated that in 2018 about 4 % of the European population and about 2 % of both the total European population without Turkey and the EU-28 population lived in areas with NO_2 annual average concentrations above the EU limit value of 40 $\mu g \cdot m^{-3}$. CSI004 (EEA, 2020c) also estimates that around 4 % of the population in urban agglomerations in the EU-28 was exposed in 2018 to levels above the EU limit value.

The European-wide and EU-28 only population-weighted concentration of the NO_2 annual average for 2018 has been estimated to be about 19 $\mu g \cdot m^{-3}$ and 18 $\mu g \cdot m^{-3}$, respectively, being this last value the same also for the total European population without Turkey.

Figure 5.1 shows, for the whole mapped area, the population frequency distribution for exposure classes of 1 $\mu g \cdot m^{-3}$. The frequency distribution is centred around 17-18 $\mu g \cdot m^{-3}$.

Figure 5.1 Population frequency distribution, NO_2 annual average, 2018

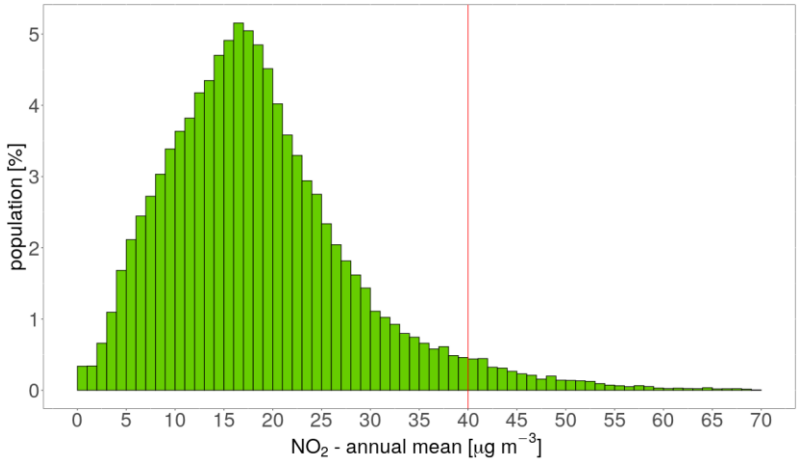

5.2 NO_x – Annual mean

5.2.1 Concentration maps

The AQ Directive (EC, 2008) sets a Critical Level (CL) for the protection of vegetation for the NO_x annual mean at 30 µg·m^{-3}. According to this directive, the sampling points targeted at the protection of vegetation and natural ecosystems shall be in general sited more than 20 km away from agglomerations or more than 5 km away from other built-up areas. Thus, only the observations at rural background stations are used for the NO_x mapping and the resulting map is representative for rural areas only.

The number of NO_x measurement stations is limited. The mapping of the NO_x annual average has been therefore performed on the basis of an approach presented in Horálek et al. (2007). This approach derives additional *pseudo* NO_x annual mean concentrations from NO_2 annual mean measurement concentrations and increases as such the number and spatial coverage of NO_x 'data points', and applies these data to the NO_x mapping. Section A1.1 of Annex 1 provides some details.

Map 5.2 presents the concentration map of NO_x annual average. It concerns rural areas only, representing an indicator for vegetation exposure to NO_x. The relative mean uncertainty of this rural map is 41 %.

Most of the European area shows NO_x levels below 20 µg·m^{-3}. However, in the Po Valley, southern part of the Netherlands, northern Belgium, the German Ruhr region and around some larger European cities (typically being the national capitals) elevated NO_x concentrations above the Critical Level (CL) are observed. Furthermore, around many larger European cities concentrations just below the CL are observed. These concentrations are expected to be the result of large emissions from transport in and around the cities, as well as energy production and industrial facilities taking place at these areas. However, this is relevant only if there is vegetation around those larger cities. On the contrary, low concentrations (below 10 µg·m^{-3}) are observed in large areas of Spain, France, Italy, the Balkan area, Turkey, Scandinavia, Iceland, Ireland and the Baltic States.

The NO_x annual average rural map including the data measured at rural background stations is presented in Map A5.10 of Annex 5. The map illustrates the lack of the NO_x rural stations in the Balkan area.

Map 5.2 Concentration map of NO_x annual average, rural map, 2018

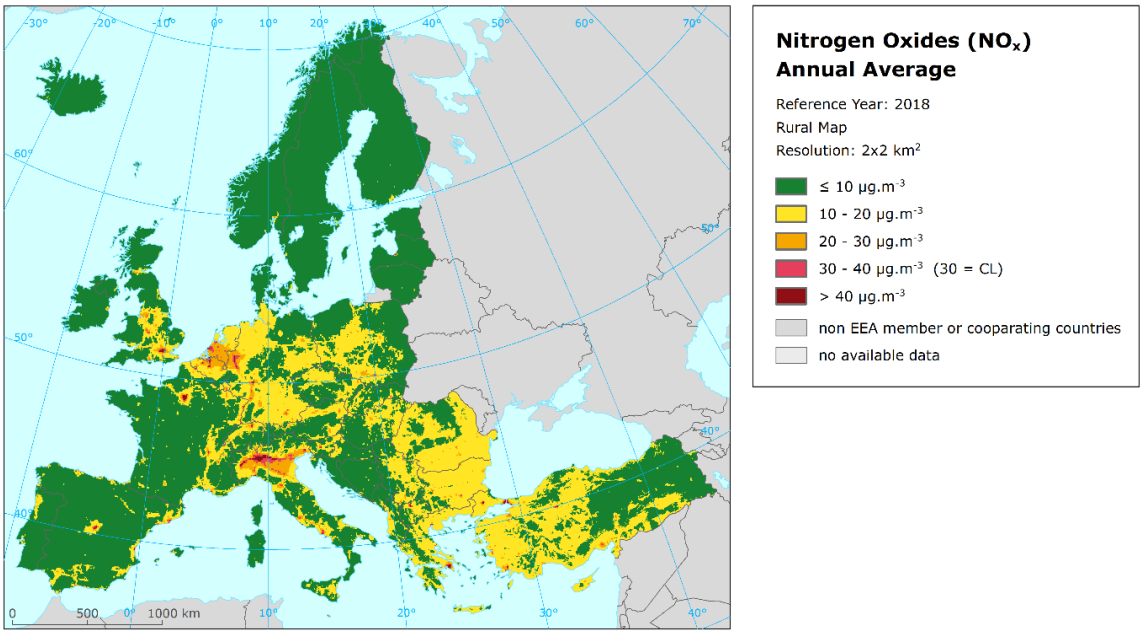

Vegetation exposure has not been calculated for NO_x, as the Critical Level (CL) applies actually to vegetation only, which is by nature mostly allocated in rural areas where there has been limited CL exceedance observed. Therefore, the vegetation exposure exceedance would occur in limited vegetation areas only and, as such, is considered not to provide essential information from the European scale perspective. Furthermore, contrary to vegetation exposure to high ozone concentrations in Europe that leads to considerable damage, vegetation exposure to NO_x pollution is of minor importance in terms of actual impacts. On the other hand, NO_x concentrations contribute in part to the total N-deposition, which leads to acidifying and eutrophying effects on vegetation. These effects, especially eutrophication, are still very important in Europe (e.g. EMEP, 2019). However, these effects on vegetation cannot be easily expressed by an exposure NO_x table.

Concerning the potential exposure estimate of vegetation and natural ecosystems to NO_x there is an additional dilemma: which receptor types should be selected to estimate the exposure and Critical Level exceedance of vegetation and natural ecosystems? An option would be the use of CLC classes (e.g. like in Horálek et al., 2008); nevertheless this classification is too general. Another option would be the NATURA 2000 database. However, that data source contains a wide series of receptor types, species and classes. Serious additional efforts would be needed to conclude on the most relevant set of receptors from the NATURA 2000 geographical database.

6 Exposure trend estimates

This report has presented the interpolated maps for 2018 on the PM_{10}, $PM_{2.5}$, ozone and NO_2 *human health* related air pollution indicators (annual average and the 90.4 percentile of PM_{10} daily means, annual average for $PM_{2.5}$, the 93.2 percentile of maximum daily 8-hour means, SOMO35 and SOMO10 for ozone, and the annual average for NO_2), together with tables showing the frequency distribution of the estimated population exposures and exceedances per country and as European totals.

Furthermore, interpolated maps of ozone and NO_x *vegetation* related air pollution indicators have been produced. More specifically, these include a map of the ozone indicator AOT40 for vegetation and AOT40 for forests, and tables with the frequency distribution of estimated land area exposures and exceedances per country and the European totals. In addition, the maps of the Phytotoxic Ozone Dose (POD) for wheat and potato and the NO_x annual average map have been produced, but without exposure estimates.

A mapping approach similar to previous years (Horálek et al., 2020a and references therein) based primarily on observational data has been used. With the interpolated air pollution maps and exposure estimates for the year 2018 completed, a fourteen-year overview of comparable exposure estimates has been obtained (with full time series coverage for PM_{10} and ozone, except SOMO10 and POD indicators, with one year missing for $PM_{2.5}$ and with four years missing for NO_2). In this chapter we provide these multi-annual overviews of exposure estimates for each of the indicators of PM_{10}, $PM_{2.5}$ and ozone (except SOMO10 and POD), including a trend analysis.

For the previous years, mapping results as presented in Horálek et al. (2020a) and previous mapping reports have been used, with additions and changes as follows. The merge of the rural and urban layers has been re-calculated using the Geostat population data (see Annex 2) for years 2005-2012, in which the JRC population data was originally used. For PM_{10}, $PM_{2.5}$ and NO_2 annual averages and for ozone indicator SOMO35, mapping results for 2005 and 2009 as presented in Horálek et al. (2020b) have been used. Next to this, PM_{10} and $PM_{2.5}$ results for 2015-2018 (and partly also for 2005 and 2009) are presented in two variants, i.e. based on the old and the updated (i.e. based on Horálek et al., 2019) methodologies, for comparability reasons.

For the human health indicators, we express the exposure estimates, on one hand, as population-weighted concentration and, on the other hand, as percentage of population exposed to concentrations above the limit/target value. For the vegetation related indicators, the exposure estimates are expressed as the agricultural- and forest-weighted concentrations, as well as the agricultural or forest areas exposed to concentrations above defined thresholds.

It should be noted that the percentage of population, agricultural area, or forest area exposed is a less robust indicator compared to the population-weighted, agricultural-weighted, or forest-weighted concentration, as a small concentration increase (or decrease) may lead to a major increase (or decrease) of population, agricultural or forest area exposed. This is not the case when taking the population-weighted or agricultural/forest-weighted concentration as indicator. Therefore, the trend analysis is done based on the population-weighted, agricultural-weighted and forest-weighted concentrations only.

When thinking about a trend, we should take into account (i) the meteorologically induced variations, (ii) the uncertainties involved in the interpolation (Annex 3), and (iii) the year to year variation of the station density and their spatial distribution, which induce a variation in interpolated maps from year to year. In addition, we should be aware of the fact that different trends in various parts of Europe may occur. However, bearing in mind these limitations we provide here a trend analysis for the period 2005-2018 on the population-, agricultural- and forest-weighted concentrations for Europe as a whole.

For comparability reasons, we present in this chapter the results for Europe as a whole without Turkey, because 2016 was the first year for which the area of Turkey was mapped.

6.1 Human health PM_{10} indicators

Table 6.1 summarises the average concentration to which the European population has been exposed to over the fourteen year period 2005-2018 for both *human health PM_{10} indicators*, expressed as the population-weighted concentration, and the percentage of population exposed to PM_{10} concentrations above limit values (LV), i.e. the annual (ALV) and daily (DLV) limit value, respectively.

For the years 2012 and 2013 both the 36th highest value and the 90.4 percentile of daily mean(s) have been calculated. Their results demonstrate an underestimation of almost 1 µg·m^{-3} at the 36th highest daily mean. One may conclude that this underestimation is caused by the fact that when calculating the 36th highest daily mean value there is no correction for the missing values at incomplete time series. Whereas the 90.4 percentile of daily means adjusts for such missing data.

As the PM_{10} maps for 2018 (as presented in Chapter 2) have been constructed using the updated methodology as developed and tested in Horálek et al. (2019), the table presents the results for 2015-2018 (and 2005 and 2009, for annual average) both based on the updated and the old methodologies, for comparability reasons.

Table 6.1 Population-weighted concentration and percentage of the European population (without Turkey) exposed to concentrations above the PM_{10} limit values (LV) for the protection of health for 2005 to 2018

PM_{10}		method	2005	2006	2007	2008	2009	2010	2011	2012	2013	2014	2015	2016	2017	2018
Annual average																
Population-weighted concentration	[µg.m^{-3}]	old	28.0	28.9	26.6	25.1	24.6	24.5	25.3	22.9	22.2	21.1	21.2	20.2	20.2	20.1
		new	28.6				25.3						21.6	20.5	20.8	20.8
Population exposed > ALV (40 µg.m^{-3})	[%]	old	13.3	10.9	7.1	5.9	6.0	5.2	7.2	3.4	2.6	2.0	0.6	1.7	2.9	2.1
		new	11.5				6.2						0.7	1.7	3.3	2.4
36th highest daily mean / 90.4 percentile of daily means																
Popul.-weighted conc. [µg.m^{-3}]	36th highest d. m.	old	47.4	48.3	44.7	41.9	41.6	42.0	44.9	40.0	38.6					
	90.4 perc. of d. m.	old								40.8	39.4	37.1	36.9	35.7	36.1	34.5
	90.4 perc. of d. m.	new											37.5	36.1	37.0	35.4
Popul. exposed > DLV (50 µg.m^{-3}) [%]	36th highest d. m.	old	35.9	37.2	27.6	20.3	17.0	20.8	24.8	16.9	16.4					
	90.4 perc. of d. m.	old								18.1	17.3	13.3	14.7	14.0	15.8	12.0
	90.4 perc. of d. m.	new											16.2	14.6	17.0	13.2

In 2018 the population exposed to *annual mean* concentrations of PM_{10} above the limit value of 40 µg·m^{-3} has been 2.4 % of the total population; using the old methodology, it would be 2.1 %, which is lower percentage compared to the years 2005-2013 and 2017, but higher compared to the years 2014-2016. Furthermore, it is estimated that European inhabitants have been exposed on average to an annual mean PM_{10} concentration of 21 µg·m^{-3}; using the old methodology, it would be 20 µg·m^{-3}, the lowest value (together with the years 2016 and 2017) in the fourteen years' time series. The comparison of results for 2015-2018 illustrates well that a clear decrease in the population-weighted concentration does not lead necessarily to a similar decrease in the percentage of population exposed to an exceedance.

In the fourteen-year time series, the number of people living in areas with concentrations above the annual LV is lower in the latest six years (2013-2018) than in the first eight years. The overall picture of the population-weighted annual mean concentration of the European totals (i.e. totals of 40 European countries considered) demonstrates a downward trend approximately of -0.7 µg·m^{-3}.year^{-1} for the years 2005-2018, based on the old mapping method results for the whole period (for trend estimation methodology, see Annex 1, Section A1.2). This trend is statistically significant (at the strongest level ***, i.e. 0.001) and expresses a mean decrease of 0.7 µg·m^{-3} per year.

In 2018 about 13 % of the European population have lived in areas where the PM_{10} daily limit value (calculated using the *90.4 percentile* and the new methodology) has been exceeded (using the old methodology, it would be 12 %), being the lowest of the fourteen year period (also in the case of the old methodology). The overall European population-weighted concentration of the 90.4 percentile of the PM_{10} daily means (formerly the 36th highest daily mean) for the background areas is estimated to be about 35 µg·m^{-3} in 2018 (according to the old mapping methodology, it would be 34.5 µg·m^{-3}), which is the lowest of the fourteen years considered (again with both methodologies). This is the case even though the 36th highest daily means (i.e. possibly underestimated data if applied instead of the 90.4 percentiles, see above) have been used in the 2005-2011 calculations. The population-weighted concentrations of the European total (i.e. total of 40 European countries considered) show a statistically significant (at the strongest level ***, i.e. 0.001) downward trend of about -1.0 µg·m^{-3} per year for the years 2005-2018, for the daily LV related indicator 90.4 percentile of daily means (formerly the 36th highest daily mean), as calculated based on the old mapping method results for the whole period.

6.2 Human health $PM_{2.5}$ indicators

Table 6.2 summarises for *human health $PM_{2.5}$ indicator* (annual average) the population-weighted concentration and the percentage of European population exposed to $PM_{2.5}$ concentrations above the EU LV for the years 2005 to 2018 (without 2006, for which neither a map nor a population exposure was prepared).

As in the case of PM_{10}, the $PM_{2.5}$ maps for 2018 (as presented in Chapter 3) has been constructed using the updated methodology. Due to this reason, the table presents the results for 2018 (and 2005, 2009 and 2015-2017) both based on the updated and the old methodology, for comparability reasons.

Table 6.2 Population-weighted concentration and percentage of the European population (without Turkey) exposed to concentrations above the $PM_{2.5}$ limit value (LV) for the protection of health for 2005 to 2018

$PM_{2.5}$		method	2005	2006	2007	2008	2009	2010	2011	2012	2013	2014	2015	2016	2017	2018
Annual average																
Population-weighted concentration	[µg.m^{-3}]	old	18.8	not mapped	16.2	16.4	16.2	16.9	17.8	15.7	15.3	14.1	14.2	13.4	13.6	13.2
		new	19.0				16.6						14.3	13.6	13.8	13.5
Population exposed > LV (25 µg.m^{-3})	[%]	old			8.2	7.9	7.6	8.3	13.3	9.1	5.8	4.2	6.3	5.4	7.0	4.1
		new	20.9				7.6						6.5	5.4	7.2	4.5

The percentage of population exposed in 2018 to annual mean concentrations of $PM_{2.5}$ above the LV of 25 µg·m^{-3} has been 4.5 %, which is a lower value compared to the previous three years. Furthermore, it is estimated that European inhabitants have been exposed on average to an annual mean $PM_{2.5}$ concentration of 14.5 µg·m^{-3} in 2018 (according to the old methodology it would be 13 µg·m^{-3}), being the lowest value in the time series.

The trend analysis of the population-weighted concentrations across the period 2005-2018 for Europe as a whole has been executed, based on the old mapping method results across the whole period. At European scale a statistical significant (at the level ***, i.e. 0.001) downward trend can be observed, estimated to be -0.4 µg·m^{-3} per year.

6.3 Human health ozone indicators

Table 6.3 summarises the exposure levels of the European inhabitants in terms of population-weighted concentrations for both *human health ozone indicators*. Furthermore, it presents the percentage of European population exposed to concentrations above the target value (TV) and above a level of 6 000 $\mu g \cdot m^{-3} \cdot d$ for the SOMO35 for the years 2005 to 2018.

Table 6.3 Population-weighted concentration and percentage of the European population (without Turkey) exposed to concentrations above the target value (TV) threshold for the protection of health and a SOMO35 threshold of 6 000 µg·m^{-3}·d for 2005 to 2018

Ozone		2005	2006	2007	2008	2009	2010	2011	2012	2013	2014	2015	2016	2017	2018
26th highest daily max. 8-h mean / 93.2 percentile of daily max. 8-h means															
Pop.-weighted conc. [µg.m^{-3}]	26th highest d. max8h	111.4	117.6	110.0	109.4	107.7	106.5	108.4	107.3	108.3					
Pop.-weighted conc. [µg.m^{-3}]	93.2 perc. of d. max8h								107.9	108.9	102.9	110.4	104.8	105.0	114.4
Pop. exp. > TV (120 µg.m^{-3}) [%]	26th highest d. max8h	29.5	49.8	24.9	13.6	14.9	15.8	15.0	19.0	15.0					
Pop. exp. > TV (120 µg.m^{-3}) [%]	93.2 perc. of d. max8h								20.2	15.9	5.6	34.0	8.4	12.9	34.8
SOMO35															
Pop.-weighted concentration	[µg.m^{-3}.d]	4622	5045	4291	4164	4233	3850	4318	4174	4089	3500	4312	3619	3890	4962
Pop. exposed > 6000 µg.m^{-3}.d	[%]	26.8	27.1	26.3	17.0	23.2	15.9	22.0	23.2	18.8	9.4	22.2	11.7	19.1	31.3

The table presents the results obtained with the 1x1 km^2 merging resolution as tested on the 2006 data in Horálek et al (2010), then recomputed for 2005 and 2007, and finally implemented fully on the 2008 data and onwards. For 2012 and 2013, both the 26th highest value and the 93.2nd percentile of maximum daily 8-hour mean(s) have been calculated. It demonstrates an underestimation of about 0.6 $\mu g \cdot m^{-3}$ at the 26th maximum daily 8-hour mean, which is caused by the fact that when calculating this indicator there is no correction for the missing values in the incomplete measurement time series.

Using the *93.2 percentile of ozone maximum daily 8-hour means* it is estimated that 35 % of the population have lived in 2018 in areas where concentrations were above the ozone target value (TV) of 120 $\mu g \cdot m^{-3}$, which is the second highest number of the fourteen year period. The overall European population-weighted ozone concentration in terms of the 93.2 percentile maximum daily 8-hour means in the background areas is estimated at about 114 $\mu g \cdot m^{-3}$, which is also the second highest value of the whole fourteen year period (it should be noted that for 2005-2011 the 26th highest value of the maximum daily eight-hour mean was considered instead).

Examining the time series for 2005-2018, it can be concluded that 2006, but also 2005, 2015 and 2018 are exceptional years with high ozone concentrations, leading to increased exposure levels compared to the other ten years. The years 2014, 2016 and 2017 show the lowest exposure levels in the fourteen years' time series for the 93.2 percentile of the maximum daily 8-hour means.

The trend analysis of the population-weighted concentrations for the 93.2 percentile of the maximum daily 8-hour means across the period 2005-2018 of the European totals (i.e. totals of 40 European countries considered) does not estimate a statistically significant trend.

A similar tendency is observed for *SOMO35*. In 2006-2007, almost one-third of the population have lived in areas where a level of 6 000 $\mu g \cdot m^{-3} \cdot d$[3] has been exceeded, with the highest level in 2006. In the period of 2008-2017, it fluctuated from about 16 % to 23 % of the population, except 2014 with about 9 % and 2016 with about 12 %. In 2018, it has been again about one-third of the population.

The population-weighted SOMO35 concentrations show a quite similar pattern over time. Trend analysis on the population-weighted concentration of the European totals shows no trend for the period 2005-2018.

6.4 Vegetation related ozone indicators

Exposure indicators describing the *agricultural and forest areas exposed to accumulated ozone* concentrations above defined thresholds are summarised in Table 6.4. Those thresholds are the target value (TV) of 18 000 $\mu g \cdot m^{-3} \cdot h$ and the long-term objective (LTO) of 6 000 $\mu g \cdot m^{-3} \cdot h$ for the AOT40 for vegetation, and the former Reporting Value (RV) of 20 000 $\mu g \cdot m^{-3} \cdot h$ and the Critical Level (CL) of 10 000 $\mu g \cdot m^{-3} \cdot h$ for the AOT40 for forests.

[3] Note that the 6 000 $\mu g \cdot m^{-3} \cdot d$ does not represent a health-related legally binding 'threshold'. In this and previous papers it represents a somewhat arbitrarily chosen threshold to facilitate the discussion of the observed distributions of SOMO35 levels in their spatial and temporal context. For motivation of this choice, see Section 4.2.

Table 6.4 Percentages of the European agricultural and forest area (without Turkey) exposed to ozone concentrations above the target value (TV) and the long-term objective (LTO) for AOT40 for vegetation, and above Critical Level (CL) and Reporting Value (RV) for AOT40 for forests and agricultural- and forest-weighted concentrations for 2005 to 2018

Ozone	2005	2006	2007	2008	2009	2010	2011	2012	2013	2014	2015	2016	2017	2018
AOT40 for vegetation														
Agricultural area % > TV (18 000 µg.m^{-3} [%]	48.5	69.1	35.7	37.8	26.0	21.3	19.2	30.0	22.1	17.8	31.4	14.7	23.8	39.7
Agricultural area % > LTO (6 000 µg.m^{-3}. [%]	88.8	97.6	77.5	95.5	81.0	85.4	87.9	86.4	81.0	85.5	79.7	74.1	73.4	95.1
Agricultural-weighted concentration (µg.m-3	17481	22344	14597	15214	13157	13310	13255	14041	12838	12427	14223	10942	11750	16311
AOT40 for forests														
Forest area exposed > RV (20 000 µg.m^{-3}. [%]	59.1	69.4	48.4	50.2	49.2	49.3	53.0	47.2	44.1	37.7	52.4	41.9	38.9	56.1
Forest area exposed > CL (10 000 µg.m^{-3} [%]	76.4	99.8	62.1	79.6	67.4	63.4	68.6	65.0	67.2	68.2	59.8	60.0	55.4	86.7
Forest-weighted concentration (µg.m-3.h)	25900	31154	23744	21951	23532	19625	21892	21580	21753	17124	21150	17573	16798	25397

In 2018, some 40 % of all agricultural land (crops) has been exposed to accumulated ozone concentrations (AOT40 for vegetation) exceeding the target value (TV) threshold, which is the highest percentage in the last twelve years considered. About 95 % of all agricultural land has been exposed to levels in excess of the long-term objective (LTO), which is the third highest number of all fourteen years.

The trend analysis of the agricultural-weighted concentrations for the AOT40 for vegetation across the period 2005-2018 of the European totals (i.e. totals of 40 European countries considered) estimates a statistically significant (at the level *, i.e. 0.05) downward trend of -320 µg·m^{-3}·h per year.

For the ozone indicator AOT40 for *forests*, the level of 20 000 µg·m^{-3}·h (earlier used Reporting Value, RV) has been exceeded in about 56 % of the European forest area in 2018, which is the third highest of the whole time series. The forest area exceeding the Critical Level (CL) has been in 2018 about 87 %, which is the second highest percentage of the fourteen years period.

The temporal pattern of the AOT40 for forests exceedances shows some similarity with those of the AOT40 for vegetation, despite their different definitions and receptors and their natural difference in area type characteristics and occurrence. Their annual variability is, however, heavily dependent on meteorological variability.

The trend analysis of the forest-weighted concentrations for the AOT40 for forests across the period 2005-2018 of the European totals (i.e. totals of 40 European countries considered) estimates a statistically significant (at the strongest level **, i.e. 0.01) downward trend of -590 µg·m^{-3}·h per year.

6.5 Human health NO_2 indicators

Table 6.5 summarises the development in exposure levels of the European population for the *human health NO_2 indicator* (annual average), in terms of population-weighted concentrations and of percentage population exposed to concentrations above the annual LV (40 µg·m^{-3}), for the years 2005, 2009, 2010 and 2013 to 2018, for which the maps based on the current methodology are available. The population-weighted concentration is presented additionally also for 2007, although based on different mapping methodology than the other years. This 2007 value is probably slightly underestimated; based on Horálek et al. (2017b), we can suppose the true value would be of about 1 % higher (i.e. it would be about 23.5 µg·m^{-3}).

Table 6.5 Population-weighted concentration and percentage of the European population (without Turkey) exposed to concentrations above the NO_2 limit value (LV) of 40 µg·m^{-3} for the protection of health for 2005 to 2018

NO_2	2005	2006	2007	2008	2009	2010	2011	2012	2013	2014	2015	2016	2017	2018
Annual average														
Popul.-weighted concentr. [µg.m^{-3}]	23.3	not mapped	23.3	not mapped	22.1	22.1	not mapped		19.4	18.6	18.8	18.6	18.4	17.6
Pop. exp. > LV (40 µg.m^{-3}) [%]	7.9				5.6	4.9			3.2	2.8	3.2	2.8	3.0	1.8

In 2018 the population exposed to NO_2 annual mean concentrations above the limit value of 40 µg·m^{-3} has been 2 % of the total population, which is the lowest in the whole series. Furthermore, it is estimated that European inhabitants have been exposed on average to an annual mean NO_2 concentration of 18 µg·m^{-3}, again the lowest in the whole series.

Trend analysis on the population-weighted concentration of the European totals shows a slight downward trend of about -0.5 µg·m^{-3}·d per year, for the period 2005-2018, which is statistically significant (at the level ***, i.e. 0.001).

7 References

Alonso, R., et al., 2014, 'Drought stress does not protect Quercus ilex L. from ozone effects: results from a comparative study of two subspecies differing in ozone sensitivity', *Plant Biology 16*, pp. 375-384 (https://onlinelibrary.wiley.com/doi/10.1111/plb.12073) accessed 21 January 2021.

Ashmore, M., et al., H., 2004, 'New directions: a new generation of ozone critical levels for the protection of vegetation in Europe', *Atmospheric Environment* 38, pp. 2213-2214 (https://doi.org/10.1016/j.atmosenv.2004.02.029) accessed 20 November 2020.

Cressie, N., 1993, *Statistics for spatial data,* Wiley series, New York.

CLRTAP, 2017, *Manual for modelling and mapping critical loads & levels. Chapter III: "Mapping Critical levels for Vegetation"*, UNECE Convention on Long Range Transboundary Air Pollution (https://icpvegetation.ceh.ac.uk/sites/default/files/FinalnewChapter3v4Oct2017_000.pdf) accessed 26 August 2020.

Colette, A., et al., 2018, *Long term evolution of the impacts of ozone air pollution on agricultural yields in Europe. A modelling analysis for the 1990-2010 period*, Eionet Report – ETC/ACM 2018/15 European Environment Agency (https://www.eionet.europa.eu/etcs/etc-atni/products/etc-atni-reports/eionet_rep_etcacm_2018_15_o3impacttrends) accessed 26 August 2020.

Copernicus, 2019, *Copernicus European State of the Climate 2018 Summary* (https://climate.copernicus.eu/sites/default/files/2019-04/Brochure_Final_Interactive.pdf) accessed 20 November 2020.

Danielson, J. J. and Gesch, D. B., 2011, *Global multi-resolution terrain elevation data 2010 (GMTED2010)*, U.S. Geological Survey Open-File Report, pp. 2011-1073 (https://pubs.er.usgs.gov/publication/ofr20111073) accessed 19 November 2020.

De Leeuw, F., 2012, *AirBase: a valuable tool in air quality assessments at a European and local level*, ETC/ACM Technical Paper 2012/4 (http://www.eionet.europa.eu/etcs/etc-atni/products/etc-atni-reports/etcacm_tp_2012_4_airbase_aqassessment) accessed 26 August 2020.

Denby, B., et al., 2008, 'Comparison of two data assimilation methods for assessing PM_{10} exceedances on the European scale', *Atmospheric Environment* 42, pp. 7122-7134 (https://doi.org/10.1016/j.atmosenv.2008.05.058) accessed 26 August 2020.

Denby, B., et al., 2011a, *Calculation of pseudo $PM_{2.5}$ annual mean concentrations in Europe based on annual mean PM10 concentrations and other supplementary data*, ETC/ACC Technical Paper 2010/9 (http://www.eionet.europa.eu/etcs/etc-atni/products/etc-atni-reports/etcacc_tp_2010_9_pseudo_pm2-5_stations) accessed 26 August 2020.

Denby, B., et al., 2011b, *Mapping annual mean $PM_{2.5}$ concentrations in Europe: application of pseudo $PM_{2.5}$ station data*, ETC/ACM Technical Paper 2011/5 (http://www.eionet.europa.eu/etcs/etc-atni/products/etc-atni-reports/etcacm_tp_2011_5_spatialpm2-5mapping) accessed 26 August 2020.

De Smet, P., et al., 2011, *European air quality maps of ozone and PM_{10} for 2008 and their uncertainty analysis*, ETC/ACC Technical Paper 2010/10 (http://www.eionet.europa.eu/etcs/etc-atni/products/etc-atni-reports/etcacc_tp_2010_10_spataqmaps_2008) accessed 26 August 2020.

Deumier, J. M. and Hannon, C., 2010, 'La période d' initiation de la tubérisation: comment la repérer?' (in French), CNIPT (http://www.cnipt.fr/wp-content/uploads/2013/10/Irrigation-juin-2010.pdf) accessed 8 February 2021.

EC, 2008, *Directive 2008/50/EC of the European Parliament and of the Council of 21 May 2008 on ambient air quality and cleaner air for Europe,* OJ L 152, 11.06.2008, 1-44 (http://eur-lex.europa.eu/LexUriServ/LexUriServ.do?uri=OJ:L:2008:152:0001:0044:EN:PDF) accessed 26 August 2020.

EEA, 2010, *ORNL Landscan 2008 Global Population Data conversion into EEA ETRS89-LAEA5210 1km grid* (by Hermann Peifer of EEA) (https://sdi.eea.europa.eu/catalogue/geoss/api/records/1d68d314-d07c-4205-8852-f74b364cd699) accessed 26 August 2020.

EEA, 2018, *Guide for EEA map layout. EEA operational guidelines*, January 2015, version 5 (https://www.eionet.europa.eu/gis/docs/GISguide_v5_EEA_Layout_for_map_production.pdf) accessed 26 August 2020.

EEA, 2020a, *Air Quality e-Reporting. Air quality database (*https://www.eea.europa.eu/data-and-maps/data/aqereporting-8). Data extracted in March 2020.

EEA, 2020b, *Air quality in Europe – 2020 Report*, EEA Report 9/2020 (https://www.eea.europa.eu/publications/air-quality-in-europe-2020-report) accessed 8 December 2020.

EEA, 2020c, *Exceedance of air quality standards in Europe. CSI004 indicator assessment* (https://www.eea.europa.eu/data-and-maps/indicators/exceedance-of-air-quality-limit-2/assessment) accessed 19 November 2020.

EEA 2020d, *Exposure of Europe's ecosystems to ozone* (https://www.eea.europa.eu/data-and-maps/indicators/exposure-of-ecosystems-to-acidification-15/assessment) accessed 19 November 2020.

Emberson, L. D., et al., 2000, 'Modelling stomatal ozone flux across Europe', *Environmental Pollution* 109, pp. 403-413 (https://doi.org/10.1016/S0269-7491(00)00043-9) accessed 19 November 2020.

EU, 2020, *Corine land cover 2018 (CLC2018) raster data*, 100x100m^2 gridded version 2020_20 (https://land.copernicus.eu/pan-european/corine-land-cover/clc2018) accessed 19 November 2020.

EMEP, 2019, *Transboundary particular matter, photo-oxidants, acidifying and eutrophying components*, EMEP Report 1/2019 (https://emep.int/publ/reports/2019/EMEP_Status_Report_1_2019.pdf) accessed 26 August 2020.

Eurostat, 2014, *GEOSTAT 2011 grid dataset. Population distribution dataset* (http://ec.europa.eu/eurostat/web/gisco/geodata/reference-data/population-distribution-demography) accessed 26 August 2020.

Eurostat, 2020, *Total population for European states for 2018* (http://epp.eurostat.ec.europa.eu/tgm/table.do?tab=table&language=en&pcode=tps00001&tableSelection=1&footnotes=yes&labeling=labels&plugin=1) accessed 26 August 2020.

Gilbert, R. O., 1987, *Statistical Methods for Environmental Pollution Monitoring*, Van Nostrand Reinhold, New York.

Haberle, J. and Svoboda, P., 2015, 'Calculation of available water supply in crop root zone and the water balance of crop's, *Contributions to Geophysics and Geodesy* 45, pp. 285-298 (https://www.researchgate.net/publication/293194127_Calculation_of_available_water_supply_in_crop_root_zone_and_the_water_balance_of_crops) accessed 21 January 2021.

Horálek, J., et. al., 2005, *Interpolation and assimilation methods for European scale air quality assessment and mapping, Part II: Development and testing new methodologies*, ETC/ACC Technical paper 2005/8 (http://www.eionet.europa.eu/etcs/etc-atni/products/etc-atni-reports/etcacc_technpaper_2005_8_spatial_aq_dev_test_part_ii) accessed 26 August 2020.

Horálek, J., et. al., 2007, *Spatial mapping of air quality for European scale assessment*, ETC/ACC Technical paper 2006/6 (http://www.eionet.europa.eu/etcs/etc-atni/products/etc-atni-reports/etcacc_technpaper_2006_6_spat_aq) accessed 26 August 2020.

Horálek, J., et. al., 2008, *European air quality maps for 2005 including uncertainty analysis*, ETC/ACC Technical paper 2007/7 (http://www.eionet.europa.eu/etcs/etc-atni/products/etc-atni-reports/etcacc_tp_2007_7_spataqmaps_ann_interpol) accessed 26 August 2020.

Horálek, J., et. al., 2010, *Methodological improvements on interpolating European air quality maps*, ETC/ACC Technical Paper 2009/16 (http://www.eionet.europa.eu/etcs/etc-atni/products/etc-atni-reports/etcacc_tp_2009_16_improv_spataqmapping) accessed 26 August 2020.

Horálek, J., et. al., 2016a, *Application of FAIRMODE Delta tool to evaluate interpolated European air quality maps for 2012*, ETC/ACM Technical Paper 2015/2 (http://www.eionet.europa.eu/etcs/etc-atni/products/etc-atni-reports/etcacm_tp_2015_2_delta_evaluation_aqmaps2012) accessed 26 August 2020.

Horálek, J., et. al., 2016b, *European air quality maps of PM and ozone for 2013 and their uncertainty*, ETC/ACM Technical Paper 2015/5 (http://www.eionet.europa.eu/etcs/etc-atni/products/etc-atni-reports/etcacm_tp_2015_5_aqmaps2013) accessed 26 August 2020.

Horálek, J., et. al., 2017a, *Potential improvements on benzo(a)pyrene (BaP) mapping*, ETC/ACM Technical Paper 2016/3 (http://www.eionet.europa.eu/etcs/etc-atni/products/etc-atni-reports/etcacm_tp_2016_3_bap_improved_mapping) accessed 26 August 2020.

Horálek, J., et. al., 2017b, *Inclusion of land cover and traffic data in NO_2 mapping methodology*, ETC/ACM Technical Paper 2016/12 (http://www.eionet.europa.eu/etcs/etc-atni/products/etc-atni-reports/etcacm_tp_2016_12_lc_and_traffic_data_in_no2_mapping) accessed 26 August 2020.

Horálek, J., et. al., 2018, *Satellite data inclusion and kernel based potential improvements in NO_2 mapping*, ETC/ACM Technical Paper 2017/14 (http://www.eionet.europa.eu/etcs/etc-atni/products/etc-atni-reports/etcacm_tp_2017_14_improved_aq_no2mapping) accessed 26 August 2020.

Horálek, J., et. al., 2019, *Land cover and traffic data inclusion in PM mapping*, Eionet Report ETC/ACM 2018/18 (http://www.eionet.europa.eu/etcs/etc-atni/products/etc-atni-reports/etc-acm-report-18-2018-land-cover-and-traffic-data-inclusion-in-pm-mapping) accessed 26 August 2020.

Horálek, J., et. al., 2020a, *European air quality maps for 2017*, Eionet Report ETC/ATNI 2019/9 (https://doi.org/10.5281/zenodo.4309292) accessed 8 December 2020.

Horálek, J., et. al., 2020b, *Reference air quality maps 2005 and 2009*, Eionet Report ETC/ATNI 2020/1 (https://doi.org/10.5281/zenodo.4293744) accessed 8 December 2020.

ICP Vegetation, 2017, *Scientific Background Document A of Chapter 3 of "Manual on methodologies and criteria for modelling and mapping critical loads and levels of air pollution effects, risks and trends", UNECE Convention on Long-range Transboundary Air Pollution* (https://icpvegetation.ceh.ac.uk/sites/default/files/ScientificBackgroundDocumentAOct2018.pdf) accessed 11 December 2020.

ICP Vegetation, 2020, *Scientific Background Document B of Chapter 3 of "Manual on methodologies and criteria for modelling and mapping critical loads and levels of air pollution effects, risks and trends", UNECE Convention on Long-range Transboundary Air Pollution* (https://icpvegetation.ceh.ac.uk/sites/default/files/Scientific%20Background%20document%20B%20June%202020.pdf) accessed 11 December 2020.

Jarvis, P. G., 1976, 'The interpretation of the variation in leaf water potential and stomatal conductance found in canopies in the field', *Philosophical Transactions of the Royal Society of London*, Series B: Biological Sciences 273, pp. 593-610 (https://doi.org/10.1098/rstb.1976.0035) accessed 8 December 2020.

JRC, 2009, *Population density disaggregated with Corine land cover 2000,* 100x100 m^2 grid resolution, EEA version (http://www.eea.europa.eu/data-and-maps/data/population-density-disaggregated-with-corine-land-cover-2000-2) accessed 26 August 2020.

JRC, 2016, Maps of indicators of soil hydraulic properties for Europe, dataset/maps downloaded from the European Soil Data Centre (http://esdac.jrc.ec.europa.eu/content/maps-indicators-soil-hydraulic-properties-europe) accessed 8 December 2020.

Krupa, S., et al., 2000, 'Ambient ozone and plant health', *Plant Disease* 85, pp. 4-12 (https://apsjournals.apsnet.org/doi/pdf/10.1094/pdis.2001.85.1.4) accessed 8 December 2020.

Mareckova, K., et al., 2019, *Inventory Review 2019, Review of emission data reported under the LRTAP Convention and NEC Directive*, EEA & CEIP Technical Report 4/2019 (https://www.ceip.at/fileadmin/inhalte/ceip/00_pdf_other/2019/inventoryreport_2019.pdf) accessed 19 November 2020.

Mills, G., et al., 2011, 'New stomatal flux-based critical levels for ozone effects on vegetation', *Atmospheric Environment* 45, pp. 5064-5068 (https://doi.org/10.1016/j.atmosenv.2011.06.009) accessed 19 November 2020.

Musselman, R. C. and Massman, W. J., 1998, 'Ozone flux to vegetation and its relationship to plant response and ambient air quality standards', *Atmospheric Environment* 33, pp. 65-73 (https://doi.org/10.1016/S1352-2310(98)00127-7) accessed 11 December 2020.

NASA, 2020, *OMNO2d level 3 satellite data* (https://acdisc.gsfc.nasa.gov/opendap/HDF-EOS5/Aura_OMI_Level3/OMNO2d.003) accessed 26 March 2020.

NILU, 2020, *EBAS, database of atmospheric chemical composition and physical properties* (http://ebas.nilu.no) accessed 26 March 2020.

NMI, 2020, *EMEP/MSC-W modelled air concentrations and depositions, Gridded data for 2018, using 2017 emission (2019 Reporting)* (https://thredds.met.no/thredds/catalog/data/EMEP/2019_Reporting/catalog.html) accessed 26 March 2020.

Nussbaum, S., et al., 2003, 'High-resolution spatial analysis of stomatal ozone uptake in arable crops and pastures', *Environmental International* 129, pp. 385-392 (https://www.ncbi.nlm.nih.gov/pubmed/12676231) accessed 11 December 2020.

Pleijel, H., et al., 2007, 'Ozone risk assessment for agricultural crops in Europe: Further development of stomatal flux and flux-response relationships for European wheat and potato', *Atmospheric Environment* 41, pp.3022-3040 (https://doi.org/10.1016/j.atmosenv.2006.12.002) accessed 8 December 2020.

Reich, P. B., 1987, 'Quantifying plant response to ozone: a unifying theory, 'Tree Physiology' 3, pp. 63-91 (https://doi.org/10.1093/treephys/3.1.63) accessed 19 November 2020.

Simpson, D., et al., 2012, 'The EMEP MSC-W chemical transport model – technical description', *Atmospheric Chemistry and Physics* 12, pp. 7825-7865 (https://doi.org/10.5194/acp-12-7825-2012) accessed 26 August 2020.

UNECE, 2016, Forest condition in Europe, 2016 report of ICP Forests, UNECE Convention on Long-range Transboundary Air Pollution (https://www.icp-forests.org/pdf/TR2016.pdf) accessed 19 November 2020.

WHO, 2005, *WHO Air quality guidelines for particulate matters, ozone, nitrogen dioxide and sulphur dioxide, Global update 2005,* World Health Organization (http://www.who.int/phe/health_topics/outdoorair/outdoorair_aqg/en/index.html) accessed 26 August 2020.

WHO, 2013, *Health risks of air pollution in Europe – HRAPIE project, Recommendations for concentration-response functions for cost-benefit analysis of particulate matter, ozone and nitrogen dioxide*, World Health Organization (http://www.euro.who.int/__data/assets/pdf_file/0006/238956/Health_risks_air_pollution_HRAPIE_project.pdf) accessed 26 August 2020.

Annexes

Annex 1 – Methodology

A1.1 Mapping method

Previous technical papers prepared by Horálek et al. (2005, 2007, 2008, 2010, 2017b, 2018, 2019), De Smet et al. (2011) and Denby et al. (2011a, 2011b) discuss methodological developments and details on spatial interpolations and their uncertainties. No changes took place in the mapping methodology compared to the preceding report (Horálek et al., 2020a). This annex summarizes the currently applied method for all the considered indicators. The mapping method has been evaluated with the FAIRMODE Delta tool in Horálek et al. (2016a). The method is called the *Regression – Interpolation – Merging Mapping*.

Pseudo $PM_{2.5}$ and NO_x station data estimation

To supplement $PM_{2.5}$ measurement data, in the mapping procedure we also use data from so-called *pseudo $PM_{2.5}$ stations.* These data are the estimates of $PM_{2.5}$ concentrations at the locations of PM_{10} stations with no $PM_{2.5}$ measurement. These estimates are based on PM_{10} measurement data and different supplementary data, using linear regression:

$$\hat{Z}_{PM_{2.5}}(s) = c + b.Z_{PM_{10}}(s) + a_1X_1(s) + a_2X_2(s) \quad \text{(A1.1)}$$

where $\hat{Z}_{PM_{2.5}}(s)$ is the estimated value of $PM_{2.5}$ at the station *s*,

$Z_{PM_{2.5}}(s)$ is the measurement value of PM_{10} at the station *s*,

$X_1(s),\ldots, X_n(s)$ are the values of other supplementary variables at the station *s*,

$c, b, a_1,\ldots, a_n$ are the parameters of the linear regression model calculated based on the data at the points of measuring stations with both $PM_{2.5}$ and PM_{10} measurements,

n is the number of other supplementary variables used in the linear regression model (apart from PM_{10}).

When applying this estimation method, all background stations (either classified as rural, urban or suburban) are handled together for estimating $PM_{2.5}$ values at background pseudo stations. For details, see Denby et al. (2011b). For estimating $PM_{2.5}$ values at urban traffic pseudo stations, Equation A1.1 is applied for the urban traffic stations. For details, see by Horálek et al. (2019).

To supplement NO_x measurement data, we estimate NO_x values at the locations of NO_2 stations with no NO_x data. The estimates are calculated similarly as in Horálek et al. (2007), using quadratic regression:

$$\hat{Z}_{NO_x}(s) = a_1Z_{NO_2}(s)^2 + a_2Z_{NO_2}(s) + c \quad \text{(A1.2)}$$

where $\hat{Z}_{NO_x}(s)$ is the estimated value of NO_x at the station *s*,

$Z_{NO_2}(s)$ is the measurement value of NO_2 at the station *s*,

a_1, a_2, c are the parameters of the quadratic regression calculated based on the data at the points of measuring stations with both NO_x and NO_2 measurements.

Interpolation

The mapping method used is a linear regression model followed by kriging of the residuals produced from that model (residual kriging). Interpolation is therefore carried out according to the relation:

$$\hat{Z}(s_0) = c + a_1 X_1(s_0) + a_2 X_2(s_0) + \cdots + a_n X_n(s_0) + \eta(s_0) \quad \text{(A1.3)}$$

where $\hat{Z}(s_0)$ is the estimated value of the air pollution indicator at the point s_o,

$X_1(s_0), X_2(s_0),\ldots, X_n(s_0)$ are the n number of individual supplementary variables at the point s_o

$c, a_1, a_2,\ldots, a_n$ are the $n+1$ parameters of the linear regression model calculated based on the data at the points of measurement,

$\eta(s_0)$ is the spatial interpolation of the residuals of the linear regression model at the point s_o calculated based on the residuals at the points of measurement.

For different pollutants and area types (rural, urban background, and in the case of PM and NO_2 , also urban traffic), different supplementary data are used, depending on their improvement to the fit of the regression. Ordinary kriging is used to interpolate the residuals:

$$\hat{R}(s_i) = \sum_{i=1}^{N} \lambda_i R(s_i), \lambda_i = 1 \quad \text{(A1.4)}$$

where $R(s_i)$ are the residuals in the points of the measuring stations s_i ,

$\lambda_1, \ldots, \lambda_N$ are the weights estimated based on variogram,

N is the number of the stations used in the interpolation.

The variogram (as a measure of a spatial correlation) is estimated using a spherical function (with parameters *nugget, sill, range*). For details, see Horálek et al. (2007), Section 2.3.5 and Cressie (1993).

For $PM_{2.5}$ and NO_x, both measurement data and the estimated data from the pseudo stations are used.

For the PM_{10} and $PM_{2.5}$ indicators we apply, prior to linear regression and interpolation, a logarithmic transformation to measurement and EMEP model concentrations. After interpolation, we apply a back-transformation. For details, see De Smet et al. (2011) and Denby et al. (2008).

For the vegetation related indicators (AOT40 for vegetation and forests, POD, and NO_x) we only construct rural maps based on rural background stations, based on the assumption that no vegetation is located in urban areas. For the health related indicators, we construct the rural and urban background map layers (and for PM and NO_2 also urban traffic map layer) separately and then we merge them.

Merging of rural and urban background (and urban traffic) map layers

Health related indicator map layers for ozone are constructed (using linear regression with kriging of its residuals) for the rural and urban background areas separately on a grid at 10x10 km^2 resolution, while for PM_{10}, $PM_{2.5}$ and NO_2 on a grid at 1x1 km^2 resolution. The rural map is based on rural background stations and the urban background map on urban and suburban background stations. Subsequent to this, the rural and urban background maps are merged into one combined air quality indicator map using a European-wide population density grid at 1x1 km^2 resolution. For the 1x1 km^2 grid cells with a population density less than a defined value of α_1, we select the rural map value and for grid cells with a population density greater than a defined value α_2, we select the urban background map value. For areas with population density within the interval (α_1, α_2) a weighting function of α_1 and

α_2 is applied (for details and the setting of the parameters α_1 and α_2, see Horálek et al., 2005, 2007, 2010). This applies to the grid cells where the estimated rural value is lower (PM_{10}, $PM_{2.5}$ and NO_2) or higher (ozone), than the estimated urban background map value. In limited areas when this criterion does not hold, we apply a joint urban/rural map layer (created using all background stations regardless their type), as far as its value lies in between the rural and urban background map value. Thus, the adjusted rural and urban background map layers are calculated and further used. For details, see De Smet et al. (2011).

In the case of ozone, the separate ozone rural and urban (adjusted) map layers are constructed at a resolution of 10x10 km^2; their merging however takes place on the basis of the 1x1 km^2 resolution population density grid, resulting in a final combined pollutant indicator map on this 1x1 km^2 resolution grid. This map is used both for the population exposure estimates and for presentational purposes.

In the case of PM_{10}, $PM_{2.5}$ and NO_2, separate map layers are created for rural, urban background and urban traffic areas on a grid at 1x1 km^2 resolution. The (adjusted) rural background map layer is based on the rural background stations, the (adjusted) urban background map layer on the urban and the suburban background stations, and the urban traffic map layer on the urban and the suburban traffic stations. For different map layers (rural, urban background, urban traffic) different supplementary data are used, depending on their improvement to the fit of the regression. The three map layers are merged into one final map using a weighting procedure

$$\hat{Z}_F(s_0) = \big(1 - w_U(s_0)\big)\hat{Z}_R(s_0) + w_U(s_0)\big(1 - w_T(s_0)\big)\hat{Z}_{UB}(s_0) + w_U(s_0)w_T(s_0)\hat{Z}_{UT}(s_0) \quad \text{(A1.5)}$$

where $\hat{Z}_F(s_0)$ is the resulting estimated concentration in a grid cell s_o for the final map,

$\hat{Z}_R(s_0)$ is the estimated concentration in a grid cell s_o for the rural background map layer,

$\hat{Z}_{UB}(s_0)$ is the estimated concentration in a grid cell s_o for the urban background map layer,

$\hat{Z}_{UT}(s_0)$ is the estimated concentration in a grid cell s_o for the urban traffic map layer,

$w_U(s_0)$ is the weight representing the ratio of the urban character of the a grid cell s_o,

$w_T(s_0)$ is the weight representing the ratio of areas exposed to traffic air quality in a grid cell s_o.

The weight $w_U(s_0)$ is based on the population density grid, while $w_T(s_0)$ is based on the buffers around the roads. For further details, see Horálek et al. (2017b).

In all calculations and map presentations the EEA standard projection ETRS89-LAEA5210 (also known as ETRS89 / LAEA Europe, see www.epsg-registry.org) is used. The interpolation and mapping domain consists of the areas of all EEA member and cooperating countries, and other microstates, as far as they fall into the EEA map extent *Map_2c* (EEA, 2018). The mapping area covers the whole Europe apart from Belarus, Moldova, Ukraine and the European parts of Russia and Kazakhstan.

A1.2 Calculation of population and vegetation exposure

Population and vegetation exposure estimates are based on the interpolated concentration maps, population density data and land cover data.

Population exposure

Population exposure for individual countries and for Europe as a whole is calculated for ozone from the air quality maps and population density data, both at 1x1 km^2 resolution. For each concentration class, the total population per country as well as the European-wide total is determined.

For PM and NO_2, the population exposure is calculated separately for the areas where the air quality is considered to be directly influenced by traffic and for the background (both rural and urban) areas. For each concentration class '*j*', the percentage population per country as well as the European-wide total is determined according to:

$$P_j = \frac{\sum_{i=1}^{N} I_{Bij}\left(1 - w_U(i)w_T(i)\right)p_i + \sum_{i=1}^{N} I_{Tij} w_U(i) w_T(i) p_i}{\sum_{i=1}^{N} p_i} \cdot 100 \qquad \text{(A1.6)}$$

where P_j is the percentage population living in areas of the *j*-th concentration class in either the country or in Europe as a whole,

p_i is the population in the *i*-th grid cell,

I_{Bij} is the Boolean 0-1 indicator showing whether the background air quality concentration (estimated by the combined rural/urban background map layer) in the *i*-th grid cell is within the *j*-th concentration class (I_{Bij} = 1), or not (I_{Bij} = 0),

I_{Tij} is the Boolean 0-1 indicator showing whether the traffic air quality concentration in the *i*-th grid cell is within the *j*-th concentration class (I_{Tij} = 1), or not (I_{Tij} = 0),

N is the number of grid cells in the country or in Europe as a whole.

In addition, we express per-country and European-wide exposure as the population-weighted concentration, i.e. the average concentration weighted according to the population in a 1x1 km^2 grid cell:

$$\hat{c} = \frac{\sum_{i=1}^{N} c_i p_i}{\sum_{i=1}^{N} p_i} \qquad \text{(A1.7)}$$

where $\hat{c}$ is the population-weighted average concentration in the country or in the whole of Europe,

p_i is the population in the i^{th} grid cell,

c_i is the concentration in the i^{th} grid cell (based on the final merged map),

N is the number of grid cells in the country or in Europe as a whole.

Estimation of trends

For detecting and estimating the trends in time series of annual values of population exposure, the non-parametric Mann-Kendall's test for testing the presence of the monotonic increasing or decreasing trend is used. Next to that, the non-parametric Sen's method for estimating the slope of a

linear trend is executed. For details, see Gilbert (1987). The significance of the Mann-Kendal test is shown by the usual way, i.e. + for 0.1, * for 0.05, ** for 0.01, and *** for 0.001.

Vegetation exposure

Vegetation exposure for individual countries and for Europe as a whole is calculated based on the air quality maps and land cover data, both in 2x2 km^2 grid resolution. For each concentration class, the total agricultural and forest area per country as well as European-wide is determined.

Next to this, we express per-country and European-wide exposure as the agricultural- and forest-weighted concentration, i.e. the average concentration weighted according to the agricultural and forest area in a 1x1 km^2 grid cell, similarly like in Eq. A1.7.

A1.3 Phytotoxic Ozone Dose above a threshold flux Y (POD_Y) calculation

The calculation of POD_Y as described below follows precisely the methodology described in the Manual for modelling and mapping critical loads & levels of the Long-Range Transboundary Air Pollution Convention (CLRTAP) in its most recent available revision (CLRTAP, 2017), including some specifications presented in the Scientific background documents of this manual (ICP Vegetation, 2017, 2020), as prepared by the International scientific Cooperative Programme on effects of air pollution on natural vegetation and crops of the Working Group on Effects of the CLRTAP (ICP Vegetation). The steps to be taken are presented in Table A1.1.

Table A1.1 Steps to calculate exceedance of flux-based (POD_YSPEC or POD_YIAM) critical levels

1	Decide on the species and biogeographical region(s) to be included.
2	Obtain the ozone concentrations at the top of the canopy for the species or vegetation-specific accumulation period.
3	Calculate the hourly stomatal conductance of ozone (g_{sto}).
4	Model the hourly stomatal flux of ozone (F_{sto}).
5	Calculation of POD_Y (POD_YSPEC or POD_YIAM) from F_{sto}.
6	Calculation of exceedance of flux-based critical levels.

Source: CLRTAP, 2017

The cumulative stomatal ozone fluxes (F_{sto}) are calculated over the course of the growing season based on ambient ozone concentration and stomatal conductance (g_{sto}) to ozone. g_{sto} was calculated using a multiplicative stomatal conductance model proposed by Jarvis (1976) and modified by Emberson et al. (2000) as a function of species-specific maximum g_{sto} (expressed on a single leaf-area basis), phenology, and prevailing environmental conditions (photosynthetic photon flux density (PPFD)), air temperature, vapour pressure deficit (VPD), and soil moisture.

Hourly averaged stomatal ozone fluxes (F_{sto}) in excess of a threshold Y (expressed in mmol m^{-2} PLA ([4])) are accumulated over a species or vegetation-specific accumulation period using the equation:

$$POD_Y = \sum_n (F_{sto}(n) - Y) \cdot \frac{3600}{10^6} \qquad [\text{mmol.m}^{-2}\,\text{PLA}] \qquad \text{(A1.8)}$$

where the value *Y* [nmol m^{-2} PLA s^{-1}] is subtracted from each hourly averaged F_{sto} [nmol m^{-2} PLA s^{-1}] value only when $F_{sto} > Y$, during daylight hours (when global radiation is more than 50 W m^{-2}).

As can be been in Equation A1.8, the accumulated stomatal ozone fluxes in excess of the threshold Y is converted to hourly fluxes by multiplying by 3600 and to mmol by dividing by 10^6 , to get the stomatal ozone flux in mmol m^{-2} PLA.

For the wheat as for other crop species, the Y value is taken equal to 6 nmol m^{-2} PLA s^{-1}. Although several POD indicators are proposed in the Modelling and Mapping Manual, POD_6 is recommended for wheat, as the hourly averaged stomatal ozone fluxes above a value of 6 are more relevant for that crop. For potato and tomato, POD_6 is also recommended. Two POD_6 versions are available: POD_6IAM is a simplified version recommended for Integrated Assessment Modelling. We preferred to use here POD_6SPEC, which is specific to a given specie (Colette et al., 2018).

Obtaining the ozone concentrations at the top of the canopy for the species or vegetation-specific accumulation period

The ozone concentration at canopy top (nmol.m^{-3}) in the given hour H is calculated according to

$$c(z_1) = c(z_{m,O3}) * \left(1 - \frac{R_a(z_{tgt},\ z_{m,O3})}{R_a\left(d+z_0,\ z_{m,O3}\right) + R_b + R_{surf}}\right) \qquad \text{(A1.9)}$$

where
- $c(z_1)$ is ozone concentration at the top of the canopy
- $c(z_{m,O3})$ is the ozone concentration measured at the height z_m
- $R_a(x, y)$ is the aerodynamic resistance between the height of y and the height of x
- R_b is the resistance to ozone diffusion in the laminar sub-layer
- R_{surf} is the overall resistance to ozone deposition to the underlying surfaces

while

$$R_a(z_{tgt},\ z_{m,O3}) = \frac{1}{k.u*}\left[ln\left(\frac{z_{m,O3}-d}{z_{tgt}-d}\right) - \Psi_H\left(\frac{z_{m,O3}-d}{L}\right) + \Psi_H\left(\frac{z_{tgt}-d}{L}\right)\right] \qquad \text{(A1.9a)}$$

$$R_a(d+z_0,\ z_{m,O3}) = \frac{1}{k.u*}\left[ln\left(\frac{z_{m,O3}-d}{z_0}\right) - \Psi_H\left(\frac{z_{m,O3}-d}{L}\right) + \Psi_H\left(\frac{z_0}{L}\right)\right] \qquad \text{(A1.9b)}$$

$$R_b = \frac{2}{k\,.u*}\left(\frac{Sc}{Pr}\right)^{2/3} \qquad \text{(A1.9c)}$$

([4]) PLA, or the projected leaf area, is the total area of the sides of the leaves that are projected towards the sun. PLA is different to the total leaf area, which accounts for both sides of the leaves.

$$R_{surf} = \frac{1}{\frac{LAI}{R_{sto}} + \frac{SAI}{R_{ext}} + \frac{1}{R_{inc} + R_{soil}}} \quad \text{(A1.9d)}$$

where k is the von Kármán constant (equal to 0.41)

z_{tgt} is the top canopy height (the target height)

$z_{m,\,O3}$ is the height of the available ozone measurement above the canopy

z_0 is the roughness length, usually assumed as 1/10 of the canopy height

L is the Obukhov length

d is the displacement height, usually assumed as 2/3 of the canopy height

u^* is the friction velocity

Sc is the Schmidt number for ozone (equal to 0.41)

Pr is the Prandtl number of air (equal to 0.71)

LAI is the projected leaf area ($m^2.m^{-2}$)

SAI is the surface area of the canopy ($m^2.m^{-2}$)

$\Psi_H(..) = \Psi_H(\zeta)$ is the similarity function for heat with ζ as the argument ([5]), according to

$$\Psi_H(\zeta) = 2\ ln\left(\frac{1+x^2}{2}\right) \quad \text{when } \zeta < 0$$
$$= -5\zeta \quad \text{when } \zeta \geq 0 \quad \text{(A1.9e)}$$

with $x = (1 - 16 * \zeta)^{1/4}$ (A1.9f)

and R_{ext} is the resistance to cuticular deposition of ozone (equal to 2 500 $s.m^{-1}$)

R_{soil} is the soil resistance (equal to 200 $s.m^{-1}$)

while $R_{sto} = 1/g_{sto}$ (A1.9g)

$R_{inc} = b.SAI.h / u^*$ (A1.9h)

where g_{sto} is the actual stomatal conductance

b is the empirical constant (equal to 14 m^{-1})

h is the height of the canopy

Calculation of the hourly stomatal conductance of ozone (g_{sto})

The basis of the approach used for calculating phytotoxic ozone doses is the calculation of an instantaneous stomatal conductance g_{sto} in the given hour H, according to the equation

$$g_{sto} = g_{max} * [min(f_{phen}, f_{O3})] * f_{light} * max\{f_{min}, (f_{temp} * f_{VPD} * f_{SW})\} \quad \text{(A1.10)}$$

([5]) For more details see ICP Vegetation (2017).

where g_{sto} is the actual stomatal conductance (mmol O_3 m^{-2} PLA s^{-1})

g_{max} is the species-specific maximum stomatal conductance (mmol O_3 m^{-2} PLA s^{-1}); see Table A1.2

f_{phen} is the relative proportion function for the phenology for the different stage of growing

f_{O3} is the relative proportion function for the influence of ozone on stomatal flux by promoting premature senescence

f_{min} is the species-specific relative minimum stomatal conductance that occurs during daylight hours, see Table A1.2

f_{temp}, f_{VPD}, f_{SW}, f_{light} are relative proportion functions for leaf stomata respond to temperature, air humidity, soil moisture and light

Parameters f_{phen}, f_{O3}, f_{light}, f_{temp}, f_{VPD}, f_{SW} and f_{min} are expressed as relative proportion functions, taking values between 0 and 1 as a proportion of g_{max}. These functions allow taking into account irradiance (f_{light}), temperature (f_{temp}), water vapour deficit at leaves level (f_{vpd}), soil moisture (f_{sw}), phenology for the different stage of growing (f_{phen}) and the influence of ozone on stomatal flux by promoting premature senescence (f_{O3}). f_{min} is the minimum relative value of stomatal conductance during the daylight.

The parameter f_{phen} is calculated based on the accumulation of thermal time over the growing season of the crop being considered (Colette, 2018), according to CLRTAP (2017). For wheat and potato, the accumulation period is defined for each year using the effective temperature sum (ETS) in ˚C for days in excess of 0 ˚C, while for tomato for days in excess of 10 ˚C.

For wheat, the total accumulation period during which wheat is sensitive to ozone exposure is 200 °C days before mid-anthesis (mid-point in flowering) to 700 °C days after mid-anthesis. The timing of mid-anthesis is estimated by starting at the first date after 1 January (or just 1 January) when the temperature exceeds 0 °C. The mean daily temperature is then accumulated (temperature sum), and mid-anthesis is estimated to be a temperature sum of 1075 °C days, which in general corresponds to bread wheat. (For future, it is recommended to use a specific mid-anthesis for Mediterranean region.)

For potato, the accumulation period stands between 330 °C days before the tuber initiation date and 800 °C days after this date. The tuber initiation date is considered homogeneous throughout Europe due to a lack of local data availability. As discussed ([6]) with the French national Chamber of agriculture (APCA, http://chambres-agriculture.fr), the tuber initialization starts 15 days after the transplantation in the field, which occurs in May. Therefore, we set the fixed date for the tuber initialization to June 1st.

For tomato, the accumulation period is from 250 ˚C days to 1500 ˚C days after transplantation in the field over a base temperature of 10 °C. The timing of the transplantation is set on the fixed date 1 June.

The parameter f_{phen} is calculated according to equation

([6]) There is a lack of information on a date of potato tuber initiation in Europe. It should ideally rely on existing models based on agricultural practices, local climatology, ground properties, and location. INERIS, while developing the POD script, relied on contents of discussions with the French National Chamber of Agriculture (personal consultation, Quentin Mathieu, APCA, March 2018; Deumier and Hannon, 2010). Based on the information given that the tuber initialization starts 15 days after the transplantation in the field, which occurs in May in France, it has chosen a fixed date of June 1st for France and for Europe. This date might be revised according to the availability of more accurate information on potato plantations in Europe.

in the case of wheat:

$f_{phen} = 1$ when $(f_{phen\_2\_ETS} + f_{phen\_1\_ETS}) \leq ETS \leq (f_{phen\_2\_ETS} + f_{phen\_3\_ETS})$

$= 1 - \left(\frac{f_{phen\_a}}{f_{phen\_4\_ETS} - f_{phen\_3\_ETS}}\right) * (ETS - f_{phen\_3\_ETS})$ when $(f_{phen\_2\_ETS} + f_{phen\_3\_ETS}) < ETS \leq (f_{phen\_2\_ETS} + f_{phen\_4\_ETS})$

$= f_{phen\_e} - \left(\frac{f_{phen\_e}}{f_{phen\_5\_ETS} - f_{phen\_4\_ETS}}\right) * (ETS - f_{phen\_4\_ETS})$ when $(f_{phen\_2\_ETS} + f_{phen\_4\_ETS}) < ETS \leq f_{phen\_5\_ETS}$ (A1.10a)

in the case of potato (formulated based on ICP Vegetation, 2017):

$f_{phen} = 1 - \left(\frac{1 - f_{phen\_a}}{f_{phen\_1\_ETS}}\right) * ETS$ when $f_{phen\_1\_ETS} \leq ETS < 0$

$= 1 - \left(\frac{1 - f_{phen\_e}}{f_{phen\_2\_ETS}}\right) * ETS$ when $0 < ETS \leq f_{phen\_2\_ETS}$ (A1.10b)

in the case of tomato (formulated based on ICP Vegetation, 2017):

$f_{phen} = \frac{\mathrm{ETS} - f_{phen\_2\_ETS}}{A_{start\_ETS} - f_{phen\_2\_ETS}}$ when $A_{start\_ETS} \leq ETS < A_{end\_ETS}$ (A1.10c)

where *ETS* is the effective temperature sum in ˚C days using a base temperature of 0 ˚C for wheat and potato and a base temperature of 10 °C for tomato (see Table A1.2); for wheat, ETS is set to 0 °C days at mid-anthesis day. Then A_{start_ETS} will be at 200 ˚C days before mid-anthesis, and A_{end_ETS} will be at 700 ˚C days after mid-anthesis;

for potato, ETS is set to 0 °C days at tuber initiation day. Then A_{start_ETS} will be at 330 ˚C days before tuber initiation and A_{end_ETS} at 800 ˚C days after tuber initiation;

for tomato, ETS is set to 0 °C days at transplantation day in the field. Then A_{start_ETS} will be at 250 ˚C days after transplantation in the field and A_{end_ETS} at 1500 ˚C days after transplantation in the field,

f_{phen_a}, f_{phen_e} is the phenology function, which consists of terms describing rate changes of g_{max} expressed as fractions (see Table A1.2),

$f_{phen\_1\_ETS}$, $f_{phen\_2\_ETS}$, $f_{phen\_3\_ETS}$, $f_{phen\_4\_ETS}$, $f_{phen\_5\_ETS}$ are °C days (see Table A1.2; $f_{phen\_1\_ETS}$ and $f_{phen\_5\_ETS}$ define period crops to be sensitive to ozone exposure),

A_{start_ETS} and A_{end_ETS} are the effective temperature sums (counted from the day of the mid-anthesis for wheat, from the day of the tuber initiation for potato and from the day of the transplantation in the field for tomato) above a base temperature of 0 ˚C for wheat and potato and 10 ˚C for tomato at the start and end of the O_3 accumulation period respectively; in the case of tomato, A_{start_ETS} is 250 °C days and A_{end_ETS} is 1500 °C days after transplantation in the field over a base temperature of 10 °C, see Table A1.2 and CLRTAP (2017).

The parameter f_{O3} in the case of wheat is calculated according to equation

$f_{O3} = ((1+(POD_0/14)^8)^{-1}$ (A1.10d)

while $POD_0 = \sum_{n=A_{start}}^{H-1} F_{sto}(n) \cdot \frac{3600}{10^6}$ (A1.10e)

where POD_0 is the ozone flux already accumulated since the beginning of the vegetation period A_{start} up to the last hour *H-1*,

$F_{sto}(n)$ is the hourly ozone flux in the hour *n*, calculated in the previous steps based on Equation 2.4, while $F_{sto}(A_{start})$ is equal to 0.

The parameter (ozone function) f_{O3} in the case of potato is calculated according to equation

$$f_{O3} = ((1+(AOT0/40)^5)^{-1} \quad \text{(A1.10f)}$$

where *AOT0* is accumulated ozone concentration from the start of the vegetation period A_{start} up to the last hour *H-1.*

The parameter (ozone function) f_{O3} in the case of tomato is not determined.

The parameter f_{light} is calculated according to

$$f_{light} = 1 - EXP((-light\_a)*PPFD) \quad \text{(A1.10g)}$$

while $$PPFD = SSRD * 0.5 * 4.5 \quad \text{(A1.10h)}$$

where *PPFD* represents the photosynthetic photon flux density [µmol m^{-2} s^{-1}],

light_a is a light parameter (see Table A1.2),

SSRD represents the surface net solar radiation [$W.m^{-2}$].

The parameter f_{temp} is calculated according to:

$$f_{temp} = max\{f_{min}, [(T - T_{min}) / (T_{opt} - T_{min})] * [(T_{max} - T) / (T_{max} - T_{opt})]^{bt}\} \text{ when } T_{min} < T < T_{max}$$
$$= f_{min} \text{ when } T_{min} > T > T_{max} \quad \text{(A1.10i)}$$

while $$bt = (T_{max} - T_{opt}) / (T_{opt} - T_{min}) \quad \text{(A1.10j)}$$

where T_{min}, T_{max} and T_{opt} are minimum, maximum and optimum temperatures determining leaf stomata opening (see Table A1.2)

The parameter f_{VPD} is calculated according to:

$$f_{VPD} = min\{1, max\{f_{min}, ((1-f_{min})*(VPD_{min} - VPD) / (VPD_{min} - VPD_{max})) + f_{min}\}\} \quad \text{(A1.10k)}$$

while $$VPD = e_s(Ta) * (1-hr) \quad \text{(A1.10l)}$$
$$e_s(Ta) = a \exp(bT_a/(T_a+c)) \quad \text{(A1.10m)}$$

where VPD_{min} is the minimum vapour pressure deficit determining leaf stomata opening

VPD_{max}	is the maximum vapour pressure deficit determining leaf stomata opening
T_a	is the air temperature [°C]
h_r	is the relative humidity [%]/100
$e_s(Ta)$	is the potential (saturation) water vapour pressure
a, b, c	are the empirical constants (a = 0.611 kPa, b = 17.502, c = 240.97°C)

The ΣVPD (i.e. the function describing stomatal re-opening in the afternoon) is not taken into account.

The parameter f_{SW} is replaced by f_{SMI}**,** where *SMI* represents Soil Moisture Index, taking values between 0 and 1 (i.e. between 0 for soil moisture at wilting point and 1 for soil moisture at field capacity); SMI, taking values between 0 and 1 as a proportion of g_{max}, following the parameterization given in Simpson et al., 2012, similar to the plant available water (PAW) parameterization, f_{PAW}, defined for wheat in CLRTAP (2017). The basic equation used for f_{SW} resp. f_{SMI} is:

$$SMI = (SWLL - PWP) / (FC - PWP) \quad \text{(A1.10n)}$$

where	*SWLL*	is the soil moisture ($m^3\ m^{-3}$)
	PWP	is the permanent wilting point ($cm^3\ cm^{-3}$)
	FC	is the field capacity ($cm^3\ cm^{-3}$)

We use the Soil Moisture Index using the EMEP methodology as described in Simpson et al. (2012) and ICP Vegetation (2020). It is computed using the *soil moisture* variable available from a meteorological model, which represents the water content in m^3 of water per m^3 of ground [m^3. m^{-3}] in a specific ground level, in dependence on the available dataset. For soil moisture, we have used the ECWMF's ERA5-Land variable Volume of water in soil layer 3 (i.e. 28-100 cm), see Section 3.3. The level of soil layer was chosen based on recommendation of Haberle and Svoboda **(**2015**).** The soil moisture is quite a sensitive parameter in the calculation of the POD. Next to the soil moisture, the soil moisture index also takes into account the *permanent wilting point* and the *field capacity*; they are taken from JRC database soil hydraulic properties maps for Europe (JRC, 2016), see Annex 2, Section A2.3.

Table A1.2 Parametrisation for POD_6SPEC for wheat flag leaves and the upper-canopy sunlit leaves of potato and tomato, for different biogeographical regions

Parameter	Units	(Bread) Wheat		Potato	Tomato
		Atlantic, Boreal, Continental *(Pannonia, Steppic)*	Mediterranean	Atlantic, Boreal, Continental *(Pannonia, Steppic)*	Mediterranean
g_{max}	mmol $O_3.m^{-2}$ PLA.s^{-1}	500	430	750	330
f_{min}	fraction	0.01	0.01	0.01	0.06
light_a	-	0.0105	0.0105	0.005	0.0125
T_{min}	°C	12	12	13	18
T_{opt}	°C	26	28	28	28

Parameter	Units	(Bread) Wheat		Potato	Tomato
		Atlantic, Boreal, Continental *(Pannonia, Steppic)*	Mediterranean	Atlantic, Boreal, Continental *(Pannonia, Steppic)*	Mediterranean
T_{max}	°C	40	39	39	37
VPD_{max}	kPa	1.2	3.2	2.1	1
VPD_{min}	kPa	3.2	4.6	3.5	4
f_{O3}	POD0 mmol $O_3.m^{-2}$.PLA s^{-1}	14	-	-	-
f_{O3}	AOT0, ppmh	-	-	40	-
f_{O3}	exponent	8	-	5	-
Astart_ETS	ºC day	-	-	-	250
Aend_ETS	ºC day	-	-	-	1500
Leaf dimension	cm	2	2	4	3
Canopy height	m	1	0.75	1	2
f_{phen_a}	fraction	0.3	0.0	0.4	1
f_{phen_b}	fraction	-	-	-	-
f_{phen_c}	fraction	-	-	-	-
f_{phen_d}	fraction	-	-	-	-
f_{phen_e}	fraction	0.7	0.99	0.2	0.0
$f_{phen\_1\_ETS}$	ºC	-200	-300	-330	0
$f_{phen\_2\_ETS}$	°C	0	0	800	2770
$f_{phen\_3\_ETS}$	°C	100	70	-	-
$f_{phen\_4\_ETS}$	°C	525	0	-	-
$f_{phen\_5\_ETS}$	°C	700	550	-	-

Source: CLRTAP, 2017.

Modelling the hourly stomatal flux of ozone (F_{sto})

Once the hourly stomatal conductance of ozone (g_{sto}) and all relevant variables are computed, thejstomatal flux of ozone (F_{sto}) can be calculated, based on the assumption that the concentration of ozone at the top of the canopy represents a reasonable estimate of the concentration at the upper surface of the laminar layer for a sunlit upper canopy leaf. F_{sto} is calculated according to the ICP Vegetation methodology, thus the fraction of the ozone taken up by the stomata is given using a combination of the stomatal conductance, the external leaf, or cuticular, resistance and the leaf surface resistance. The hourly stomatal flux in the given hour H is calculated according to

$$F_{sto} = c(z_1) * g_{sto} * \frac{r_c}{r_b + r_c} \qquad \text{(A1.11)}$$

where F_{sto} is the hourly stomatal flux of ozone [nmol.m^{-2} PLA.s^{-1}]

$c(z_1)$ is the concentration of ozone at canopy top [nmol.m^{-3}]

r_b is the quasi-laminar resistance [s.m^{-1}]

r_c is the leaf surface resistance [s.m^{-1}]

g_{sto} is the actual stomatal conductance [(m.s^{-1}],

while $r_c = 1/(g_{sto} + g_{ext})$ (A1.11a)

$g_{ext} = 1/2500$ [m.s^{-1}] (A1.11b)

$$r_b = 1.3 * 150 * \sqrt{\frac{L}{u(z_1)}} \quad \text{(A1.11c)}$$

where g_{ext} is the external leaf, or cuticular, resistance (m.s^{-1}),

$u(z_1)$ is the wind speed at height z_1 (z_1 is the canopy top)

L is the cross-wind leaf dimension (2 cm, see Table A1.2)

while $$u_{(z1)} = \frac{u*}{k} * ln\left(\frac{z_1 - d}{z_0}\right) \quad \text{(A1.11d)}$$

where k is the von Kármán constant (equal to 0.41)

d is the displacement height usually assumed as 2/3 of the canopy height,

z_1 is the top of the canopy

z_0 is the roughness length usually assumed as 1/10 of the canopy height

$u*$ is the friction velocity

Box A1.1 shows the conversion of stomatal conductance and ozone concentration to units demanded for POD calculation.

Box A1.1 Conversion of stomatal conductance g_{sto} and ozone concentration to units demanded for POD$_y$ calculation

Stomatal conductance g_{sto} has to be converted from units mmol·m^{-2}·s^{-1} to units m·s^{-1} (since all the resistances are expressed in the unit of s·m^{-1}). At standard temperature (20 °C) and air pressure (1.013 x 10^5 Pa), the conversion is made by dividing the conductance in mmol·m^{-2}·s^{-1} by 41 000 to give conductance in m·s^{-1}.

To convert the **ozone concentration (C)** at canopy height from µg·m^{-3} resp. ppb to nmol m^{-3}, the following equation should be used:

C [nmol·m^{-3}] = C [ppb] * P/(R·T) = C [µg·m^{-3}] / 2 * P/(R·T) (A1.12)

where P is the atmospheric pressure in Pa,

R is the universal gas constant of 8.31447 J mol^{-1}·K^{-1}

T is the air temperature in Kelvin.

At standard temperature (20 °C) and air pressure (1.013 x 10^5 Pa), the concentration in ppb should be multiplied by 41.56 to calculate the concentration in nmol.m^{-3}.

Source: CLRTAP, 2017

In the routine used in this report (Section 2.3), an alternative conversion of the ozone concentrations from µg·m^{-3} resp. ppb to nmol·m^{-3} is done, using the air density instead of the atmospheric pressure, according to

$$C\ [nmol \cdot m^{-3}] = C\ [ppb] * \rho / N_a * 10^6 = C\ [\mu g \cdot m^{-3}] / 2 * \rho / N_a * 10^6 \quad \text{(A1.13)}$$

where ρ is the air density showing the number of the molecules in cm^{-3},

N_a is the Avogadro constant, which is equal to $6.022 \cdot 10^{23}$ mol^{-1}.

Calculation of POD_Y (POD_YSPEC or POD_YIAM) from F_{sto}

Hourly averaged stomatal ozone fluxes (F_{sto}) in excess of a Y threshold are accumulated over a species or vegetation-specific accumulation period using the following equation:

$$POD_Y = \sum_n (F_{sto}(n) - Y) \cdot \frac{3600}{10^6} [\text{mmol.m}^{-2}\ \text{PLA}] \quad \text{(A1.14)}$$

while Y (for wheat, potato or tomato) = 6 nmol m^{-2} PLA s^{-1}

where POD_Y is the phytotoxic ozone dose related to the threshold *Y*, in mmol.m^{-2} PLA

$F_{sto}(n)$ is the hourly ozone flux in the hour *n* of the accumulation period.

The value *Y* [nmol m^{-2} PLA s^{-1}] is subtracted from each hourly averaged F_{sto} [nmol m^{-2} PLA s^{-1}] value only when F_{sto}>*Y*, during daylight hours (when global radiation is more than 50 W m^{-2}). The value is then converted to hourly fluxes by multiplying by 3600 and to mmol by dividing by 10^6 to get the stomatal ozone flux in mmol m^{-2} PLA.

Calculation of exceedance of flux-based critical levels

If the calculated POD_Y value is larger than the flux-based Critical Level for O_3, then there is exceedance of the Critical Level ($CL_{exceedance}$). Exceedance of the Critical Level (CL) is calculated at follows:

$$CL_{exceedance} = POD_Y - CL \quad \text{(A1.15)}$$

A1.4 Methods for uncertainty analysis

The uncertainty estimation of the European map is based on cross-validation. The cross-validation method computes the quality of the spatial interpolation for each measurement point from all available information except from the point in question, i.e. it withholds one data point and then makes a prediction at the spatial location of that point. This procedure is repeated for all measurement points in the available set. The predicted and measurement values at these points are plotted in the form of a scatter plot. With help of statistical indicators the quality of the predictions is demonstrated objectively. The advantage of the nature of this cross-validation technique is that it enables evaluation

of the quality of the predicted values at locations without measurements, as long as they are within the area covered by the measurements.

In addition, we make a simple comparison between the point measurements and estimated values of the 10x10 km^2 grid for the separate rural and urban maps and the 1x1 km^2 grid for the final combined maps, for the health-related indicators, resp. the 2x2 km^2 grid in the case of AOT40 and NO_x. Note that the grid cell value is the averaged result of the estimation in this grid cell area. The estimated value within a grid cell will only approximate the predicted value(s) at the station(s) lying within that cell.

Another method to estimate uncertainties is based on geostatistical theory: together with the prediction, the prediction standard error is computed at all the grid cells, which represents in fact the interpolation uncertainty map (see Cressie, 1993 for a detailed discussion). Based on the concentration and the uncertainty map, the exceedance probability map is created.

Cross-validation

The results of cross-validation are described by the statistical indicators and scatter plots. The main indicator used is root mean squared error (RMSE) and additional is bias (mean prediction error, MPE):

$$RMSE = \sqrt{\frac{1}{N}\sum_{i=1}^{N}\left(\hat{Z}(s_i) - Z(s_i)\right)^2} \quad \text{(A1.16)}$$

$$bias(MPE) = \frac{1}{N}\sum_{i=1}^{N}\left(\hat{Z}(s_i) - Z(s_i)\right) \quad \text{(A1.17)}$$

where $Z(s_i)$ is the air quality indicator value derived from the measured concentration at the i^{th} point, *i = 1, …, N*,

$\hat{Z}(s_i)$ is the air quality estimated indicator value at the i^{th} point using other information, without the indicator value derived from the measured concentration at the i^{th} point,

N is the number of the measuring points.

Next to the RMSE expressed in the absolute units, one could express this uncertainty in relative terms by relating the RMSE to the mean of the air pollution indicator value for all stations:

$$RRMSE = \frac{RMSE}{\bar{Z}}.100 \quad \text{(A1.18)}$$

where *RRMSE* is the relative RMSE, expressed in percent,

$\bar{Z}$ is the arithmetic average of the indicator values $Z(s_1)$, …, $Z(s_N)$, as derived from measurement concentrations at the station points *i = 1, … , N*.

Other indicators are R^2 and the regression equation parameters *slope* and *intercept*, following from the scatter plot between the predicted (using cross-validation) and the observed concentrations.

RMSE should be as small as possible, bias (MPE) should be as close to zero as possible, R^2 should be as close to *1* as possible, slope *a* should be as close to *1* as possible, and intercept *c* should be as close to zero as possible (in the regression equation *y = a.x + c*).

In the cross-validation of $PM_{2.5}$ and NO_x, only stations with $PM_{2.5}$, resp. NO_x, measurement data are used (not the pseudo $PM_{2.5}$, resp. NO_x, stations).

Comparison of the point measurement and interpolated grid values

The comparison of point measurement and predicted grid values is described by the linear regression equation and its parameters and statistical values. The comparison is executed separately for rural and

urban background maps and for the final combined map. In the case of $PM_{2.5}$ and NO_x, only the stations with actual $PM_{2.5}$ resp. NO_x measurement data are used (not the pseudo $PM_{2.5}$ resp. NO_x stations).

The point observation – point cross-validation prediction analysis (Annex 3) describes interpolation performance at point locations when there is no observation (as it follows the leave-one-out approach). In this case, the smoothing effect of the interpolation is most prevalent.

The point observation – grid prediction approach indicates performance of the value for the 10x10 km^2 (resp. 2x2 km^2 or 1x1 km^2) grid cell with respect to the observations that are located within that cell. As such, some variability is due to smoothing but it also includes smoothing due to spatial averaging into the 10x10 km^2 (2x2 km^2, 1x1 km^2) grid cells. As such, the point-grid validation approach tells us how well our interpolated and aggregated grid values approximate the measurements at the actual station (point) locations. Whereas the point-point approach tells us how well our interpolated values estimate the indicator at a point where there is no actual measurement at that location, under the constrained that the point lies within the area covered by measurements.

Annex 2 – Input data

The types of input data in this paper are similar as in Horálek et al. (2020a), supplemented with the data needed for POD calculation. The air quality and meteorological data has been updated. For readability of this paper, we reproduce here the list of the input data. The key data is the air quality measurements at the monitoring stations extracted from Air Quality e-Reporting database, including geographical coordinates (*latitude*, *longitude*). The supplementary data cover the whole mapping domain and are converted into the EEA reference projection ETRS89-LAEA5210 on a 1 x 1 km^2 grid resolution (for health related indicators apart from ozone) resp. a 10x10 km^2 grid resolution (ozone). The data for the maps of vegetation related indicators (particularly AOT40) were converted – like in the previous reports (Horálek et al., 2020a, and references cited therein) – into a 2 x 2 km^2 resolution to allow accurate land cover exposure estimates to be prepared for use in Core Set Indicator 005 of the EEA.

A2.1 Air quality monitoring data

Air quality station monitoring data for the relevant year as extracted from the official EEA Air Quality e-Reporting database, EEA (2020a) in March 2020 has been used. This data set is supplemented with several EMEP rural stations from the database EBAS (NILU, 2020) not reported to the Air Quality e-Reporting database. Specifically, 6 additional stations for PM_{10}, 8 for $PM_{2.5}$, 11 for NO_2 and 5 for NO_x from the EBAS database (NILU, 2020) are added. Only data from stations classified as *background* (for the three types of area, *rural*, *suburban* and *urban*) are used for ozone. *Industrial* and *traffic* station types are not considered; they represent local scale concentration levels not applicable at the mapping resolution employed. For PM and NO_2, next to the background stations, also the stations classified as *traffic* for the types of area *suburban* and *urban* are used.

The following pollutants and aggregations are considered:

PM_{10} – annual average [$\mu g \cdot m^{-3}$], year 2018

– 90.4 percentile of the daily average values [$\mu g \cdot m^{-3}$], year 2018

$PM_{2.5}$ – annual average [$\mu g \cdot m^{-3}$], year 2018

Ozone – 93.2 percentile of the maximum daily 8-hour average values [$\mu g \cdot m^{-3}$], year 2018

– SOMO35 [$\mu g \cdot m^{-3} \cdot day$], year 2018

– SOMO10 [$\mu g \cdot m^{-3} \cdot day$], year 2018

– AOT40 for vegetation [$\mu g \cdot m^{-3} \cdot hour$], year 2018

– AOT40 for forests [$\mu g \cdot m^{-3} \cdot hour$], year 2018

– hourly values [$\mu g \cdot m^{-3}$], all hours of the year 2018 (for the purpose of POD mapping)

NO_2 – annual average [$\mu g \cdot m^{-3}$], year 2018

NO_x – annual average [$\mu g \cdot m^{-3}$], year 2018

NO – annual average [$\mu g \cdot m^{-3}$], year 2018 (for the purposes of NO_x mapping only)

The exact values of percentiles are actually 90.41 in the case of PM_{10} daily means and 93.15 in the case of ozone maximum daily 8-hour means.

For a considerable number of stations NO_x is measured, but it is not reported as such but separately as NO and NO_2. For these stations reporting NO and NO_2 separately, the NO_x concentrations were derived according to the equation

$$NO_x = NO_2 + \frac{46}{30} \cdot NO \qquad \text{(A2.1)}$$

In this equation, all components are expressed in µg·m^{-3}, with a molecular mass for NO of 30 g·mol^{-1} and for NO_2 of 46 g·mol^{-1}.

SOMO35 is the annual sum of the differences between maximum daily 8-hour concentrations above 70 µg·m^{-3} (i.e. 35 ppb) and 70 µg·m^{-3}. SOMO10 is the annual sum of the differences between maximum daily 8-hour concentrations above 20 µg·m^{-3} (i.e. 10 ppb) and 20 µg·m^{-3}. AOT40 is the sum of the differences between hourly concentrations greater than 80 µg·m^{-3} (i.e. 40 ppb) and 80 µg·m^{-3}, using only observations between 08:00 and 20:00 CET, calculated over the three months from May to July for AOT40 for vegetation and over the six months from April to September for AOT40 for forests.

Only the stations with annual data coverage of at least 75 percent are used. In the case of SOMO35, SOMO10 and AOT40 indicators, a correction for the missing data is applied according to the equation

$$I_{corr} = I \cdot \frac{N_{max}}{N} \qquad \text{(A2.2)}$$

where I_{corr} is the corrected indicator (SOMO35, SOMO10, AOT40 for vegetation or AOT40 for forests),

I is the value of the given indicator without any correction,

N is the number of the available daily resp. hourly data in a year for the given station,

N_{max} is the maximum possible number of the days or hours applicable for the given indicator.

For the indicators relevant to human health (i.e. for all PM_{10} and $PM_{2.5}$ indicators, ozone indicators 93.2 percentile of maximum daily 8-hour means, SOMO35 and SOMO10, and NO_2 annual average), data from *rural*, *urban* and *suburban background* stations are considered. (Throughout the paper, the urban and suburban stations are handled together). For PM_{10} and $PM_{2.5}$ and NO_2, also *urban* and *suburban traffic* stations are considered. For the indicators relevant to vegetation damage (i.e. for ozone AOT40 and POD parameters and NO_x annual average), only *rural background* stations are considered. In case of existing data (with sufficient annual time coverage) from two or more different measurement devices in the same station location, the average of these data is used.

We excluded the stations from French overseas areas (departments), Svalbard, Azores, Madeira and Canary Islands. These areas outside the EEA map extent *Map_2c* (EEA, 2018) were excluded from the interpolation and mapping domain.

Table A2.1 shows the number of the measurement stations selected for the individual pollutants and their respective indicators.

Table A2.1 Number of stations selected for each pollutant indicator and area type, 2018

Station type	PM_{10}		$PM_{2.5}$	ozone						NO_2	NO_x
	Ann. avg.	90.4 perc. of d. means	Annual average	93.2 perc. of dmax- 8h	SOMO35	SOMO10	AOT40 for veg.	AOT40 for forests	POD	Ann. avg.	Ann. avg.
Rural background	386	380	209	551	551	551	555	555	550	480	401
Urban/suburb. backgr.	1422	1409	688	1201	1201	1201				1381	
Urban/suburb. traffic	758	747	348							1060	

Compared to 2017, the number of rural background stations selected for 2018 increased by approximately 14 % for NO_x, 6-8 % for PM_{10} and NO_2, and 3-5 % for $PM_{2.5}$ and ozone. The number of the urban/suburban background stations increased by approximately 3-5 % for PM_{10} , ozone and NO_2,

while it remained almost the same for $PM_{2.5}$. The number of the NO_2 urban/suburban traffic stations increased by approximately 8 % for NO_2, 5 % for $PM_{2.5}$ and 1 % for PM_{10}.

For the $PM_{2.5}$ mapping, 199 additional rural background, 714 additional urban/suburban background and additional 428 urban/suburban traffic PM_{10} stations (at locations without $PM_{2.5}$ measurement) have been also used for the purpose of calculating the pseudo $PM_{2.5}$ station data.

In the case of NO_x, 352 stations with NO_x reported data have been used, while for 49 stations NO_x values are calculated from reported NO_2 and NO data using Eq. A2.1. Next to this, for the NO_x mapping 100 additional rural background NO_2 stations (at locations without NO_x measurement) were also used for the purpose of calculating the pseudo NO_x station data.

A2.2 EMEP MSC-W model output

The chemical dispersion model used in this paper is the EMEP MSC-W (formerly called Unified EMEP) model (version rv4.33), which is an Eulerian model. Simpson et al. (2012) and https://wiki.met.no/emep/page1/emepmscw_opensource (web site of Norwegian Meteorological Institute) describe the model in more detail. Emissions for the previous year 2017 (Mareckova et al., 2019) are used and the model is driven by ECMWF meteorology for the relevant year 2018. EMEP (2019) provides details on the EMEP modelling for 2018 using 2017 emission. The resolution of the model is 0.1°x0.1°, i.e. circa 10x10 km^2. For the second time, the model output based on the emission for the previous (not actual) year has been used, in agreement with conclusion of Horálek et al. (2016b), in order to enable the map creation a half year earlier than using the model results based on the actual emission.

We downloaded the EMEP data from NMI (2020) in the form of annual means, daily means and hourly means. Where relevant, we aggregated these primary data to the same set of parameters as we have for the air quality observations:

PM_{10} – *annual average* [µg·m^{-3}], year 2018

– *90.4 percentile of the daily average value* [µg·m^{-3}], year 2018 (aggregated from daily means)

$PM_{2.5}$ – *annual average* [µg·m^{-3}], year 2018

Ozone – *93.2 percentile of the highest maximum daily 8-hour average value* [µg·m^{-3}], year 2018 (aggregated from hourly means)

– *SOMO35* [µg·m^{-3}·day], year 2018 (aggregated from hourly means)

– *SOMO10* [µg·m^{-3}·day], year 2018 (aggregated from hourly means)

– *AOT40 for vegetation* [µg·m^{-3}·hour], year 2018 (aggregated from hourly means)

– *AOT40 for forests* [µg·m^{-3}·hour], year 2018 (aggregated from hourly means)

NO_2 – *annual average* [µg·m^{-3}], year 2018

NO_x – *annual average* [µg·m^{-3}], year 2018

Due to the complete temporal data coverage available at the modelled data, the PM_{10} indicator 90.4 percentile of daily means is identical with the 36th highest daily mean and the ozone indicator 93.2 percentile of maximum daily 8-hour means is identical with the 26th highest maximum daily 8-hour mean.

In the original format of the model results, a point represents the centre of a grid cell (in 0.1°x0.1° resolution). The data was imported into *ArcGIS* as a point shapefile and converted into ETRS89-LAEA5210 projection, subsequently converted into a 100x100 m^2 resolution raster grid and spatially aggregated into the reference EEA 10x10 km^2 grid (for ozone health related indicators), 1x1 km^2 grid (for PM and NO_2), resp. into the 2x2 km^2 grid (for vegetation related indicators).

A2.3 Other supplementary data

Altitude

We use the altitude data field (in meters) of *Global Multi-resolution Terrain Elevation Data 2010 (GMTED2010)*, with an original grid resolution of 15x15 arcseconds (some 463x463 m at 60N). Source: U.S. Geological Survey Earth Resources Observation and Science, see Danielson et al. (2011). We converted the field into the ETRS 1989 LAEA projection. (The resolution after projection was in 449.2x449.2 m). In the following step, we resampled the raster dataset to 100x100 m^2 resolution and shifted it to the extent of EEA reference grid. As a final step, the dataset was spatially aggregated into 1x1 km^2, 2x2 km^2 and 10x10 km^2 resolutions.

Meteorological parameters

The meteorological data used are the ECWMF data extracted from the CDS (Climate Data Store, https://cds.climate.copernicus.eu/cdsapp#!/home). Hourly data for 2018 are used. The most of the data come from the reanalysed data set ERA5-Land in 0.1°x0.1° resolution, namely the indicators:

Surface solar radiation [MWs.m^{-2}] – variable "Surface solar radiation downwards"

Temperature [K] – variable "2m temperature"

Wind speed [m.s^{-1}] – calculated based on variables "10m u-component of wind" and "10m v-component of wind"

Relative humidity [%] – calculated based on variables "2m temperature" and "2m dewpoint temperature"

Soil water – variable "Volumetric soil water layer 3", i.e. layer of 28-100 cm (used for POD only)

Wind speed (WV) is derived from the "10m u-component of wind" (10U) and "10m v-component of wind" (10V) according to relation

$$WV = \sqrt{(10U)^2 + (10V)^2} \qquad (3.1)$$

Relative humidity (RH) is derived by means of the saturated water vapour pressure (e_t) as a function of "2m temperature" *(2T)* and "2m dew point temperature" *(2D)* according to relation

$$RH = \frac{e_{2D}}{e_{2T}} \cdot 100 \text{ , with } e_t = 6.1365^{(17.502 \cdot t/(240.97+t))} \qquad (3.2)$$

where *t* is 2T and 2D respectively.

In the coastal areas (where the data from ERA5-Land are not available), the same parameters from the reanalysed data set ERA5 in 0.25°x0.25° resolution are applied. Next to this, the following data (not available in the ERA5-Land data set) from the ERA5 data set is also used:

Friction velocity – variable “Friction velocity”

Next to the meteorological data of ERA5-Land and ERA5, the following indicators based on the meteorological ECWMF’s IFS (Integrated Forecasting System) data and coming from the CHIMERE pre-processing are used, being the hourly data for 2018 in 0.1°x0.1° resolution:

Obukhov length

Air density

The most of the meteorological parameters is used for POD maps only. For other maps than POD, annual aggregations based on hourly data are used, namely for the parameters:

Wind speed	– annual average [$m \cdot s^{-1}$], year 2018
Relative humidity	– annual average [%], year 2018
Surface solar radiation	– annual average of daily sum [$MWs.m^{-2}$], year 2018

The annual data are imported into *ArcGIS* as a point shapefile. Each point represents the centre of a grid cell. The shapefile is converted into ETRS89-LAEA5210 projection, converted into a 100x100 m^2 resolution raster grid and spatially aggregated into the reference EEA 1x1 km^2 grid, 10x10 km^2 grid, and 2x2 km^2 grid.

Population density and population totals

Population density (in $inhbs.km^{-2}$, census 2011) is based on *Geostat 2011* grid dataset, Eurostat (2014). The dataset is in 1x1 km^2 resolution, in the EEA reference grid.

For regions not included in the Geostat 2011, alternative sources were used. Primarily, *JRC (Joint Research Centre)* population data in resolution 100x100 m^2 were used (JRC, 2009). The JRC 100x100 m^2 population density data is spatially aggregated into the reference 1x1 km^2 EEA grid. For regions that are neither included in the Geostat 2011 nor in the JRC database, we used population density data from *ORNL LandScan Global Population Datase*, https://landscan.ornl.gov/. This dataset in 30x30 arcsec resolution; based on the annual mid-year national population estimates for 2008 (from the Geographic Studies Branch, US Bureau of Census, http://www.census.gov) was earlier re-projected and converted from its original WGS1984 30x30 arcsecs grids into EEA's reference projection ETRS89-LAEA5210 at 1x1 km^2 resolution by the EEA (EEA, 2010).

The areas lacking Geostat 2011 data, and supplemented with JRC or ORNL data were: Gibraltar (JRC); Faroe Islands, British crown dependencies (Jersey, Guernsey and Man) and northern Cyprus (ORNL). As such, the Geostat 2011 1x1 km^2 data and these supplements cover the entire mapping area.

To verify the consistency of merging Geostat 2011 with JRC and ORNL data, we compared the Geostat 2011 data and the JRC supplemented with ORNL data on the basis of the national population totals of the individual countries. Additionally, we verified the national population totals for the Geostat 2011 gridded data with the Eurostat national population data for 2018 (Eurostat, 2020). Figure A2.1 presents both comparisons. From these verifications, one can conclude a high correlation of the national population totals of each data source. Slight underestimation of the supplemented JRC and ORNL data

in comparison with the Geostat 2011 data can be seen, which is caused by the fact that the Geostat 2011 data is more up-to-date than both the JRC and the ORNL data source. Geostat 2011 and Eurostat 2018 data correlate even better and leads to a similar conclusion. Based on this, we used in the further calculations on national population totals the actual Eurostat data for 2018 (Eurostat, 2020), as described further.

Population density data can be used to classify the spatial distribution of each type of area (rural, urban or mixed population density) in Europe. We use this information to select and weight the air quality values, grid cell by grid cell and merge them into a final combined map (Annex 1). Furthermore, we use it to estimate population health exposure and exceedance numbers per country and for Europe as a whole, including involved uncertainties. These activities take place on the 1x1 km^2 resolution grid in accordance with the recommendations of Horálek et al. (2010). The supplemented Geostat data (as described above) are used in all the calculations.

Figure A2.1 Correlation of national population totals for JRC supplemented with ORNL (left) and Eurostat 2018 (right) with Geostat 2011

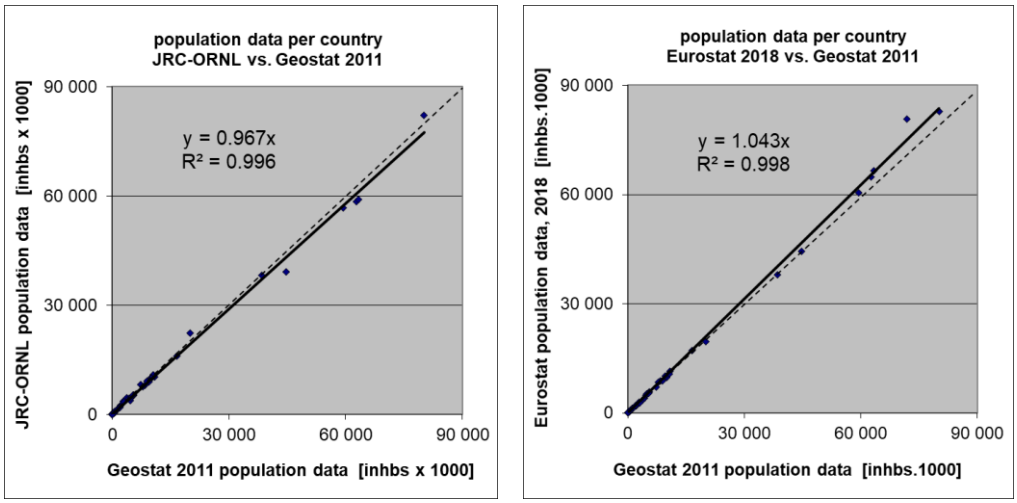

National population totals presented in the exposure tables of this paper are based on Eurostat national population data for 2018 (Eurostat, 2020). For France, Portugal and Spain, the population totals of areas outside the mapping area (i.e. French oversea departments Azores, Madeira and Canarias) are subtracted. For northern part of Cyprus which do not have 2018 data in the Eurostat database, the population total is based on alternative data (namely http://www.devplan.org/frame-eng.html).

Land cover

CORINE Land Cover 2018 – grid 100 x 100 m^2, Version 2020_20 is used (EU, 2020). The country missing in this database is Andorra, the area missing in this database is Jan Mayen. Due to the lack of land cover data for Andorra, we excluded this country from the process of exposure estimates related to the vegetation based AOT40 ozone indicators.

In agreement with Horálek et al. (2017b), the 44 CLC classes have been re-grouped into the 8 more general classes. In this paper we use four of these general classes, see Table A2.2.

Table A2.2 General land cover classes, based on CLC2012 classes, used in mapping

Label	General class description	CLC classes grid codes	CLC classes codes	CLC classes description
HDR	High density residential areas	1	111	Continuous urban fabric
LDR	Low density residential areas	2	112	Discontinuous urban fabric
AGR	Agricultural areas	12 - 22	211 - 244	Agricultural areas
NAT	Natural areas	23 - 34	311 - 335	Forest and semi natural areas

Two aggregations are used, i.e. into 1x1 km^2 grid and into the circle with radius of 5 km. For each general CLC class we spatially aggregated the high land use resolution into the 1x1 km^2 EEA standard grid resolution. The aggregated grid square value represents for each general class the total area of this class as percentage of the total 1x1 km^2 square area. For details, see Horálek (2017b).

Road type vector data

GRIP (Meijer et al., 2016) vector road type data base provided by PBL is used. The road types are distributed into 5 classes, from highways to local roads and streets. In agreement with Horálek et al. (2017b), road classes No. 1 "Highways", No. 2 "Primary roads" and No. 3 "Secondary roads" are used.

Percentage of the area influenced by traffic is represented by buffers around the roads: for the individual classes 1-3 and for classes 1-3 together, at all 1x1 km^2 grid cells; a buffer of 75 metres distance at each side from each road vector is taken for the roads of classes 1 and 2, while a buffer of 50 metres is taken for the roads of class 3. For motivation and calculation details, see Horálek et al. (2017b).

Satellite data

Annual average NO_2 dataset was constructed from data acquired by the *OMI* instrument onboard the Aura platform. The parameter used is

NO_2 – annual average tropospheric vertical column density (VCD) [number of NO_2 molecules per cm^2 of earth surface], year 2018 (aggregated from daily data).

The OMNO2d product generated by NASA was used as a basis, NASA (2020). The tropospheric column was used. All the orbits within a given day (typically observed between 13:00 and 14:00 local time) are mapped into a 0.25x0.25 degrees grid. For details, see Horálek et al. (2018). The data were converted to ArcGIS and spatially transformed to the reference EEA 1x1 km^2 grid, like in the case of modelled data.

Soil hydraulic properties data

JRC data called "Maps of indicators of soil hydraulic properties for Europe" in 1x1 km^2 resolution are used, JRC (2016). Namely the following indicators are used:

Wilting Point – water content at wilting point [$cm^3 \cdot cm^{-3}$]

Field Capacity – water content at field capacity [$cm^3 \cdot cm^{-3}$]

The soil hydraulic properties data are used for POD calculations only.

Annex 3 – Technical details and mapping uncertainties

This annex contains technical details on the linear regression models and the residual kriging, including the performance. Furthermore, uncertainty estimates for the maps of the indicators are given.

A3.1 PM_{10}

Technical details on the interpolation model and uncertainty estimates for both PM_{10} indicators maps annual average (Map 2.1) and 90.4 percentile of daily means (Map 2.2) are presented in this section.

Technical details on the interpolation model

Table A3.1 presents the estimated parameters of the linear regression models (c, a_1, a_2, …) and of the residual kriging (nugget, sill, range) and includes the statistical indicators of both the regression and the kriging, for both PM_{10} indicators. The linear regression and ordinary kriging on its residuals is applied on the logarithmically transformed data of both measurement and modelled PM_{10} values. In Table A3.1 the standard error and variogram parameters (nugget, sill and range) refer to these transformed data, whereas RMSE and bias refer to the interpolation after a back-transformation.

Since 2017, an updated methodology as developed and tested under Horálek et al. (2019) has been used, i.e. including land cover among the supplementary data and using the traffic urban map layer.

The adjusted R^2 and standard error are indicators for the fit of the regression relationship, where the adjusted R^2 should be as close to 1 as possible and the standard error should be as small as possible. The adjusted R^2 for the rural areas was 0.67 at the annual average and 0.61 at the P90.4; for the urban background areas 0.32 at the annual average and 0.28 at the P90.4; for the urban traffic areas 0.39 at the annual average and 0.30 at the P90.4.

RMSE (the smaller the better) and bias (the closer to zero the better), highlighted by orange, are the cross-validation indicators, showing the quality of the resulting map. The bias indicates to what extent the predictions are under- or overestimated on average. Further in this section, more detailed uncertainty analysis is presented.

Table A3.1 Parameters and statistics of linear regression model and ordinary kriging of PM_{10} indicators annual average and 90.4 percentile of daily means for 2018 in rural, urban background and urban traffic areas for the final combined map

		Annual average			90.4 percentile of daily means		
		Rural areas	Urb. b. ar.	Urb. tr. ar.	Rur. ar.	Urb. b. ar.	Urb. tr. ar.
Linear regresion model (LRM, Eq. A1.3)	c (constant)	2.02	1.60	2.13	2.06	1.68	2.54
	a1 (log. EMEP model)	0.670	0.635	0.49	0.645	0.657	0.44
	a2 (altitude GMTED)	-0.00019			-0.00015		
	a3 (wind speed)	-0.079		-0.055	-0.065		-0.067
	a4 (relative humidity)	-0.641			-0.461		
	a5 (land cover NAT)	-0.002			-0.002		
	Adjusted R^2	**0.67**	**0.32**	**0.39**	**0.61**	**0.28**	**0.30**
	Stand. Error [µg.m^{-3}]	**0.22**	**0.33**	**0.26**	**0.24**	**0.36**	**0.28**
Ordinary kriging (OK) of LRM residuals	nugget	0.023	0.013	0.014	0.027	0.016	0.012
	sill	0.047	0.065	0.040	0.051	0.086	0.049
	range [km]	1000	670	360	1000	660	450
LRM + OK of its residuals	**RMSE [µg.m^{-3}]**	**2.9**	**6.5**	**4.7**	**5.5**	**12.0**	**8.4**
	Relative RMSE [%]	**17.5**	**26.1**	**19.4**	**19.2**	**28.1**	**20.8**
	Bias (MPE) [µg.m^{-3}]	**0.4**	**0.1**	**0.2**	**0.7**	**0.3**	**0.2**

Uncertainty estimated by cross-validation

Using RMSE as the most common indicator, the *absolute mean uncertainty* of the final combined map at areas 'in between' the station measurements can be expressed in µg·m^{-3}. Table A3.1 shows that the absolute mean uncertainty of the final combined map of PM_{10} annual average resp. 90.4 percentile of daily means expressed by RMSE is 2.9 µg·m^{-3} resp. 5.5 µg·m^{-3} for the rural areas, 6.5 µg·m^{-3} resp. 12.0 µg·m^{-3} for the urban background areas, and 4.7 µg·m^{-3} resp. 8.4 µg·m^{-3} for the urban traffic areas. Alternatively, one can express this uncertainty in relative terms by relating the absolute RMSE uncertainty to the mean air pollution indicator value for all stations. This *relative mean uncertainty* (Relative RMSE) of the final combined map of PM_{10} annual average resp. 90.4 percentile of daily means is 17.5 % resp. 19.2 % for rural areas, 26.1 % resp. 28.1 % for urban background areas, and 19.4 % resp. 20.8 % for urban traffic areas. These quite high numbers in urban background areas compared to previous years up to 2015 are caused by inclusion of Turkey since 2016 mapping. For the mapping results without Turkey, the relative mean uncertainty is 16.5 % resp. 17.7 % for rural areas, 19.0 % resp. 21.0 % for urban background areas and 18.4 % resp. 19.4 % for urban traffic areas. Nevertheless, the relative uncertainty values including Turkey fulfil the data quality objectives for models as set in Annex I of the AQ Directive (EC, 2008).

Figure A3.1 shows the cross-validation scatter plots, obtained according to Annex 1, for rural, urban background and urban traffic areas, for both PM_{10} indicators. The R^2 indicates that the variability is attributable to the interpolation for about 79 % resp. 76 % at the rural areas, for about 71 % at the urban background areas, and for about 75 % % at the urban traffic areas.

Figure A3.1 Correlation between cross-validated predicted (y-axis) and measurement values for PM_{10} indicators annual average (top) and 90.4 percentile of daily means (bottom) for 2018 for rural (left) and urban background (middle) and urban traffic (right) areas

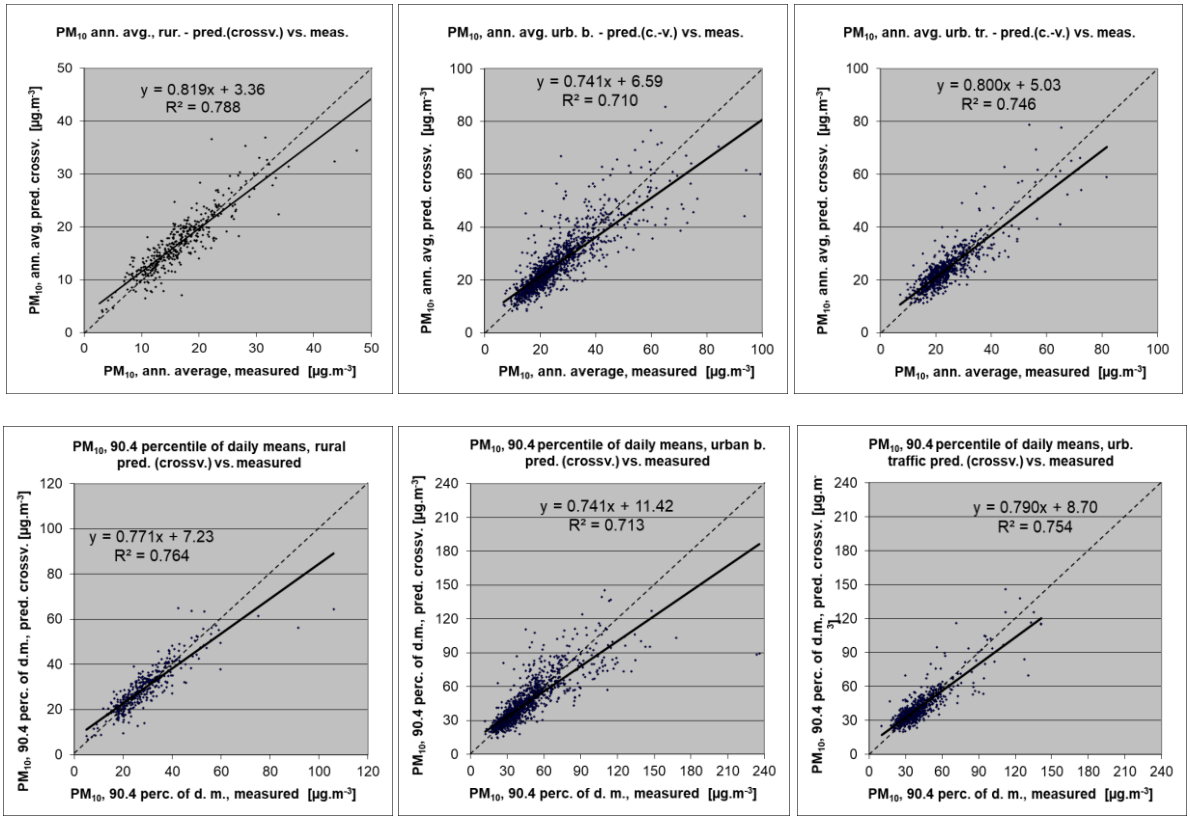

The trend line in the scatter-plots deviates at the lowest values somewhat above, and at the higher values under the symmetry axis, indicating that the interpolation methods tend to underestimate the high concentrations and overestimate the low concentrations. For example, in urban background areas for annual average an observed value of 55 µg·m^{-3} is estimated in the interpolations to be about 48 µg·m^{-3}, about 13 % lower. This underestimation at high values is common to all spatial interpolation methods. It could be reduced by either using a higher number of stations with an improved spatial distribution, or by introducing an improved regression that uses either other supplementary data or more advanced chemical transport model (resp. model in finer resolution).

Comparison of point measurement values with the predicted grid value

In addition to the above *point observation – point prediction* cross-validation, a simple comparison has been made between the point observation values and interpolated prediction values spatially averaged at grid cells. This *point observation – grid averaged prediction* comparison indicates to what extent the predicted value of a grid cell represents the corresponding measurement values at stations located in that cell. The comparison has been made primarily for the separate rural, urban background and urban traffic map layers at 1x1 km^2 resolution. (One can directly relate this comparison result to the cross-validation results of Figure A3.1). Next to this, the comparison has been done also for the final combined maps at the same 1x1 km^2 resolution. Figure A3.2 shows the scatterplots for these comparisons, for PM_{10} annual average only as an illustration. The results of the point observation – point prediction cross-validation of Figure A3.1 and those of the point observation – grid averaged prediction validation for separate rural and separate urban background maps, and for the final combined maps are summarised in Table A3.2 for both PM_{10} indicators.

Figure A3.2 Correlation between predicted grid values from rural (upper left), urban background (upper middle) and urban traffic (upper right) map layer and final combined map (all bottom) (y-axis) versus measurements from rural (left), urban/suburban background (middle) and urban/suburban traffic stations (right) (x-axis) for PM_{10} annual average 2018

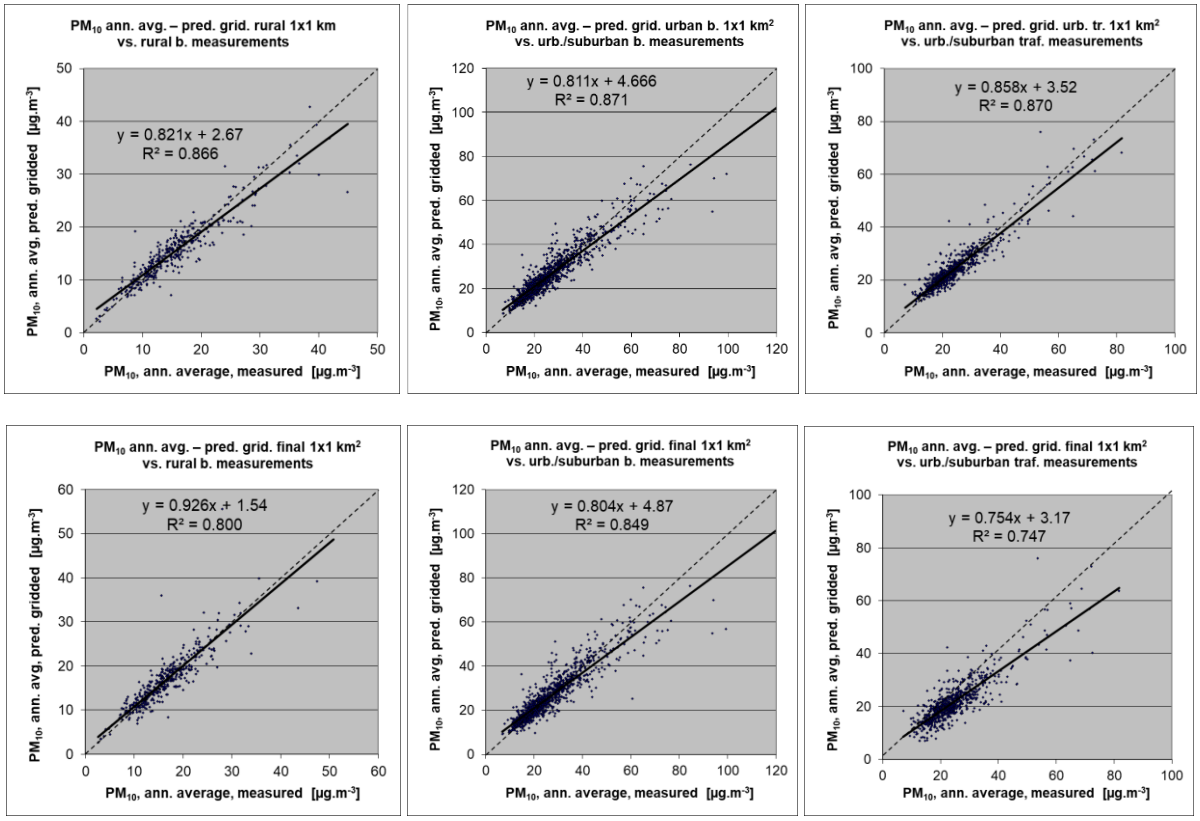

Table A3.2 Statistical indicators from the scatter plots for the predicted grid values from separate (rural, urban background or urban traffic) map layers and final combined map versus the measurement point values for rural (upper left), urban background (upper right) and urban traffic (bottom left) stations for PM_{10} indicators annual average (top) and 90.4 percentile of daily means (bottom) for 2018

PM_{10}	rural backgr. stations				urban/suburban backgr. stations			
	RMSE	bias	R^2	lin. r. equation	RMSE	bias	R^2	lin r. equation
Annual average								
cross-valid. prediction, separate (r or ub) map layer	2.9	0.4	0.778	y = 0.819x + 3.36	6.5	0.1	0.710	y = 0.741x + 6.59
grid prediction, 1x1 km^2 separ. (r or ub) map layer	2.3	-0.2	0.871	y = 0.840x + 2.50	4.4	-0.1	0.871	y = 0.811x + 4.67
grid prediction, 1x1 km^2 final combined map	2.9	0.3	0.800	y = 0.926x + 1.54	4.7	0.0	0.849	y = 0.804x + 4.87
90.4 percentile of daily means								
cross-valid. prediction, separate (r or ub) map layer	5.5	0.7	0.764	y = 0.771x + 7.23	12.0	0.3	0.764	y = 0.771x + 7.23
grid prediction, 1x1 km^2 separ. (r or ub) map layer	4.5	-0.5	0.846	y = 0.788x + 5.56	7.9	-0.2	0.881	y = 0.812x + 7.85
grid prediction, 1x1 km^2 final combined map	5.8	0.1	0.748	y = 0.840x + 4.71	8.6	-0.2	0.857	y = 0.803x + 8.23

PM_{10}	urban/suburban traffic stations			
	RMSE	bias	R^2	lin. r. equation
Annual average				
cross-valid. prediction, urban traffic map layer	4.7	0.2	0.746	y = 0.800x + 5.03
grid prediction, 1x1km^2 urban traffic map layer	3.3	0.1	0.870	z = 0.858x + 3.52
grid prediction, 1x1 km^2 final combined map	5.4	-2.8	0.747	y = 0.754x + 3.17
90.4 percentile of daily means				
cross-valid. prediction, urban traffic map layer	8.4	0.2	0.754	y = 0.790x + 8.70
grid prediction, 1x1km^2 urban traffic map layer	5.8	0.2	0.883	y = 0.873x + 5.35
grid prediction, 1x1 km^2 final combined map	9.7	-4.5	0.738	y = 0.747x + 5.73

By comparing the scatterplots and the statistical indicators for the separate rural and separate urban background map with the final combined maps in both resolutions, one can evaluate the level of representation of the rural resp. urban background areas in the final combined maps. Both the rural and the urban air quality are fairly well represented in the 1x1 km^2 final combined map, while the traffic air quality is underestimated in this spatial resolution. One can conclude that the final combined map in 1x1 km^2 resolution is representative for rural and urban background areas, but not for urban traffic areas.

The Table A3.2 shows a better relation (i.e. lower RMSE, higher R^2, smaller intercept and slope closer to 1) between station measurements and the interpolated values of the corresponding grid cells at either rural, urban background or urban traffic areas than it does at the point cross-validation predictions. That is because the simple comparison between point measurements and the gridded interpolated values shows the uncertainty at the actual station locations (points), while the point cross-validation prediction simulates the behaviour of the interpolation at point positions assuming no actual measurement would exist at that point. The uncertainty at measurement locations is introduced partly by the smoothing effect of the interpolation and partly by the spatial averaging of the values in the 1x1 km^2 grid cells. The level of the smoothing effect leading to underestimation at areas with high values is there smaller than in situations where no measurement is represented in such areas. For example, in urban background areas the predicted interpolation gridded annual average value in the separate urban background map will be about 49 $\mu g \cdot m^{-3}$ at the corresponding station point with the measurement value of 55 $\mu g \cdot m^{-3}$. This means an underestimation of about 10 %. It is a slightly less than the prediction underestimation of 13 % at the same point location, when leaving out this one actual measurement point and the interpolation is done without this station (see the previous subsection).

A3.2 $PM_{2.5}$

Technical details and uncertainty estimates for Map 3.1 with the $PM_{2.5}$ annual average are presented in this section.

Technical details on the interpolation model

Like for PM_{10}, an updated methodology as developed and tested under Horálek et al. (2019) has been used, i.e. including the land cover among supplementary data and using the traffic urban map layer.

Table A3.3 presents the regression coefficients determined for pseudo $PM_{2.5}$ stations data estimation, based on the 759 rural and urban/suburban background and 307 urban/suburban traffic stations that have both $PM_{2.5}$ and PM_{10} measurements available (see Section 2.1.1).

Table A3.3 Parameters and statistics of linear regression model for generation of pseudo $PM_{2.5}$ data, regardless of rural or urban/suburban area, for $PM_{2.5}$ annual average 2018

		Rural and urban background areas	Urban traffic areas
Linear regresion model (LRM, Eq. A1.1)	c (constant)	37.4	44.1
	b (PM_{10} measurement data)	0.666	0.531
	a1 (surface solar radiation)	-1.503	-1.358
	a2 (latitude)	-0.391	-0.531
	a3 (longitude)	0.077	0.069
	Adjusted R^2	**0.85**	**0.74**
	Standard Error [µg.m^{-3}]	**2.3**	**2.5**

The same supplementary data as in Horálek et al. (2019) has been used, apart from the wind speed, which was found not significant.

Table A3.4 presents the estimated parameters of the linear regression models (*c, a_1, a_2,…*) and of the residual kriging (*nugget, sill, range*) and includes the statistical indicators of both the regression and the kriging of its residuals. Like in the case of PM_{10}, the linear regression is applied on the logarithmically transformed data of both measurement and modelled $PM_{2.5}$ values. Thus, the standard error and variogram parameters refer to these transformed data, whereas RMSE and bias refer to the interpolation after the back-transformation.

Table A3.4 Parameters and statistics of linear regression model and ordinary kriging of $PM_{2.5}$ annual average 2018 in rural, urban background and urban traffic areas for final combined map

$PM_{2.5}$		Annual average		
		Rural areas	Urban b. areas	Urban tr.. areas
Linear regresion model (LRM, Eq. A1.3)	c (constant)	1.22	1.40	1.44
	a1 (log. EMEP model)	0.740	0.58	0.547
	a2 (altitude GMTED)	-0.00030		
	a3 (wind speed)	-0.071		
	a4 (land cover NAT1)	-0.0009		
	Adjusted R^2	**0.66**	**0.28**	**0.46**
	Standard Error [µg.m^{-3}]	**0.27**	**0.33**	**0.27**
Ordinary kriging (OK) of LRM residuals	nugget	0.034	0.020	0.017
	sill	0.063	0.085	0.043
	range [km]	650	1000	350
LRM + OK of its residuals	**RMSE [µg.m^{-3}]**	**2.2**	**2.7**	**2.8**
	Relative RMSE [%]	**20.0**	**18.1**	**20.4**
	Bias (MPE) [µg.m^{-3}]	**0.2**	**0.2**	**0.1**

The adjusted R^2 and standard error are indicators for the *quality of the fit of the regression relation*. The adjusted R^2 is 0.66 for the rural areas, 0.28 for urban background areas and 0.46 for urban traffic areas. Somewhat weaker regression relation in the urban background areas causes a higher impact of the interpolation part of the interpolation-regression-merging mapping methodology in these areas.

RMSE and bias – highlighted in orange – are the cross-validation indicators, showing the *quality of the resulting map*; the bias indicates to what extent the predictions are under- or overestimated on average. Only stations with $PM_{2.5}$ measurement data are used for calculating the RMSE and the bias (i.e. only non-pseudo $PM_{2.5}$ stations are used). These statistical indicators are calculated excluding the pseudo stations because they are estimated values only, not actual measurement values. According to Denby et al (2011b), the pseudo $PM_{2.5}$ data does not satisfy the quality objectives for fixed monitoring alone. The pseudo stations are used as they improve the mapping estimate. Whereas the actual measurements can be used for evaluating the *quality of the map*. For the future, we consider to quit the application of the $PM_{2.5}$ pseudo stations as the current number of the actual $PM_{2.5}$ measurement stations has increased over time such that the use of pseudo $PM_{2.5}$ stations may not contribute enough any longer to improve the mapping estimates.

Due to the lack of rural stations in Turkey for $PM_{2.5}$, no proper interpolation results could be presented for this country in a rural map, so we do not present the estimated $PM_{2.5}$ values for Turkey in the final map. Thus, the stations located in Turkey have not been used in the uncertainty estimates (although used in the mapping process), as they lie outside the mapping area.

Uncertainty estimated by cross-validation

Table A3.4 shows that the absolute mean uncertainty of the final combined map of $PM_{2.5}$ annual average expressed as RMSE is 2.2 µg·m^{-3} for the rural areas and 2.7 µg·m^{-3} for the urban background areas and 2.8 µg·m^{-3} for the urban traffic areas. On the other hand, the *relative mean uncertainty* (Relative RMSE) of the final combined map of $PM_{2.5}$ annual average is 20.0 % for rural areas, 18.1 % for urban background areas and 20.4 % for urban traffic areas. These relative uncertainty values fulfil the data quality objectives for models as set in Annex I of the AQ Directive (EC, 2008).

Figure A3.3 shows the cross-validation scatter plots, obtained according to Section A1.3, for both the rural and urban areas. The R^2 indicates that about 79 % of the variability is attributable to the interpolation for the rural and also for the urban background areas and 73 % for the urban traffic areas.

Figure A3.3 Correlation between cross-validated predicted and measurement values for $PM_{2.5}$ annual average 2018 for rural (left), urban background (middle) and urban traffic (right) areas

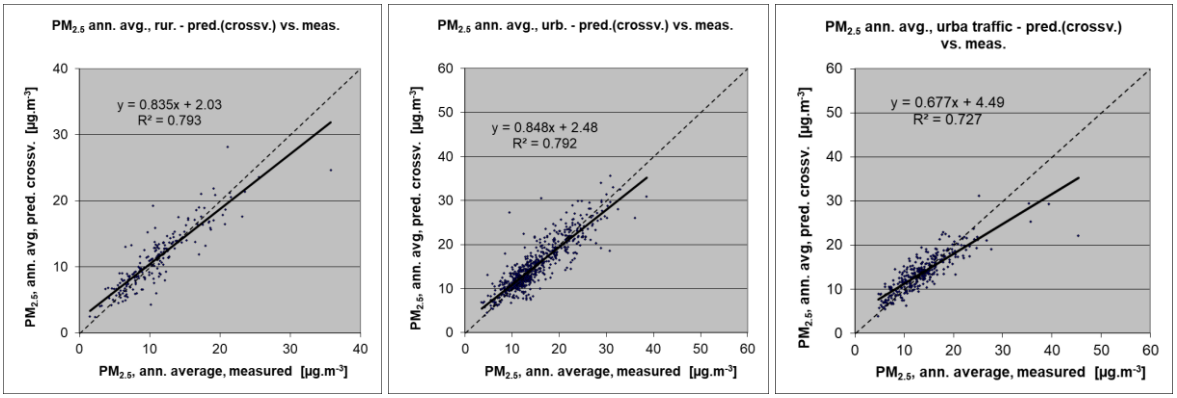

The scatter plots indicate that in areas with high concentrations the interpolation methods tend to underestimate the levels. For example, in rural areas an observed value of 25 µg·m^{-3} is estimated in the interpolations to be about 23 µg·m^{-3}, which is an underestimated prediction of about 8 %. This underestimation at high values is an inherent feature of all spatial interpolations. It could be reduced by either using a higher number of the stations at improved spatial distribution, or by introducing a closer regression that uses either other supplementary data or more improved CTM output.

Comparison of point measurement values with the predicted grid value

Like for PM_{10}, a simple comparison has been made between the point observation values and interpolated prediction values spatially averaged in grid cells, in addition to the cross-validation. The comparison has been made primarily for the separate rural, urban background and urban traffic map layers at 1x1 km^2 resolution. Next to this, the comparison has been done also for the final combined maps at the same 1x1 km^2 resolution. Figure A3.4 shows the scatterplots for these comparisons.

The results of the point observation – point prediction cross-validation of Figure A3.3 and those of the point observation – grid averaged prediction validation of Figure A3.4 for separate map layers and for the final combined map are summarised in Table A3.5.

Figure A3.4 Correlation between predicted grid values from rural (upper left), urban background (upper middle) and urban traffic (upper right) map layer and final combined map (all bottom) (y-axis) versus measurements from rural (left), urban/suburban background (middle) and urban/suburban traffic stations (right) (x-axis) for $PM_{2.5}$ annual average 2018

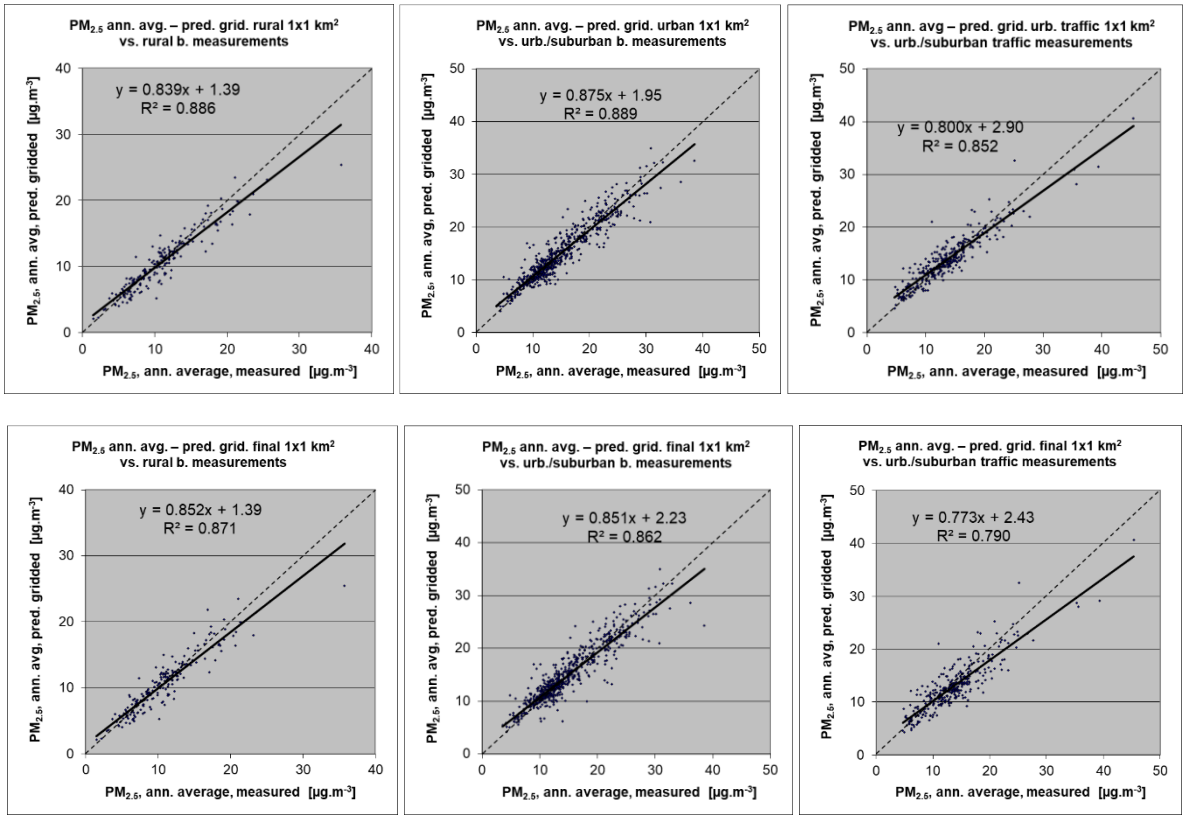

By comparing the scatterplots and the statistical indicators for separate rural, urban background and urban traffic map layers with the final combined maps, one can evaluate the level of representation of the rural, urban background and urban traffic areas in the final combined map. Similar results as for PM_{10} can be observed: the final combined map in 1x1 km^2 resolution is fairly well representative for rural and urban background areas, but not for urban traffic areas.

Like in the case of PM_{10}, Table A3.5 shows a better correlated relation with the station measurements (i.e. lower RMSE, higher R^2, smaller intercept and slope closer to 1) for the simply interpolated gridded values than for the point cross-validation predictions, at both rural and urban background map areas. That is because the simple comparison shows the uncertainty at the actual station locations, while the cross-validation prediction simulates the behaviour of the interpolation (within the area covered by measurements) at point positions assuming no actual measurements would exist at these points.

Table A3.5 Statistical indicators from the scatter plots for the predicted grid values from separate (rural, urban background or urban traffic) map layers and final combined map versus the measurement point values for rural (upper left), urban background (upper right) and urban traffic (bottom left) stations for $PM_{2.5}$ annual average 2018

$PM_{2.5}$	rural backgr. stations				urban/suburban backgr. stations			
	RMSE	bias	R^2	lin. r. equation	RMSE	bias	R^2	lin r. equation
cross-valid. prediction, separate (r or ub) map layer	2.2	0.2	0.793	y = 0.835x + 2.03	2.7	0.2	0.792	y = 0.848x + 2.48
grid prediction, 1x1 km^2 separ. (r or ub) map layer	1.9	-0.4	0.886	y = 0.839x + 1.39	1.9	0.1	0.889	y = 0.875x + 1.95
grid prediction, 1x1 km^2 final merged map	1.7	-0.2	0.871	y = 0.852x + 1.39	2.1	0.1	0.862	y = 0.851x + 2.23

$PM_{2.5}$	urban/suburban traffic stations			
	RMSE	bias	R^2	lin. r. equation
cross-valid. prediction, urban traffic map layer	2.8	0.1	0.727	y = 0.677x + 4.49
grid prediction, 1x1 km^2 urban traffic map layer	2.0	0.2	0.852	y = 0.800x + 2.90
grid prediction, 1x1 km^2 final merged map	2.5	-0.6	0.790	y = 0.773x + 2.43

The uncertainty at measurement locations is introduced partly by the smoothing effect of the interpolation and partly by the spatial averaging of the values in the 1x1 km^2 grid cells. For example, in urban background areas the predicted interpolation gridded value in the final map will be about 28 $\mu g \cdot m^{-3}$ at the corresponding station point with the measurement value of 30 $\mu g \cdot m^{-3}$ (calculated based on the linear regression equation), which coincides with an underestimation of about 6 %.

A3.3 Ozone

In this section, we present the technical details and the uncertainty estimates for the maps of ozone health-related indicators 93.2 percentile of maximum daily 8-hour means, SOMO35 and SOMO10 (Maps 4.1-4.3), as well as for the maps of ozone vegetation-related indicators AOT40 for vegetation and AOT40 for forests (Maps 4.4 and 4.5). Next to this, we present the details of POD maps.

Technical details on the interpolation model

Table A3.6 presents the estimated parameters of the linear regression models and of the residual kriging, including the statistical indicators of both the regression and the kriging.

The adjusted R^2 and standard error show the quality of the fit of the regression relation. For the rural areas, all indicators show the value of the adjusted R^2 between 0.30 and 0.39. For the urban areas, the adjusted R^2 is 0.35 for 93.2 percentile of daily 8-hour maximum and 0.29 for SOMO35, while for SOMO10 it is only 0.12. For the vegetation-related indicators the urban maps are not constructed.

RMSE and bias – highlighted by orange – are the cross-validation indicators, showing the quality of the resulting map.

Table A3.6 Parameters and statistics of linear regression model and ordinary kriging for ozone indicators 93.2 percentile of maximum daily 8-hourly means, SOMO35 and SOMO10 in rural and urban areas for the final combined map and for O_3 indicators AOT40 for vegetation and for forests in rural areas for 2018

		93.2 perc. of dmax 8h		SOMO35		SOMO10		AOT40v	AOT40f
		Rur. areas	Urb. ar.	Rur. ar.	Urb.ar.	Rur. ar.	Urb.ar.	Rur. ar.	Rur. ar.
Linear regresion model (LRM, Eq. A1.3)	c (constant)	8.4	9.0	599	1679	6015	8136	998	1456
	a1 (EMEP model)	1.02	0.97	0.71	0.62	0.69	0.37	0.83	0.68
	a2 (altitude GMTED)	*n.sign.*		0.62		1.39		*n. sign.*	*3.81*
	a3 (wind speed)		*n.sign.*		*n.sign.*		*n. sign.*		
	a4 (s. solar radiation)	*n.sign.*	*n.sign.*	102.7	*n.sign.*	*n.sign.*	248.5	565.8	910.4
	Adjusted R^2	**0.37**	**0.35**	**0.39**	**0.29**	**0.30**	**0.12**	**0.39**	**0.44**
	Stand. Err. [µg.m^{-3}.x]*	**11.4**	**13.7**	**1930**	**1901**	**3053**	**3436**	**6484**	**11517**
Ord. krig. (OK) of LRM	nugget	20	75	1.4E+06	1.6E+06	2.9E+06	4.8E+06	2.1E+07	4.7E+07
	sill	86	106	3.2E+06	2.4E+06	7.3E+06	6.4E+06	4.3E+07	1.4E+08
	range [km]	140	120	360	300	190	120	860	860
LRM + OK of its residuals	**RMSE [µg.m^{-3}.x]***	**9.6**	**10.3**	**1769**	**1518**	**2809**	**2673**	**5736**	**10230**
	Relative RMSE [%]	**7.9**	**8.8**	**27.4**	**28.8**	**12.6**	**13.6**	**29.6**	**29.7**
	Bias (MPE) [µg.m^{-3}.x]*	**0.1**	**0.1**	**-18**	**-1**	**-35**	**-4**	**-48**	**-149**

*) Units – 93.2 percentile of daily 8-h maximums: [µg·m^{-3}], SOMO35: [µg·m^{-3}·d], AOT40v and AOT40f: [µg·m^{-3}·h].

Uncertainty estimated by cross-validation

The basic uncertainty analysis is provided by cross-validation. Table A3.6 shows both absolute and relative mean uncertainty, expressed by RMSE and Relative RMSE. The relative mean uncertainty of the 2018 ozone map is at the 93.2 percentile of daily 8-h maximums about 8 % for rural areas and 9 % for urban areas, around 27-29 % for SOMO35, around 13-14 % for SOMO10 and about 30 % at AOT40 for both vegetation and forests. The small levels of the relative uncertainty for the 93.2 percentile of maximum daily 8-h means and SOMO10 are highly influenced by the low ratio between the relevant standard error and mean calculated based on all annual station concentration data: for these two indicators the ratio is at the level of about 0.12- 0.19, while for SOMO35 and for both AOT40 indicators it is at the level of about 0.38-0.45.

Figure A3.5 shows the cross-validation scatter plots for both the rural and urban areas of the 2018 map for the health-related ozone indicators.

The R^2, an indicator for the interpolation correlation with the observations, shows that for the health related ozone indicators, about 40-56 % is attributable to the interpolation in the rural areas, while in the urban areas it is about 64 % for the 93.2 percentile of maximum daily 8-h means, about 55 % for SOMO35 and about 47 % for SOMO10.

Figure A3.5 Correlation between cross-validated predicted (y-axis) and measurement values for ozone indicators 93.2 percentile of max. daily 8-hourly means (top), SOMO35 (middle) and SOMO10 (bottom) for 2018 for rural (left) and urban (right) areas

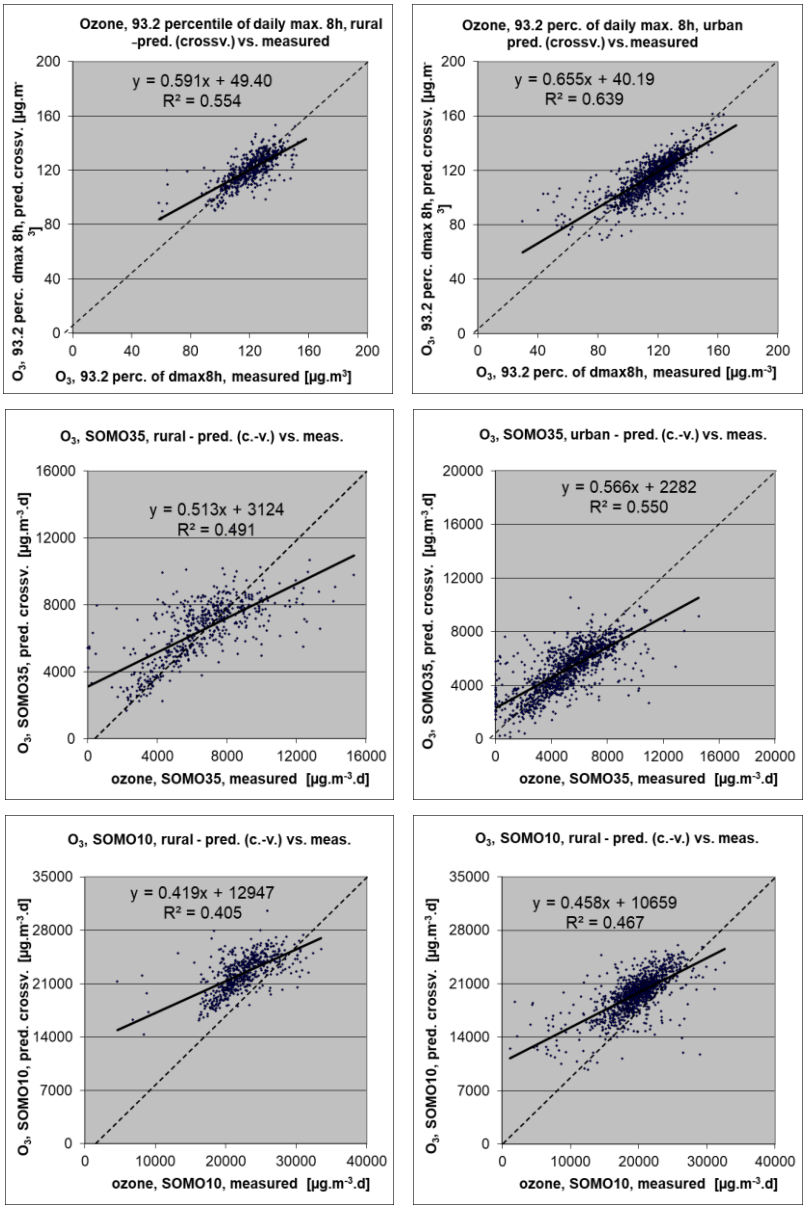

The scatter plots indicate that the higher values are underestimated and the lower values somewhat overestimated by the interpolation method; a typical smoothing effect inherent to the interpolation method with the linear regression and its residuals kriging. For example, in the case of the 93.2 percentile of daily 8-h maximums, in urban areas (Figure A.3.5, upper right panel) an observed value of 160 µg·m^{-3} is estimated in the interpolation as 144 µg·m^{-3}, which is 9 % lower. Or, in the case of SOMO35, in rural areas (Figure A3.5, middle left panel) an observed value of 9 000 µg·m^{-3}·d is estimated in the interpolation as about 7 700 µg·m^{-3}·d, which is 14 % lower.

Figure A3.6 shows the cross-validation scatter plots of the AOT40 for both vegetation and forests. R^2 indicates that about 53 % of the variability is attributable to the interpolation in the case of AOT40 for vegetation, while for AOT40 for forests it is about 56 %.

The cross-validation scatter plots show again that in areas with higher accumulated ozone concentrations the interpolation methods tend to deliver underestimated predicted values. For example, in agricultural areas (Figure A3.6, left panel) an observed value of 30 000 µg·m^{-3}·h is estimated in the interpolation as about 25 200 µg·m^{-3}·h, i.e. an underestimation of about 16 %. In addition, an overestimation at the lower end of predicted values occurred. One could reduce this under- and overestimation by extending the number of measurement stations and by optimising the spatial distribution of those stations, specifically in areas with elevated values over years.

Figure A3.6 Correlation between cross-validated predicted (y-axis) and measurement values for ozone indicators AOT40 for vegetation (left) and AOT40 for forests (right) for 2018 for rural areas

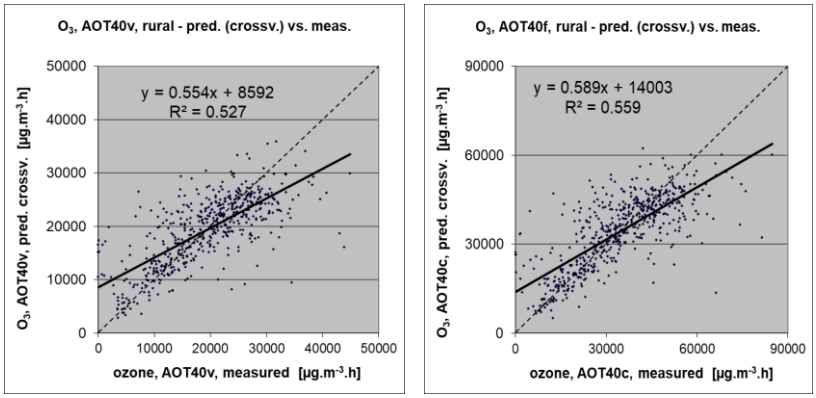

Comparison of point measurement values with the predicted grid value

In addition to the above point observation – point prediction cross-validation, a simple comparison has been made between the point observation values and interpolated predicted grid values.

For health related indicators, the comparison has been made primarily for the separate rural and separate urban background maps at 10x10 km^2 resolution. (One can directly relate this comparison result to the cross-validation of the previous section.) Next to this, the comparison has been done also for the final combined maps at 1x1 km^2 resolution.

Figure A3.7 shows the scatterplots for these comparisons, for ozone indicator 93.2 percentile of maximum daily 8-hour means only, as an illustration.

The results of the point observation – point prediction cross-validation of Figure A3.6 and those of the point observation – grid averaged prediction validation for the separate rural and the separate urban background map, and for the final combined maps are summarised in Table A3.7. By comparing the scatterplots and the statistical indicators for the separate rural and separate urban background map with the final combined maps, one can evaluate the level of representation of the rural resp. urban background areas in the final combined maps. Both the rural and the urban air quality are fairly well represented in the 1x1 km^2 final combined map.

The uncertainty of the rural and urban background maps at measurement locations is caused partly by the smoothing effect of interpolation and partly by the spatial averaging of the values in the 10x10 km^2 grid cells. The level of smoothing, which leads to underestimation in areas with high values, is weaker in areas where measurements exist than in areas where a measurement point is not available. For example, in the case of the SOMO35, in rural areas an observed value of 9 000 µg·m^{-3}·d is estimated in the interpolation as about 8 200 µg·m^{-3}·d, which is about 9 % lower. It is less than the cross-validation

underestimation of 14 % at the same point location, when leaving out this one actual measurement point and the interpolation without this station is done (see the previous subsection).

Figure A3.7 Correlation between predicted grid values from rural 10x10 km² (upper left), urban 10x10 km² (bottom left) and final combined 1x1 km² (both right) map (y-axis) versus measurements from rural (top), resp. urban/suburban (bottom) background stations (x-axis) for ozone indicator 93.2 percentile of daily max. 8-hourly means for 2018

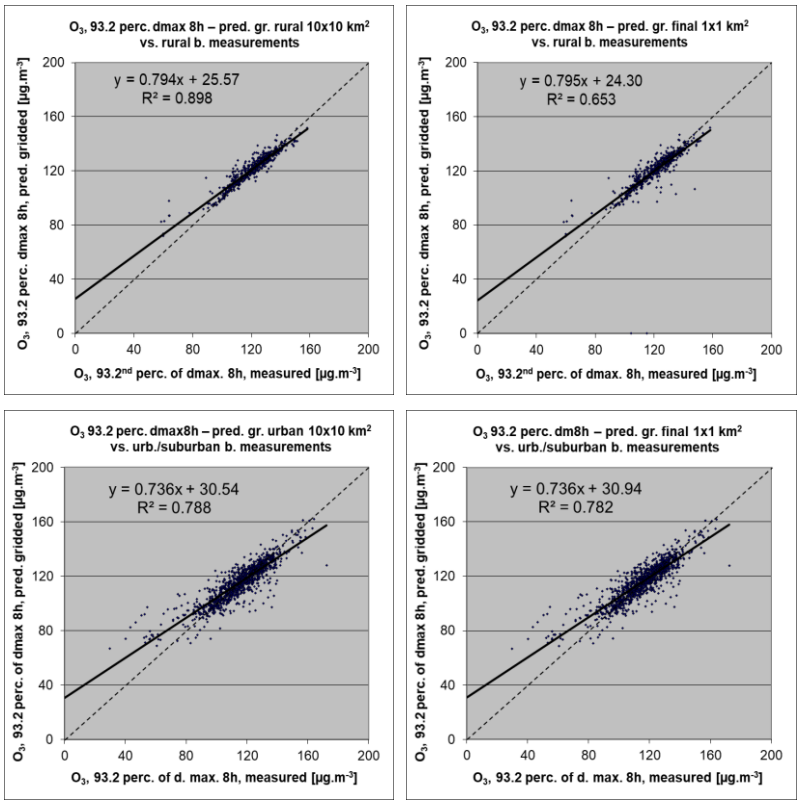

Table A3.7 Statistical indicators from the scatter plots for the predicted point values based on cross-validation and the predicted grid values from separate (rural resp. urban) 10x10 km² and final combined 1x1 km² map versus the measurement point values for rural (left) and urban (right) background stations for ozone indicators 93.2 percentile of daily max 8h means (top), SOMO35 (middle) and SOMO10 (bottom) for 2018

Ozone	rural backgr. stations				urban/suburban backgr. stations			
	RMSE	bias	R^2	lin. r. equation	RMSE	bias	R^2	lin r. equation
93.2 percentile of daily max. 8-hour means								
cross-valid. prediction, separate (r or ub) map layer	9.6	0.1	0.554	y = 0.591x + 49.40	10.3	0.1	0.639	y = 0.654x + 40.19
grid prediction, 10x10 km² separate (r or ub) map l.	4.9	0.7	0.898	y = 0.794x + 25.57	7.9	-0.1	0.788	y = 0.736x + 30.54
grid prediction, 1x1 km² final merged map	8.8	-0.4	0.653	y = 0.795x + 24.30	8.0	0.4	0.782	y = 0.736x + 30.94
SOMO35								
cross-valid. prediction, separate (r or ub) map layer	1769	-18	0.491	y = 0.513x + 3124	1518	-1	0.550	y = 0.566x + 2282
grid prediction, 10x10 km² separate (r or ub) map l.	1224	33	0.769	y = 0.668x + 2173	1260	-4	0.693	y = 0.641x + 1886
grid prediction, 1x1 km² final merged map	1317	-116	0.728	y = 0.648x + 2153	1295	73	0.674	y = 0.648x + 1927
SOMO10								
cross-valid. prediction, separate (r or ub) map layer	2809	-35	0.405	y = 0.419x + 12947	2673	-4	0.467	y = 0.458x + 10659
grid prediction, 10x10 km² separate (r or ub) map l.	1659	40	0.824	y = 0.662x + 7589	2130	-29	0.678	y = 0.572x + 8390
grid prediction, 1x1 km² final merged map	1881	-271	0.753	y = 0.647x + 7608	2145	167	0.667	y = 0.593x + 8179

Table A3.8 presents the results of the point observation – point prediction cross-validation of Figure A3.6 and those of the point-grid validation for the rural map, for vegetation related indicators AOT40 for vegetation and AOT40 for forests. Again, one can see for both indicators a better correlation between the station measurements and the averaged interpolated predicted values of the corresponding grid cells, than at the point cross-validation predictions, of Figure A3.6.

Table A3.8 Statistical indicators from the scatter plots for predicted point values based on cross-validation and predicted grid values from rural 2x2 km² map versus measurement point values for rural background stations for O_3 indicators AOT40 for vegetation (top) and forests (bottom) for 2018

Ozone	rural backgr. stations			
	RMSE	bias	R^2	linear regression equation
AOT40 for vegetation				
cross-valid. prediction, rural map	5736	-48	0.527	y = 0.554x + 8592
grid prediction, 2x2 km² rural map	4521	-18	0.709	y = 0.653x + 6709
AOT40 for forests				
cross-valid. prediction, rural map	10230	-149	0.559	y = 0.589x + 14003
grid prediction, 2x2 km² rural map	7194	-30	0.787	y = 0.716x + 9730

Details of POD maps

The hourly ozone maps needed for POD calculation have been calculated at the 2x2 km² resolution, based on rural background measurements. The maps for each hour of the year 2018 have been constructed using the same methodology as for the annual maps, i.e. the multiple linear regression followed by the kriging of its residuals (see Annex 1, Section A1.1) based on the measurement data, EMEP model output, altitude and the surface solar radiation.

POD maps have been calculated based on the methodology described in Annex 1, Section A1.3. In the POD calculations, the module to estimate phytotoxic ozone doses from a given atmospheric ozone exposure developed by INERIS has been used.

During the POD_6 maps calculation, different biogeographical regions were considered. Plant stomatal functioning varies per plant species and can vary by biogeographical region, reflecting different adaptations of plants to climate and soil water in these regions. Parametrization for POD_6 (i.e. for wheat, potato and tomato) is currently available for all different biogeographic regions of Europe apart from Alpine region, i.e. for Atlantic, Boreal, Continental, Pannonian, Steppic, and Mediterranean regions (CLRTAP, 2017). In the case of wheat, the parametrization is the same for most of these regions (namely Atlantic, Boreal, Continental, Pannonian, and Steppic), while for Mediterranean regions is different. Thus, we calculated these areas separately. For Alpine region, we used the parametrisation of the Continental and several other regions. For potato and tomato, only one parametrisation exists.

The values calculated in 0.1° x 0.1° resolution were converted into the standard ETRS89-LAEA5210 projection and transferred into the EEA 2x2 km^2 grid.

A3.4 NO_2 and NO_x

In this section, the technical details and the uncertainty estimates for the maps of NO_2 annual average and NO_x annual average, for Maps 5.1 and 5.2, are presented.

Technical details on the interpolation model

In agreement with Horálek et al. (2007) and Annex 1, the NO_x measurements are supplemented by the so-called *pseudo* NO_x stations. The pseudo NO_x data are calculated based on the NO_2 data, using quadratic regression Eq. A1.2. The regression coefficients were estimated based on the rural background stations with both NO_x and NO_2 measurements (see Section 2.1.1). The number of such stations is 380. The estimated coefficients of Eq. A1.2 are: a = 0.0164, b = 1.096, c = 0.52. Adjusted R^2 is 0.95, the standard error is 1.6 $\mu g \cdot m^{-3}$.

Table A3.9 presents the estimated parameters of the linear regression models and of the residual kriging and includes the statistical indicators of both the regression and the kriging.

Only stations with actual measurement data of the relevant pollutant (i.e. not the pseudo stations) are used for calculating the cross-validation parameters RMSE and bias.

Table A3.9 Parameters and statistics of linear regression model and ordinary kriging of NO_2 annual average for 2018 in rural, urban background and urban traffic areas for the final combined map (left) and NO_x annual average for 2018 in rural areas (right)

		NO_2 Annual average			NO_x Annual average
		Rural areas	Urb. b. areas	Urb. tr. areas	Rural areas
Linear regresion model (LRM, Eq. A1.3)	c (constant)	6.6	19.4	27.48	3.6
	a1 (EMEP model)	0.424	0.146	0.091	0.970
	a2 (altitude)	-0.0080	*non signif.*	*non signif.*	-0.0045
	a3 (altitude_5km_radius)	0.0076	*non signif.*	*non signif.*	
	a4 (wind speed)	-0.92	-2.68	-2.67	-1.94
	a5 (solar radiation)				0.63
	a6 (satellite OMI)	1.12	1.35	1.51	
	a7 (population*1000)	0.00174	0.00025		
	a8 (NAT_1km)		-0.0561		
	a9 (AGR_1km)		-0.0327		
	a10 (TRAF_1km)		0.0883		
	a11 (LDR_5km_radius)	0.0007	0.0004	0.0056	
	a12 (HDR_5km_radius)		0.0024	0.3570	
	a13 (NAT_5km_radius)	-0.0005			
	Adjusted R^2	**0.79**	**0.46**	**0.39**	**0.58**
	Standard Error [µg.m^{-3}]	**2.4**	**5.7**	**9.5**	**5.3**
Ordinary kriging (OK) of LRM residuals	nugget	0	14	45	5
	sill	5	21	80	23
	range [km]	15	50	130	36
LRM + OK of its residuals	**RMSE [µg.m^{-3}]**	**2.3**	**4.9**	**8.0**	**4.5**
	Relative RMSE [%]	**28.6**	**25.6**	**24.0**	**41.3**
	Bias (MPE) [µg.m^{-3}]	**0.0**	**0.1**	**0.0**	**0.1**

Uncertainty estimated by cross-validation

Table A3.9 shows both absolute and relative mean uncertainty, expressed by RMSE and Relative RMSE. The absolute mean uncertainty of the final combined map of NO_2 annual average expressed as RMSE is 2.3 µg·m^{-3} for the rural areas, 4.9 µg·m^{-3} for the urban background areas and 8.0 µg·m^{-3} for the urban traffic areas. For the NO_x rural map it is 4.5 µg·m^{-3}.

The relative mean uncertainty of the NO_2 annual average map is 29 % for rural, 26 % for urban background areas and 24 % for the urban traffic areas. The NO_x annual average rural map has a relative mean uncertainty of 41 %.

Figure A3.8 shows the point observation – point prediction cross-validation scatter plots for NO_2 annual average. The R^2 indicates that about 81 % of the variability is attributable to the interpolation for the rural areas, while for the urban background areas it is 60 % and for the urban traffic 57 %.

Figure A3.8 Correlation between cross-validated predicted and measurement values for NO_2 annual average 2018 for rural (left), urban background (middle) and urban traffic (right) areas

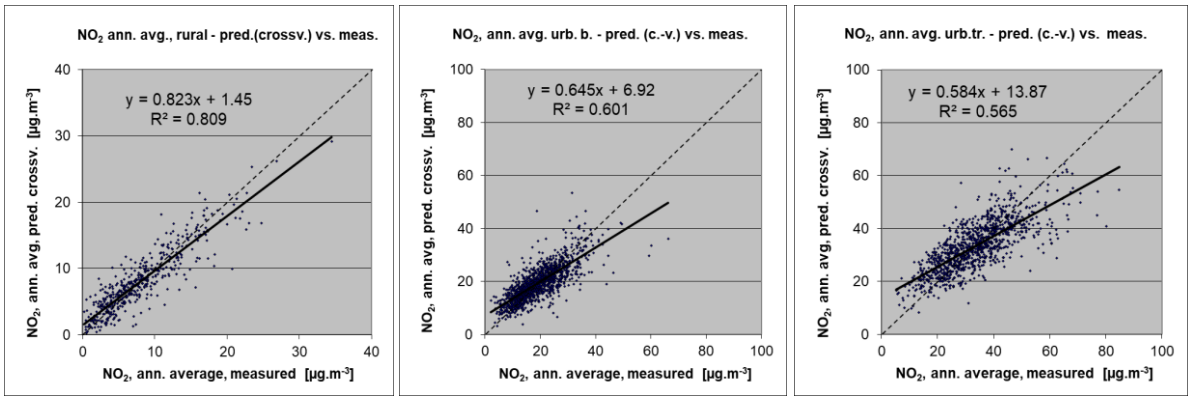

Like in the case of other pollutants, the cross-validation scatter plots show the underestimation of predictions at high concentrations at locations with no measurements. For example, in urban background areas an observed value of 40 µg·m^{-3} is estimated in the interpolations to be about 33 µg·m^{-3}, which is an underestimated prediction of about 18 %.

Figure A3.9 shows the cross-validation scatter plot for NO_x annual average rural map. The R^2 indicates that about 68 % of the variability is attributable to the interpolation.

Figure A3.9 Correlation between cross-validated predicted and measurement values for NO_x annual average 2018 for rural areas

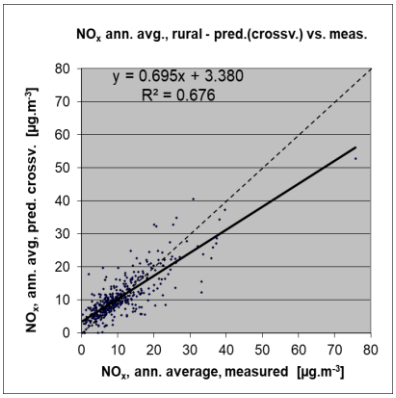

Comparison of point measurement values with the predicted grid value

Next to the above presented cross-validation, a simple comparison was made between the point observation values and interpolated predicted 1x1 km^2 resp. 2x2 km^2 grid values.

For NO_2 annual average, the comparison has been made primarily for the separate rural, separate urban background and separate urban traffic map layers at 1x1 km^2 resolution. Besides, the comparison has been done also for the final combined map. Table A3.10 presents the results of this comparison, together with the results of cross-validation prediction of Figure A3.8. One can conclude that the final combined map in 1x1 km^2 resolution is representative for rural and urban background areas, but not for urban traffic areas.

Table A3.10 Statistical indicators from the scatter plots for the predicted grid values from separate (rural, urban background or urban traffic) map layers and final combined map versus the measurement point values for rural (upper left), urban background (upper right) and urban traffic (bottom left) stations for NO_2 annual average 2018

NO_2	rural backgr. stations				urban/suburban backgr. stations			
	RMSE	bias	R^2	lin. r. equation	RMSE	bias	R^2	lin r. equation
cross-valid. prediction, separate (r or ub) map layer	2.3	0.0	0.809	y = 0.823x + 1.45	4.9	0.1	0.601	y = 0.645x + 6.92
grid prediction, 1x1 km^2 separate (r or ub) map laye	1.1	-0.3	0.960	y = 0.949x + 0.10	3.5	0.3	0.799	y = 0.753x + 5.00
grid prediction, 1x1 km^2 final merged map	2.3	0.3	0.837	y = 0.991x + 0.42	4.1	0.7	0.726	y = 0.794x + 4.69

NO_2	urban/suburban traffic stations			
	RMSE	bias	R^2	lin. r. equation
cross-valid. prediction, urban traffic map layer	8.0	0.0	0.565	y = 0.584x + 13.9
grid prediction, 1x1 km^2 urban traffic map layer	5.9	0.0	0.773	y = 0.703x + 9.92
grid prediction, 1x1 km^2 final merged map	13.6	-10.5	0.507	y = 0.431x + 8.49

Table A3.11 presents the cross-validation results of Figure A3.9 and those of the point observation – grid averaged prediction validation for the rural map of NO_x annual average.

Table A3.11 Statistical indicators from the scatter plots for predicted point values based on cross-validation and predicted grid values from rural 2x2 km^2 map versus measurement point values for rural background stations for NO_x annual average 2018

NO_x	rural background stations			
	RMSE	bias	R^2	linear regression equation
cross-valid. prediction, rural map	4.5	0.1	0.676	y = 0.695x + 3.38
grid prediction, 2x2 km^2 rural map	1.4	0.0	0.973	y = 0.924x + 0.88

Annex 4 – Inter-annual changes

In this annex, inter-annual differences between 2017 and 2018 are presented, both for the mapped concentrations and for the population-weighted and vegetation-weighted concentrations. In all cases, the 2017 maps presented in Horálek et al. (2020a) are used.

A4.1 PM_{10}

Air concentrations

Map A4.1 presents the inter-annual difference between 2017 and 2018 for annual average and the 90.4 percentile of daily means for PM_{10}. Red areas show an increase of PM_{10} concentration in 2018, while blue areas show a decrease.

Map A4.1 Difference concentrations between 2017 and 2018 for PM_{10} indicators annual average (left) and 90.4 percentile (right)

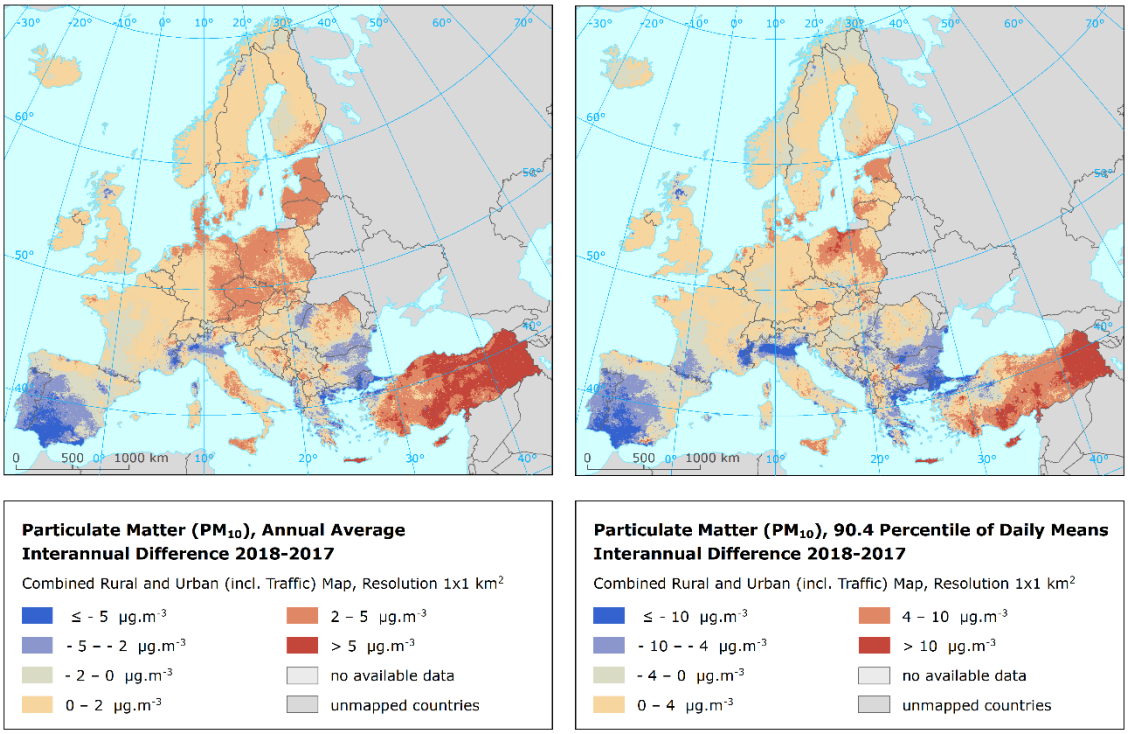

At the annual average PM_{10} difference map the highest increases are observed in Turkey, Italy (Sicilia), Austria, Czechia, Poland, Denmark, parts of Germany and the Baltic states. Contrary to that, decreases occur in Portugal, Spain, Italy (the Po Valley) and parts of the Balkan Peninsula.

At the 90.4 percentile of daily means for PM_{10} the highest increases are observed again in Turkey, Italy (Sicilia), Poland and Baltic states. The decreases are seen in Portugal, Spain, the Po Valley in Italy and parts of the Balkan Peninsula.

Be it noted that besides the actual changes in the concentrations, the variability of the linear regression model and variogram parameters, changes in the measurement network and changes in the dispersion model may cause minor differences in the concentration levels estimated.

Population exposure

Table A4.1 shows the inter-annual difference of the population-weighted concentrations between 2017 and 2018 for PM_{10} annual average and the 90.4 percentile of daily PM_{10} means, for individual countries and for Europe as a whole.

In 2018, the overall average population-weighted annual mean PM_{10} concentration for the whole of Europe was 23.4 $\mu g \cdot m^{-3}$, i.e. its value increased by about 0.3 $\mu g \cdot m^{-3}$ compared to the previous year. The steepest decreases per country were detected in Andorra and Greece, the highest increases were estimated in Bosna-Herzegovina and Malta .

In the case of the 90.4 percentile of daily means, the average European-wide population-weighted concentration for 2018 is estimated at 40.1 $\mu g \cdot m^{-3}$, which is of about 1.6 $\mu g \cdot m^{-3}$ less than in 2017. The steepest decreases were estimated in Andorra, Greece and North Macedonia, while the highest increases in Montenegro, Bosna-Herzegovina and Malta.

Table A4.1 Population-weighted concentration in 2017 and 2018 and its difference between 2017 and 2018 for PM_{10} indicators annual average (left) and 90.4 percentile of daily means (right).

Country		Population-weighted conc. [µg.m^{-3}]					
		Annual Average			90.4 Perc. of D. M.		
		2017	2018	'18 - '17	2017	2018	'18 - '17
Albania	AL	34.3	32.4	-1.9	62.1	58.6	-3.5
Andorra	AD	25.7	16.9	-8.8	49.8	26.1	-23.7
Austria	AT	17.3	19.1	1.7	31.4	33.0	1.5
Belgium	BE	19.5	20.7	1.2	34.0	35.1	1.1
Bosnia-Herzegovina	BA	29.6	34.1	4.5	60.6	67.4	6.8
Bulgaria	BG	32.3	30.9	-1.4	61.4	52.7	-8.7
Croatia	HR	24.2	23.9	-0.3	47.3	45.2	-2.1
Cyprus	CY	37.6	32.5	-5.2	55.8	54.3	-1.5
Czechia	CZ	22.8	24.8	1.9	44.1	43.5	-0.6
Denmark	DK	15.1	16.9	1.8	26.3	28.8	2.5
Estonia	EE	10.5	12.8	2.3	18.1	23.0	4.9
Finland	FI	8.6	10.8	2.2	15.2	20.0	4.8
France	FR	17.2	17.0	-0.2	29.0	27.8	-1.2
Germany	DE	16.9	18.1	1.2	29.2	29.5	0.3
Greece	GR	36.5	28.0	-8.5	65.6	45.0	-20.6
Hungary	HU	26.4	26.2	-0.2	48.5	46.7	-1.8
Iceland	IS	11.6	9.4	-2.2	19.7	16.6	-3.1
Ireland	IE	11.2	12.5	1.3	19.9	21.5	1.6
Italy	IT	26.1	24.1	-2.0	47.6	40.4	-7.2
Latvia	LV	15.2	19.2	3.9	27.0	33.0	6.0
Liechtenstein	LI	12.8	13.7	0.9	24.1	24.9	0.8
Lithuania	LT	17.2	19.5	2.3	30.8	34.8	4.0
Luxembourg	LU	16.4	16.9	0.5	27.8	26.8	-0.9
Malta	MT	25.9	30.2	4.3	39.4	46.0	6.6
Monaco	MC	22.3	20.2	-2.1	33.8	31.7	-2.1
Montenegro	ME	26	29	3.2	49	57	7.6
Netherlands	NL	18.2	19.4	1.2	29.8	32.3	2.4
North Macedonia	MK	47.3	42.1	-5.3	100.3	81.5	-18.8
Norway	NO	9.6	11.3	1.7	18.0	20.3	2.3
Poland	PL	28.5	30.3	1.8	53.2	55.4	2.2
Portugal	PT	19.7	17.4	-2.3	34.3	29.1	-5.2
Romania	RO	24.9	24.9	0.0	42.2	41.5	-0.7
San Marino	SM	22.0	20.8	-1.2	40.4	34.8	-5.6
Serbia (incl. Kosovo*)	RS	36.7	37.8	1.1	72.3	70.3	-1.9
Slovakia	SK	25.2	24.9	-0.3	48.2	44.5	-3.7
Slovenia	SI	22.6	22.1	-0.4	42.2	39.2	-3.0
Spain	ES	21.8	19.5	-2.3	37.2	31.7	-5.5
Sweden	SE	10.7	12.4	1.7	19.2	22.2	3.1
Switzerland	CH	14.8	15.0	0.1	26.3	25.7	-0.6
Turkey	TR	40.2	43.2	2.9	75.8	74.7	-1.1
United Kingdom	UK	14.6	15.3	0.7	25.1	25.9	0.7
Total		**23.1**	**23.4**	**0.3**	**41.6**	**40.1**	**-1.6**
Total without Turkey		**20.8**	**20.8**	**0.0**	**37.0**	**35.4**	**-1.6**
EU-28		**20.4**	**20.4**	**0.0**	**36.1**	**34.5**	**-1.6**

*) under the UN Security Council Resolution 1244/99

A4.2 $PM_{2.5}$

Air concentrations

Map A4.2 presents the inter-annual difference between 2018 and 2017 for annual average $PM_{2.5}$.

The highest increases are seen in the United Kingdom, Ireland, Denmark, southern Sweden, the Baltic States, Czechia, Poland, parts of Austria and Germany and the Balkan Peninsula. Decreases are estimated in the Po Valley in northern Italy, central and southern Spain, Portugal and some smaller (mostly urban) areas in the Balkan Peninsula.

Map A4.2 Difference $PM_{2.5}$ annual average concentrations between 2017 and 2018

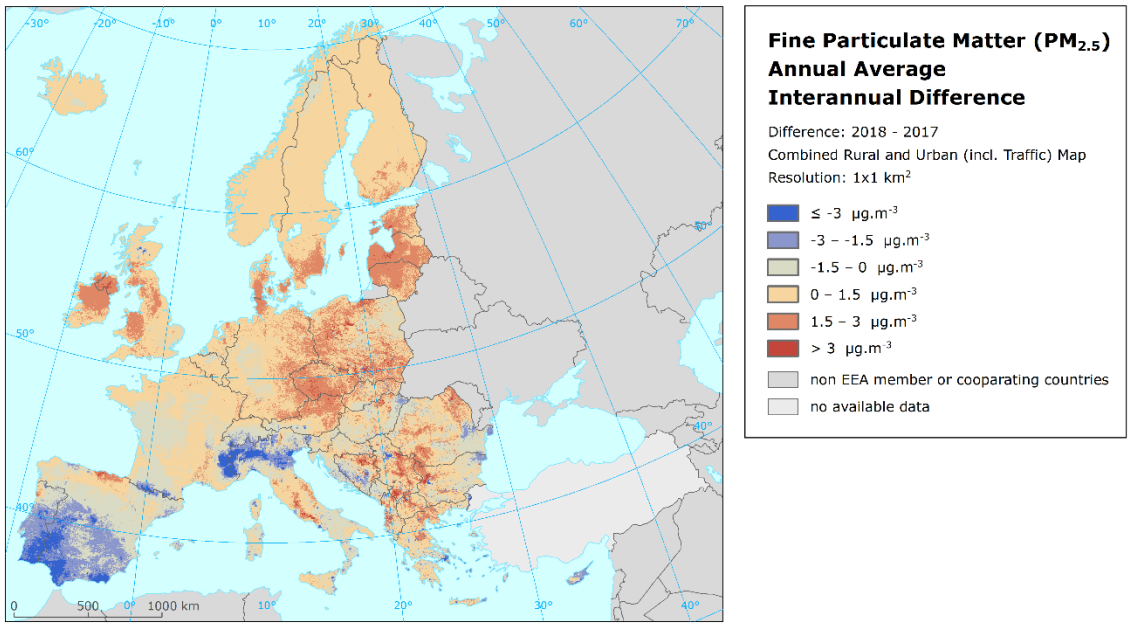

Population exposure

Table A4.2 presents the inter-annual difference of the population-weighted concentrations between 2017 and 2018 for $PM_{2.5}$ annual average, for individual countries and for Europe as a whole (without Turkey, which was not mapped neither for 2017 nor for 2018).

In 2018, the average European-wide population-weighted concentration is estimated at 13.5 $\mu g \cdot m^{-3}$, which means a slight decrease of about 0.3 $\mu g \cdot m^{-3}$ compared to 2017. The steepest decreases are shown in Greece, North Macedonia and Andorra, while the highest increases in Bosnia-Herzegovina, Latvia and Lithuania.

Table A4.2 Population-weighted concentration in 2017 and 2018 and its difference between 2017 and 2018 for $PM_{2.5}$ annual average.

Country		Pop.-weighted conc. [µg.m^{-3}]			Country		Pop.-weighted conc. [µg.m^{-3}]			Country		Pop.-weighted conc. [µg.m^{-3}]		
		2017	2018	'18 - '17			2017	2018	'18 - '17			2017	2018	'18 - '17
Albania	AL	23.1	21.6	-1.6	Greece	GR	30.0	18.3	-11.7	Norway	NO	5.2	6.4	1.2
Andorra	AD	12.5	8.5	-4.0	Hungary	HU	18.8	18.3	-0.5	Poland	PL	21.4	21.7	0.2
Austria	AT	12.3	13.6	1.3	Iceland	IS	5.1	4.7	-0.4	Portugal	PT	9.1	8.4	-0.7
Belgium	BE	12.5	12.7	0.3	Ireland	IE	6.2	7.8	1.6	Romania	RO	17.9	17.6	-0.3
Bosnia-Herzeg.	BA	22.6	26.4	3.8	Italy	IT	17.0	15.5	-1.6	San Marino	SM	14.2	13.3	-0.8
Bulgaria	BG	22.4	21.0	-1.4	Latvia	LV	9.5	12.1	2.7	Serbia (incl. Kosovo*)	RS	28.3	26.6	-1.6
Croatia	HR	17.6	18.0	0.4	Liechtenstein	LI	9.4	8.6	-0.8	Slovakia	SK	18.8	18.2	-0.6
Cyprus	CY	15.7	14.5	-1.2	Lithuania	LT	10.3	12.8	2.4	Slovenia	SI	16.2	15.8	-0.4
Czechia	CZ	17.1	18.3	1.2	Luxembourg	LU	10.0	10.0	0.0	Spain	ES	12.0	10.2	-1.8
Denmark	DK	8.5	10.5	2.0	Malta	MT	11.8	12.5	0.7	Sweden	SE	5.0	6.1	1.2
Estonia	EE	5.4	7.0	1.6	Monaco	MC	13.2	12.6	-0.6	Switzerland	CH	9.9	9.8	-0.1
Finland	FI	4.4	5.9	1.5	Montenegro	ME	18.6	20.5	1.9	United Kingdom	UK	9.3	10.0	0.7
France	FR	10.6	10.6	-0.1	Netherlands	NL	11.3	12.0	0.7	**Total**		**13.8**	**13.5**	-0.3
Germany	DE	11.8	12.3	0.5	North Macedonia	MK	36.3	30.7	-5.6	**EU-28**		**13.5**	**13.2**	-0.3

*) under the UN Security Council Resolution 1244/99

A4.3 Ozone

Air concentrations

Map A4.3 presents the inter-annual difference between 2016 and 2017 for four ozone indicators.

Map A4.3 Difference concentrations between 2017 and 2018 for ozone indicators 93.2 percentile of daily 8-hour maximums (top left), SOMO35 (top right), AOT40 for vegetation (bottom left) and AOT40 for forests (bottom right)

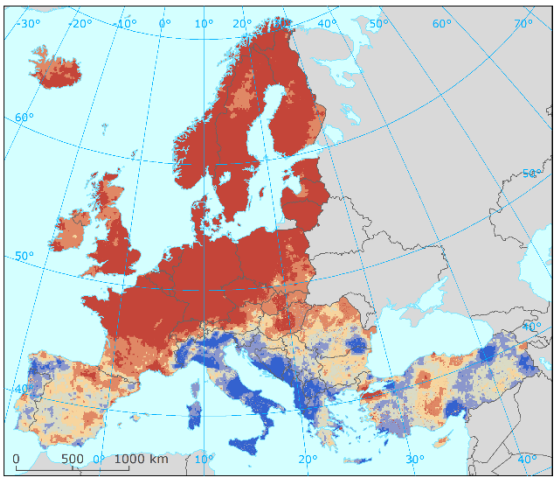

Ozone, 93.2 Percentile of Maximum daily 8-hour Means
Interannual Difference 2018-2017

Combined Rural and Urban Background Map, Resolution 1x1 km²

≤ - 10 µg.m⁻³	4 – 10 µg.m⁻³
- 10 – - 4 µg.m⁻³	> 10 µg.m⁻³
- 4 – 0 µg.m⁻³	no available data
0 – 4 µg.m⁻³	unmapped countries

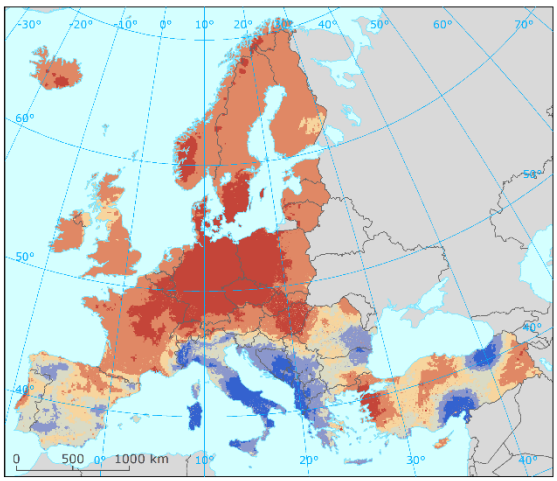

Ozone, SOMO35
Interannual Difference 2018-2017

Combined Rural and Urban Background Map, Resolution 1x1 km²

≤ - 2000 µg.m⁻³.d	800 – 2000 µg.m⁻³.d
- 2000 – - 800 µg.m⁻³.d	> 2000 µg.m⁻³.d
- 800 – 0 µg.m⁻³.d	no available data
0 – 800 µg.m⁻³.d	unmapped countries

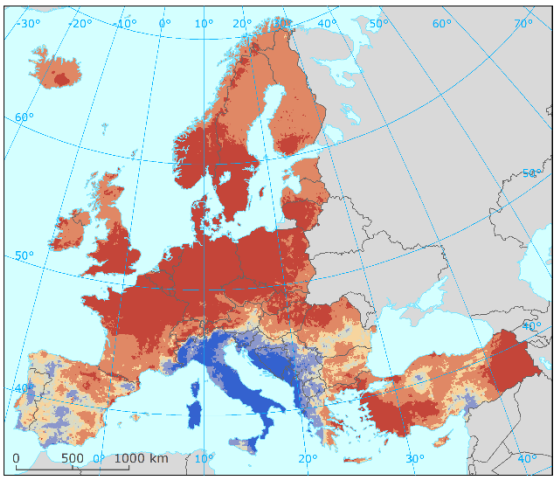

Ozone, AOT40 for Vegetation
Interannual Difference 2018-2017

Rural Map, Resolution 2x2 km²

≤ - 6000 µg.m⁻³.h	2000 – 6000 µg.m⁻³.h
- 6000 – - 2000 µg.m⁻³.h	> 6000 µg.m⁻³.h
- 2000 – 0 µg.m⁻³.h	no available data
0 – 2000 µg.m⁻³.h	unmapped countries

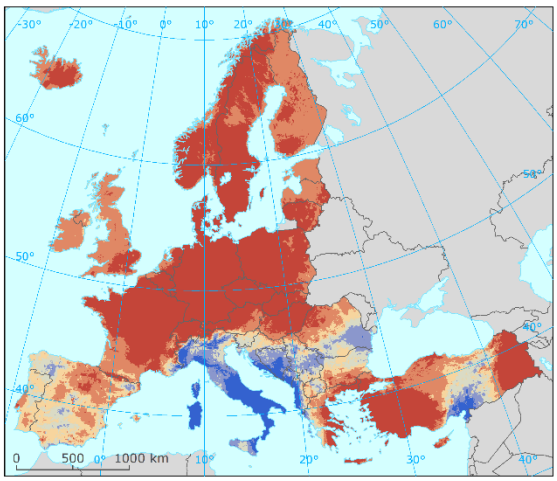

Ozone, AOT40 for Forests
Interannual Difference 2018-2017

Rural Map, Resolution 2x2 km²

≤ - 10000 µg.m⁻³.h	4000 – 10000 µg.m⁻³.h
- 10000 – - 4000 µg.m⁻³.h	> 10000 µg.m⁻³.h
- 4000 – 0 µg.m⁻³.h	no available data
0 – 4000 µg.m⁻³.h	unmapped countries

In the Map 4.3, the inter-annual difference for both the health related ozone indicators (i.e. for 93.2 percentile of maximum daily 8-hour means and SOMO35) and the vegetation related ozone indicators (i.e. for AOT40 for vegetation and AOT40 for forests) are presented. In all the maps, red areas show an increase of ozone concentrations, while blue areas show a decrease.

Most of northern, western and central Europe, parts of the Balkan Peninsula and Turkey show a quite high increase for 93.2 percentile of maximum daily 8-hour means from 2017 to 2018, which was highly influenced by the exceptional hot summer in 2018 in central and north Europe. Contrary to that, one can see a steep decline in Italy, parts of the Balkan Peninsula and parts of Spain.

The difference pattern for SOMO35 is quite similar to that of the percentile indicator. Decreases are observed in Italy, parts of Spain, the Balkan Peninsula and parts of Turkey, while increases can be seen in Northern, Western and Central Europe.

In the case of both AOT40 indicators, the state is very similar to the above indicators.

Population exposure

Table A4.3 provides the inter-annual difference of the population-weighted concentrations between 2017 and 2018 for ozone health related indicators, for individual countries and for Europe as a whole.

In 2018 the overall population-weighted concentration for ozone indicator 93.2 percentile of maximum daily 8-hour means for whole of Europe was about 113 $\mu g \cdot m^{-3}$, i.e. of about 9 $\mu g \cdot m^{-3}$ more than in 2017. The highest increases are shown in Denmark, Belgium and Germany, the highest decrease are shown in Bosnia-Herzegovina, Montenegro and Albania.

In the case of SOMO35, the average European-wide population-weighted concentration for 2018 is estimated at about 5000 $\mu g \cdot m^{-3} \cdot d$, which is of about 1000 $\mu g \cdot m^{-3} \cdot d$ more than in 2017. The highest increases are shown in Czechia, Germany and Greece, the steepest decreases are shown in Bosnia-Herzegovina, Albania and Montenegro.

Concerning SOMO10, the average European-wide population-weighted concentration for 2018 was almost 19400 $\mu g \cdot m^{-3} \cdot d$, which is of about 900 $\mu g \cdot m^{-3} \cdot d$ more than in 2017. The highest increases are shown in Greece, Czechia and Poland, the steepest decreases are shown in Bosnia-Herzegovina, Italy and Montenegro.

Table A4.3 Population-weighted concentration in 2017 and 2018 and its difference between 2017 and 2018 for ozone indicators 93.2 percentile of 8-h daily maximums (left), SOMO35 (middle) and SOMO10 (right).

Country		Population-weighted conc. [µg.m^{-3}] / [µg.m^{-3}.d]								
		93.2 perc. of 8-h d. max.			SOMO35			SOMO10		
		2017	2018	'18 - '17	2017	2018	'18 - '17	2017	2018	'18 - '17
Albania	AL	116.9	106.4	-10.4	6 898	5 601	-1 297	22 664	20 980	-1 684
Andorra	AD	111.2	112.4	1.3	5 182	6 593	1 411	21 462	20 618	-845
Austria	AT	117.3	124.3	7.0	5 311	6 731	1 420	20 021	21 481	1 460
Belgium	BE	102.6	123.8	21.3	2 553	4 298	1 745	16 020	17 689	1 670
Bosnia-Herzegovina	BA	122.1	108.1	-14.0	6 967	5 218	-1 749	22 177	19 449	-2 728
Bulgaria	BG	102.2	100.4	-1.7	3 938	3 765	-174	17 468	17 679	211
Croatia	HR	123.2	115.0	-8.2	7 110	6 342	-768	22 768	21 002	-1 767
Cyprus	CY	103.7	108.2	4.5	6 029	6 844	815	19 104	20 042	938
Czechia	CZ	112.0	127.5	15.4	4 307	6 946	2 639	19 314	22 084	2 770
Denmark	DK	87.2	109.2	22.0	1 711	3 866	2 155	17 148	19 523	2 375
Estonia	EE	84.8	98.1	13.3	1 462	2 793	1 331	15 963	17 625	1 662
Finland	FI	83.0	96.0	13.0	1 153	2 351	1 198	15 337	17 276	1 938
France	FR	104.4	119.2	14.7	3 809	5 274	1 466	18 799	20 509	1 710
Germany	DE	105.3	126.0	20.7	3 182	5 674	2 491	17 546	19 874	2 328
Greece	GR	103.7	110.8	7.1	4 858	7 157	2 299	17 926	21 685	3 759
Hungary	HU	114.8	116.0	1.2	5 010	5 892	882	19 508	20 124	617
Iceland	IS	80.4	88.6	8.2	782	1 999	1 217	15 269	16 593	1 324
Ireland	IE	87.0	95.8	8.8	1 418	2 556	1 138	16 485	17 966	1 481
Italy	IT	129.2	122.1	-7.0	7 405	6 490	-915	23 201	20 793	-2 408
Latvia	LV	87.4	98.7	11.3	1 557	2 732	1 175	16 017	17 310	1 293
Liechtenstein	LI	119.9	132.1	12.2	5 045	7 045	1 999	19 564	21 454	1 891
Lithuania	LT	84.5	102.9	18.4	1 417	3 096	1 680	15 430	17 694	2 264
Luxembourg	LU	104.4	120.1	15.6	3 001	4 604	1 603	17 017	19 011	1 995
Malta	MT	104.3	103.0	-1.2	6 174	5 498	-676	23 809	23 185	-624
Monaco	MC	120.2	126.4	6.2	8 223	7 686	-537	24 960	23 313	-1 648
Montenegro	ME	118.3	105.9	-12.4	6 787	5 630	-1 157	22 442	20 646	-1 796
Netherlands	NL	96.3	115.0	18.7	2 281	3 620	1 339	16 674	17 331	657
North Macedonia	MK	102.6	96.9	-5.7	4 248	3 533	-715	18 084	17 214	-869
Norway	NO	86.6	102.5	15.9	1 448	3 128	1 679	16 315	18 569	2 253
Poland	PL	103.2	116.2	13.0	3 111	5 095	1 983	17 116	19 612	2 496
Portugal	PT	105.8	107.6	1.8	3 914	4 672	758	19 548	20 823	1 275
Romania	RO	102.6	101.7	-0.9	3 885	3 683	-202	17 849	17 557	-292
San Marino	SM	128.1	123.9	-4.2	7 192	6 700	-493	23 209	21 121	-2 088
Serbia (incl. Kosovo*)	RS	102.3	100.3	-2.0	4 418	3 583	-835	18 367	16 999	-1 368
Slovakia	SK	113.5	118.5	5.0	4 861	6 129	1 269	19 665	20 940	1 275
Slovenia	SI	125.5	118.1	-7.4	7 035	6 494	-541	22 283	21 481	-801
Spain	ES	110.9	113.2	2.3	5 600	5 841	241	21 584	21 732	148
Sweden	SE	86.1	104.1	18.0	1 641	3 465	1 824	16 762	18 940	2 178
Switzerland	CH	117.1	133.0	15.9	5 281	7 214	1 933	19 973	21 770	1 797
Turkey	TR	100.8	104.2	3.4	4 864	5 504	640	17 435	18 194	759
United Kingdom	UK	84.5	97.7	13.2	1 218	2 314	1 095	14 875	16 089	1 214
Total		**104.5**	**113.2**	**8.7**	**4 006**	**5 027**	**1 021**	**18 417**	**19 360**	**943**
Total without Turkey		**105.0**	**114.4**	**9.5**	**3 890**	**4 962**	**1 072**	**18 551**	**19 519**	**968**
EU-28		**104.8**	**114.7**	**9.9**	**3 838**	**4 970**	**1 132**	**18 500**	**19 539**	**1 039**

*) under the UN Security Council Resolution 1244/99

Vegetation exposure

Table A4.4 provides the inter-annual difference of the agricultural-weighted concentrations for AOT40 for vegetation and the forest-weighted concentrations for AOT40 for forests between 2017 and 2018.

In 2018, the agricultural-weighted concentration of vegetation-related AOT40 shows an increase of ca. 4 680 µg·m^{-3}·h compared to 2017; the forest-weighted concentration of forest-related AOT40 shows an increase of about 8 800 µg·m^{-3}·h compared to 2017. The highest increases of vegetation-related AOT40 are seen in Denmark and Germany, while the steepest decreases in Montenegro, Italy and San

Marino. The highest increases of forest-related AOT40 are seen in Germany and Czechia, while the steepest decreases in Italy and Montenegro.

Table A4.4 Agricultural weighted (left) and forest-weighted (right) concentration in 2017 and 2018 and its difference between 2017 and 2018 for ozone indicators AOT40 for vegetation (left) and AOT40 for forests (right).

Country		Agricult.-weighted conc. AOT40 for veg. [µg.m^{-3}.h]			Forest-weighted conc. AOT40 for for. [µg.m^{-3}.h]		
		2017	2018	'18 - '17	2017	2018	'18 - '17
Albania	AL	25 124	18 066	-7 058	47 859	41 305	-6 554
Austria	AT	20 335	23 229	2 893	31 018	42 711	11 693
Belgium	BE	10 386	19 676	9 290	16 037	32 648	16 612
Bosnia-Herzeg.	BA	21 525	14 696	-6 829	38 578	30 406	-8 172
Bulgaria	BG	10 597	12 975	2 378	29 179	31 769	2 590
Croatia	HR	22 092	18 230	-3 862	39 708	35 896	-3 812
Cyprus	CY	17 882	21 728	3 846	40 798	50 036	9 238
Czechia	CZ	16 596	25 633	9 037	26 009	47 430	21 422
Denmark	DK	2 270	14 031	11 760	5 352	19 729	14 378
Estonia	EE	984	5 227	4 243	2 578	9 597	7 019
Finland	FI	348	5 601	5 253	739	9 887	9 148
France	FR	9 548	16 492	6 945	21 858	33 418	11 560
Germany	DE	10 505	22 106	11 601	18 783	40 840	22 057
Greece	GR	22 758	24 831	2 072	43 556	51 402	7 846
Hungary	HU	16 143	20 966	4 823	30 569	42 979	12 410
Iceland	IS	5	3 049	3 044	43	7 193	7 150
Ireland	IE	875	6 258	5 383	2 347	8 499	6 151
Italy	IT	28 686	20 595	-8 091	50 584	38 223	-12 362
Latvia	LV	911	6 320	5 409	2 881	11 307	8 427
Liechtenstein	LI	20 195	25 832	5 637	34 140	47 002	12 861
Lithuania	LT	1 673	8 632	6 960	4 868	15 382	10 513
Luxembourg	LU	12 078	22 251	10 172	16 978	35 173	18 195
Malta	MT	22 151	21 267	-883	47 202	46 971	-232
Monaco	MC			0	27 768	42 321	14 553
Montenegro	ME	22 879	14 373	-8 506	43 070	33 269	-9 801
Netherlands	NL	6 069	14 534	8 466	10 717	21 645	10 928
North Macedonia	MK	19 633	17 956	-1 676	42 646	43 136	490
Norway	NO	957	7 724	6 767	1 942	13 256	11 314
Poland	PL	8 077	17 259	9 182	14 954	31 544	16 590
Portugal	PT	9 647	9 591	-56	22 628	23 838	1 210
Romania	RO	8 569	11 817	3 247	21 389	24 042	2 653
San Marino	SM	28 942	20 596	-8 345	46 837	40 144	-6 692
Serbia (incl. Kosovo*)	RS	17 943	16 011	-1 932	34 714	31 060	-3 654
Slovakia	SK	14 085	20 543	6 458	24 458	39 112	14 655
Slovenia	SI	23 687	19 641	-4 046	40 259	39 655	-604
Spain	ES	16 541	17 573	1 032	28 317	30 412	2 095
Sweden	SE	2 096	11 035	8 939	2 043	13 987	11 943
Switzerland	CH	19 075	23 961	4 886	31 268	45 472	14 204
Turkey	TR	18 400	23 758	5 358	30 301	41 955	11 654
United Kingdom	UK	2 476	9 140	6 664	3 430	10 324	6 894
Total		**12 670**	**17 350**	**4 680**	**17 717**	**26 517**	**8 800**
Total without Turkey		**11 676**	**16 311**	**4 635**	**17 126**	**25 397**	**8 270**
EU-28		**11 468**	**16 362**	**4 894**	**16 628**	**25 719**	**9 092**

*) under the UN Security Council Resolution 1244/99

A4.4 NO_2 and NO_x

Air concentrations

Map A4.4 presents the inter-annual difference between 2017 and 2018 for NO_2 and NO_x annual averages. Red areas show an increase of concentration in 2018, while blue areas show a decrease.

For NO_2, the steepest decreases are shown in some parts of Italy, Spain and France. The highest increases are seen in some parts of the Northern Europe, Ireland, Balkans and Turkey.

In the case of NO_x, notable decreases are seen in southern Spain, western France, northern Italy, Serbia and Finland. The highest increases can be seen in Turkey and also in coastal parts of Ireland, central Poland and northern Switzerland. In this context, note the lack of stations in the south-east Balkan.

Map A4.4 Difference concentrations between 2017 and 2018 for NO_2 annual average (left) and NO_x annual average (right)

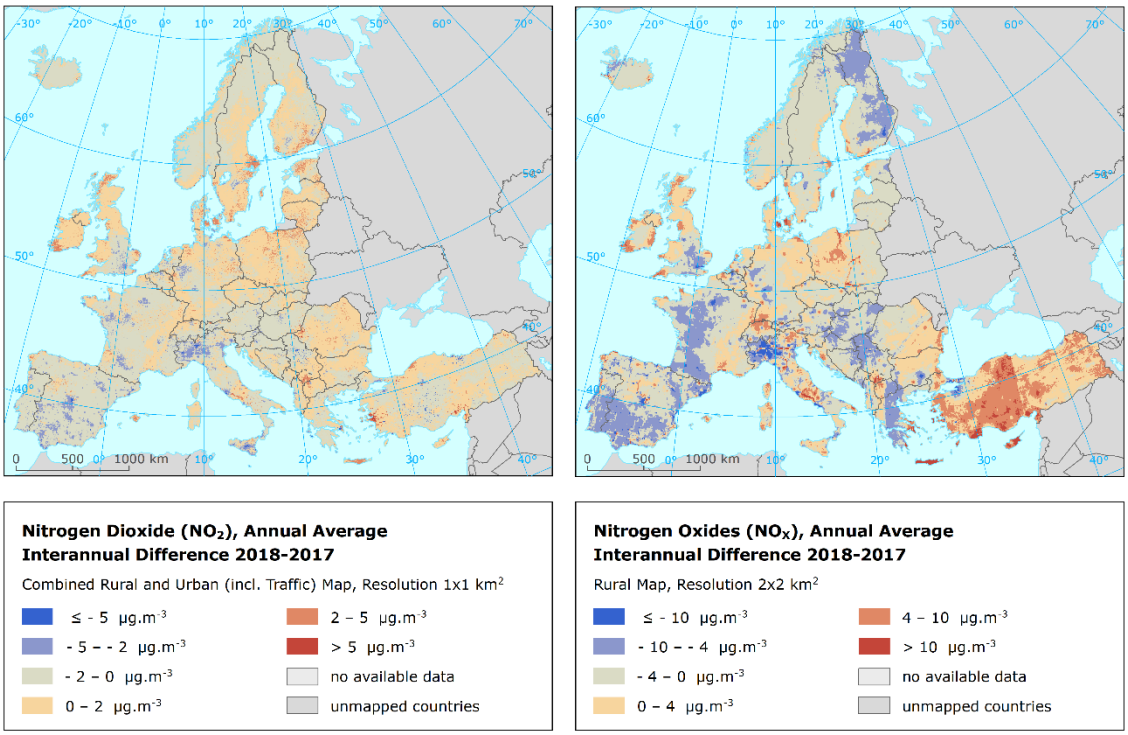

Population exposure

Table A4.5 provides the inter-annual difference between 2017 and 2018 for NO_2 annual average. In 2018 the overall population-weighted concentration for NO_2 annual average for whole of Europe was 19.2 µg·m^{-3}, i.e. the same value as in 2017. The steepest decreases are shown in Malta, Greece and Serbia, while the highest increases in Cyprus.

Table A4.5 Population-weighted concentration in 2017 and 2018 and its difference between 2017 and 2018 for NO_2 annual average.

Country		Pop.-weighted conc. [µg.m^{-3}]		
		2017	2018	'18 -
Albania	AL	16.9	14.7	-2.1
Andorra	AD	20.5	18.1	-2.4
Austria	AT	18.9	17.7	-1.2
Belgium	BE	20.9	20.4	-0.5
Bosnia-	BA	15.7	13.9	-1.8
Bulgaria	BG	19.2	19.0	-0.2
Croatia	HR	15.6	13.8	-1.8
Cyprus	CY	19.6	23.5	3.9
Czechia	CZ	15.2	15.5	0.3
Denmark	DK	8.8	9.8	1.1
Estonia	EE	6.3	7.1	0.9
Finland	FI	7.6	8.6	1.0
France	FR	16.9	15.9	-0.9
Germany	DE	19.4	19.1	-0.2
Greece	GR	23.6	21.0	-2.6
Hungary	HU	17.8	17.0	-0.7
Iceland	IS	10.2	10.4	0.1
Ireland	IE	9.3	11.0	1.7
Italy	IT	22.1	20.1	-2.0
Latvia	LV	11.1	11.9	0.8
Liechtenstein	LI	18.2	16.5	-1.7
Lithuania	LT	10.8	12.3	1.5
Luxembourg	LU	19.5	20.2	0.7
Malta	MT	16.0	10.4	-5.5
Monaco	MC	26.8	25.0	-1.8
Montenegro	ME	13.5	15.0	1.4
Netherlands	NL	20.2	20.4	0.3
North	MK	19.8	19.0	-0.8
Norw ay	NO	10.4	10.0	-0.4
Poland	PL	14.9	15.6	0.7
Portugal	PT	16.2	15.4	-0.8
Romania	RO	18.8	19.3	0.5
San Marino	SM	14.5	14.4	0.0
Serbia (incl.	RS	19.6	17.2	-2.4
Slovakia	SK	14.7	14.8	0.1
Slovenia	SI	16.2	14.5	-1.7
Spain	ES	21.6	19.4	-2.2
Sw eden	SE	7.7	8.7	1.0
Sw itzerland	CH	18.8	17.6	-1.2
Turkey	TR	25.3	25.9	0.6
United Kingdom	UK	19.8	18.8	-1.0
Total		**19.2**	**19.2**	**0.0**
Total without Turkey		**18.4**	**17.6**	**-0.7**
EU-28		**18.5**	**17.8**	**-0.7**

*) under the UN Security Council Resolution 1244/99

Annex 5 – Concentration maps including station points

Throughout the report, the concentration maps presented do not include station points. The reason is to better visualise the health related indicators with their distinct concentration levels at the more fragmented and smaller urban areas in predominant rural areas.

As presented in Annex 3, the kriging interpolation methodology somewhat smooths the concentration field. Therefore, it is valuable to present in this Annex 5 the indicator maps *including* the concentration values resulting from the measurement data at the station points. These points provide important additional visual information on the smoothing effect caused by the interpolation. For instance, maps A5.1 and A5.2 present PM_{10} indicators annual average and 90.4 percentile of daily means and include the stations points used in the interpolation. They correspond to Maps 2.1 and 2.2 of the main report, which do not have station points. Table A5.1 provides an overview on the maps of the main report and the corresponding maps including stations point values as presented in this annex.

Both the rural and the urban/suburban background stations are included in the maps of the health related indicators, while the rural stations only are shown in the maps of vegetation related indicators. For $PM_{2.5}$ and NO_x, only the stations with relevant measured data (i.e. not the pseudo stations) are presented.

Table A5.1 Overview of maps presented in this Annex 5 and their relation with the maps presented in the main report

Air pollutant	Indicator	Map including station points	Map without station points
PM_{10}	Annual average	A5.1	2.1
	90.4 percentile of daily means	A5.2	2.2
$PM_{2.5}$	Annual average	A5.3	3.1
Ozone	93.2 percentile of maximum daily 8-hour means	A5.4	4.1
	SOMO35	A5.5	4.2
	SOMO10	A5.6	4.3
	AOT40 for vegetation ([a])	A5.7	4.4
	AOT40 for forests ([a])	A5.8	4.5
NO_2	Annual average	A5.9	5.1
NO_x	Annual average ([a])	A5.10	5.2

([a]) Rural map, applicable for rural areas only.

Map A5.1 Concentration map of PM_{10} annual average including station points, 2018

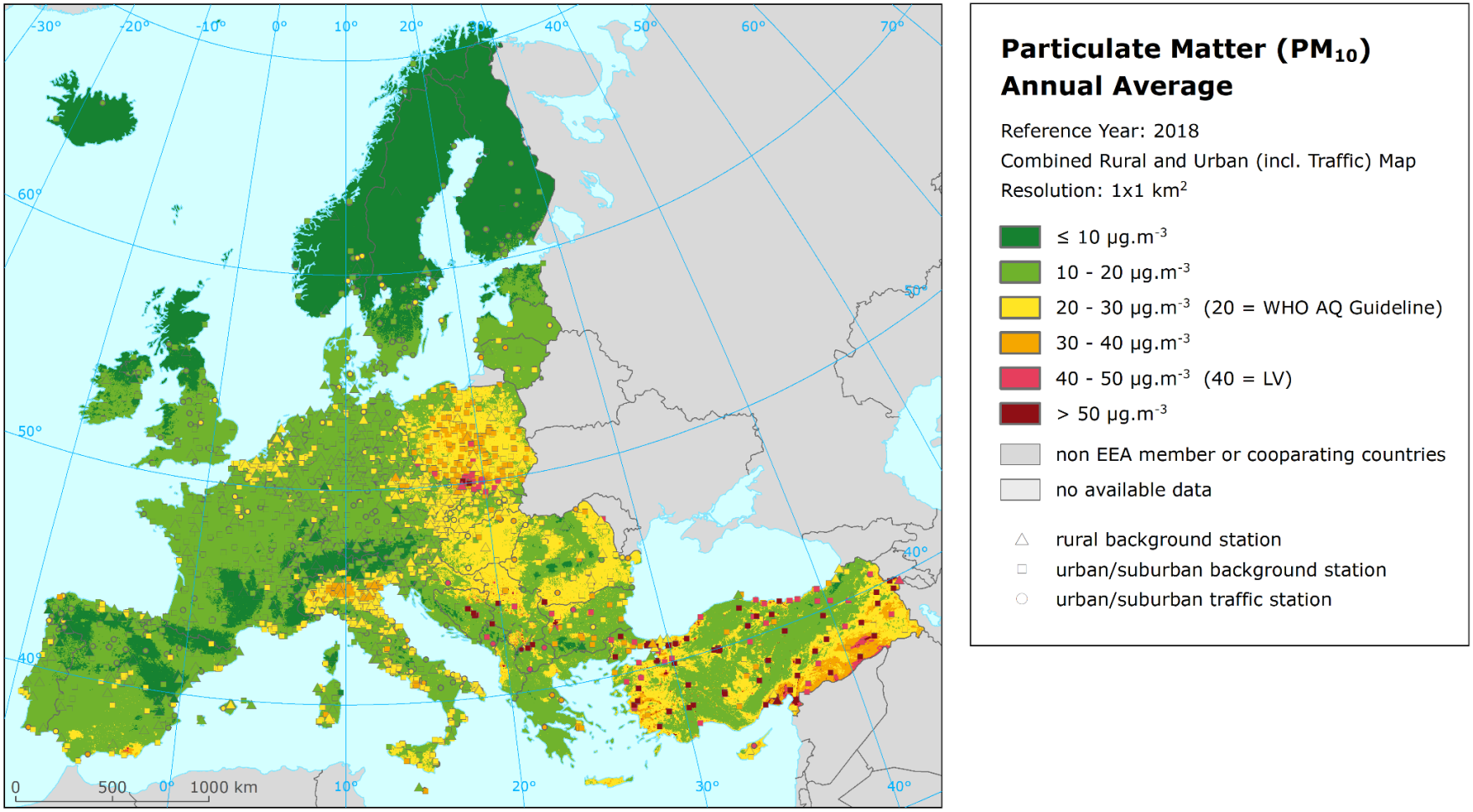

Map A5.2 Concentration map of PM_{10} indicator 90.4 percentile of daily means including station points, 2018

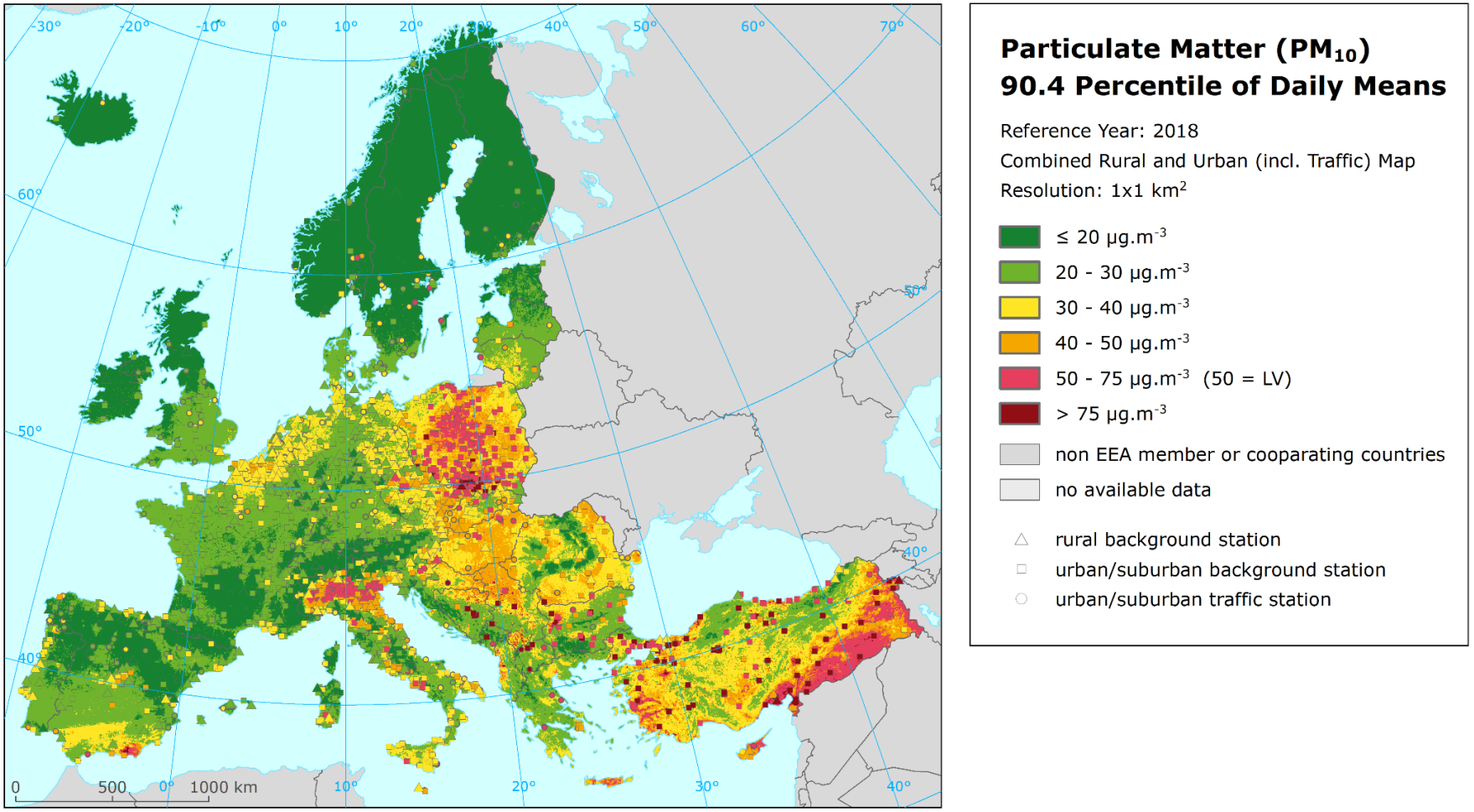

Map A5.3 Concentration map of $PM_{2.5}$ annual average including station points, 2018

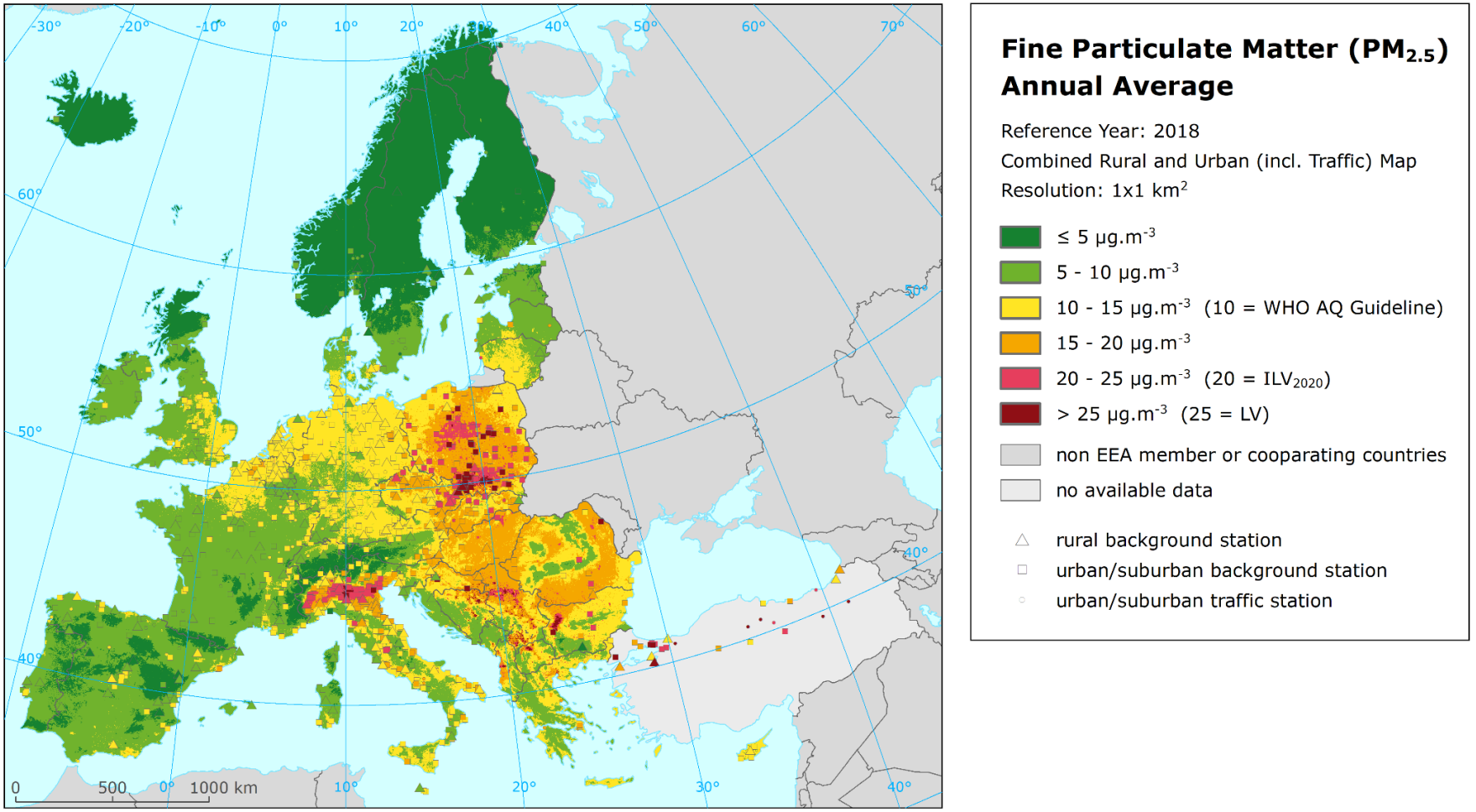

Map A5.4 Concentration map of ozone indicator 93.2 percentile of maximum daily 8-hour means including station points, 2018

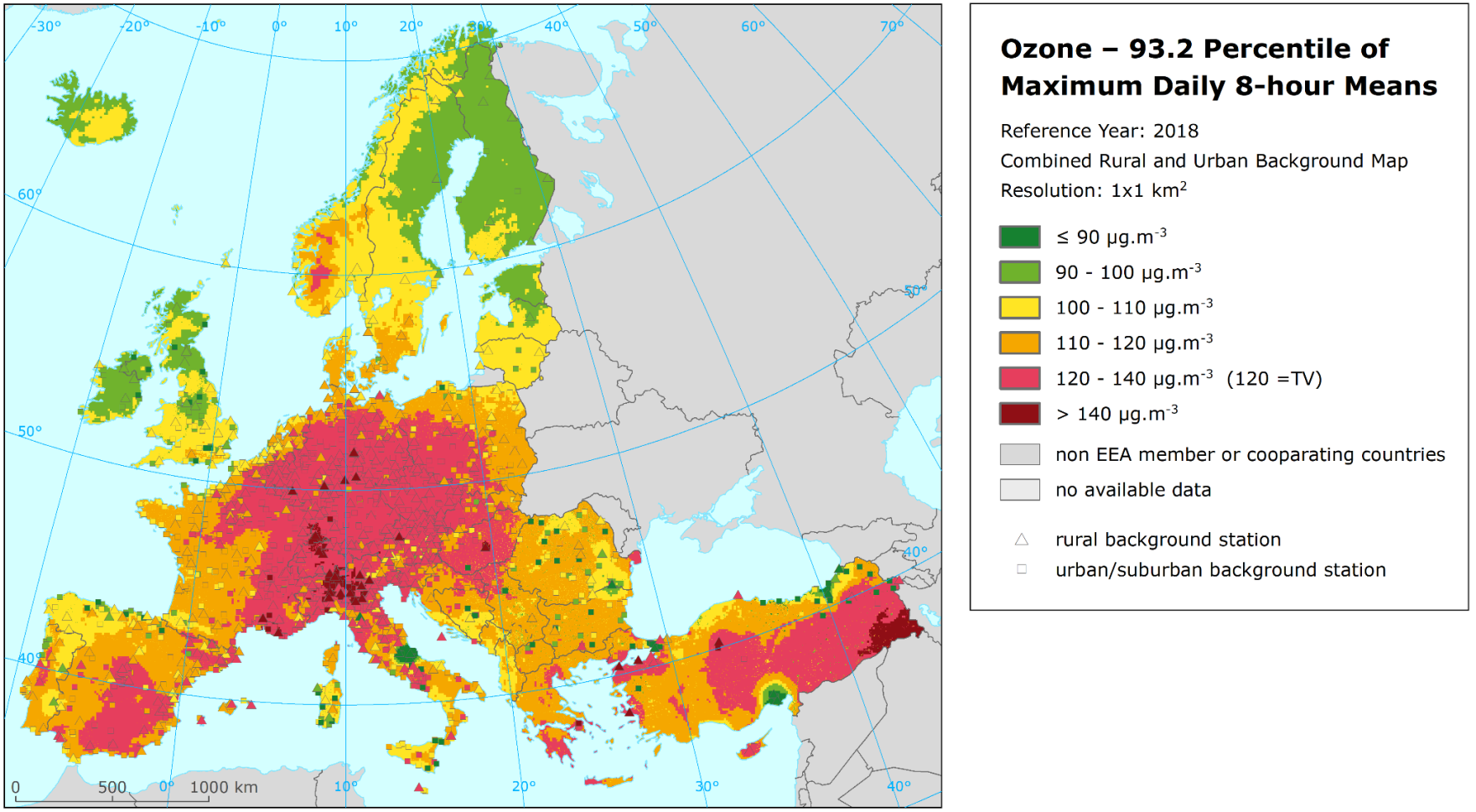

Map A5.5 Concentration map of ozone indicator SOMO35 including station points, 2018

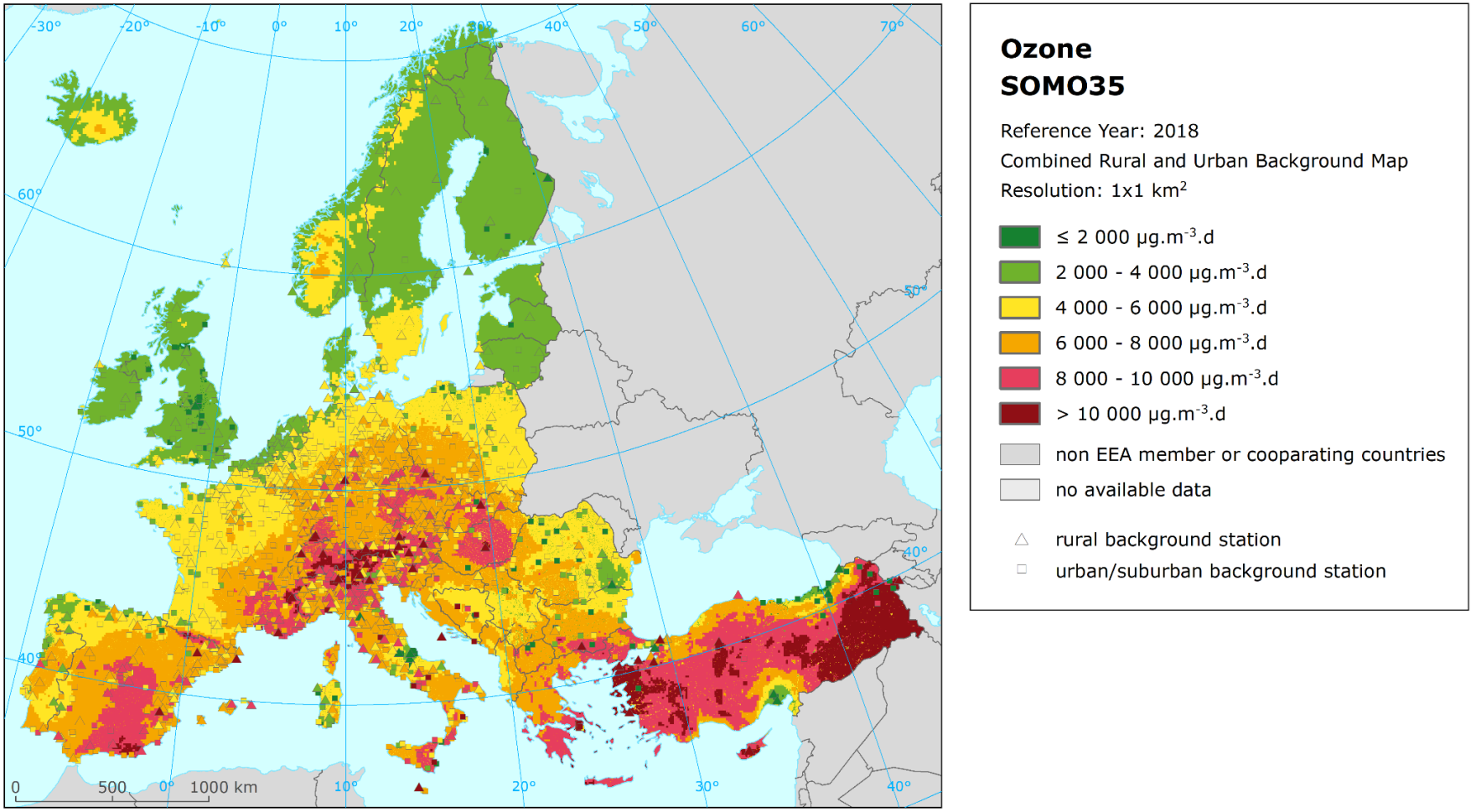

Map A5.6 Concentration map of ozone indicator SOMO10 including station points, 2018

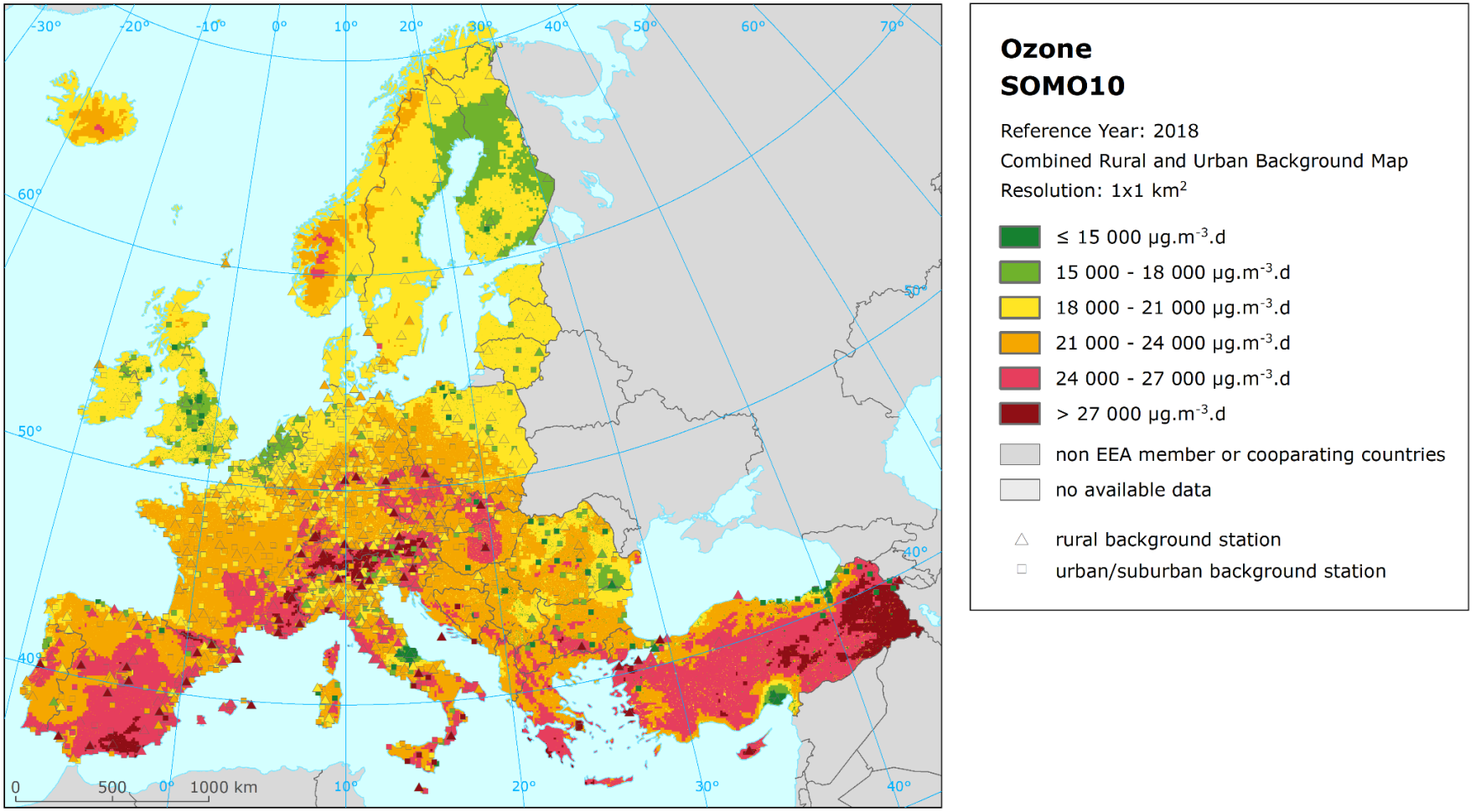

Map A5.7 Concentration map of ozone indicator AOT40 for vegetation including station points, rural air quality, 2018

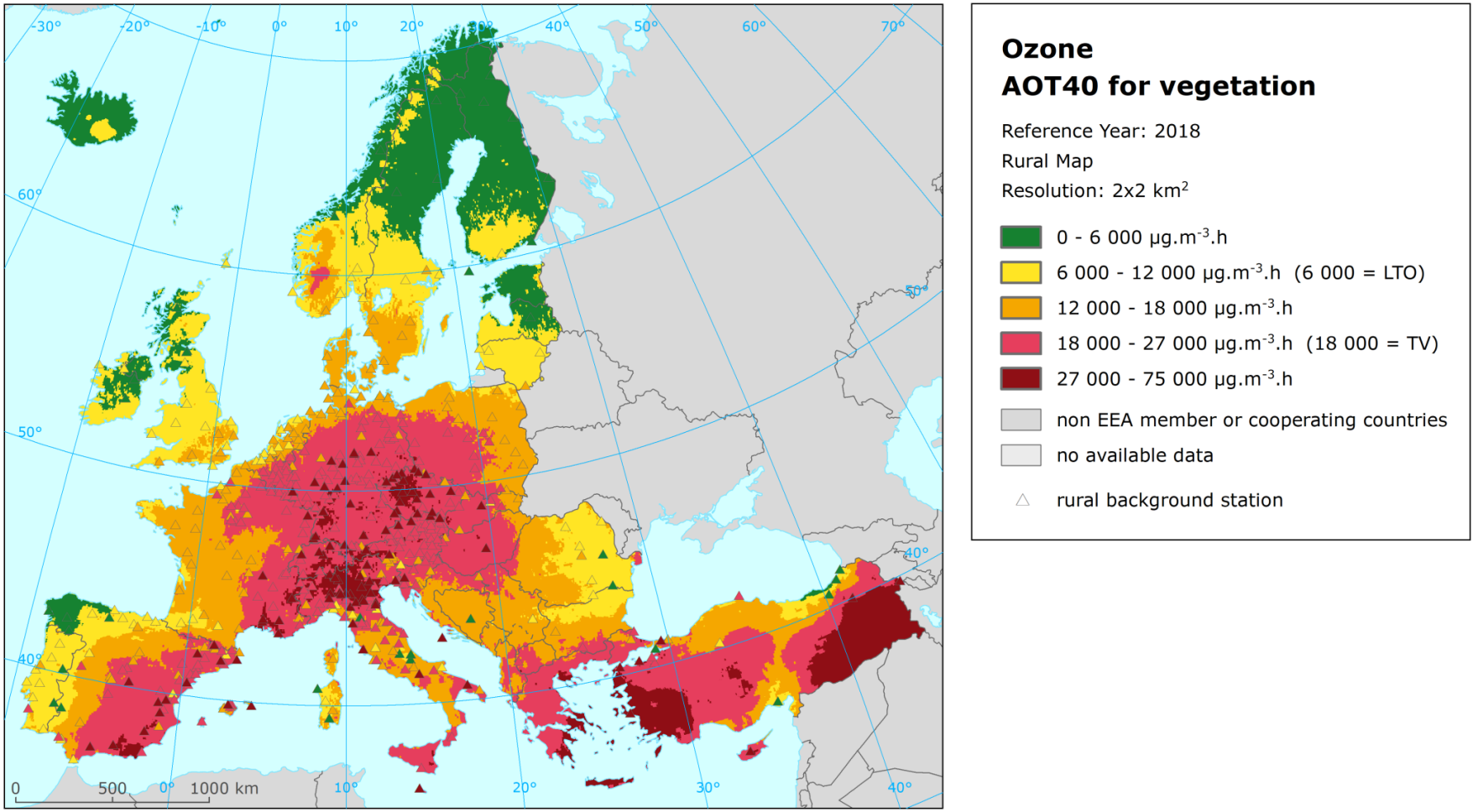

Map A5.8 Concentration map of ozone indicator AOT40 for forests including station points, rural air quality, 2018

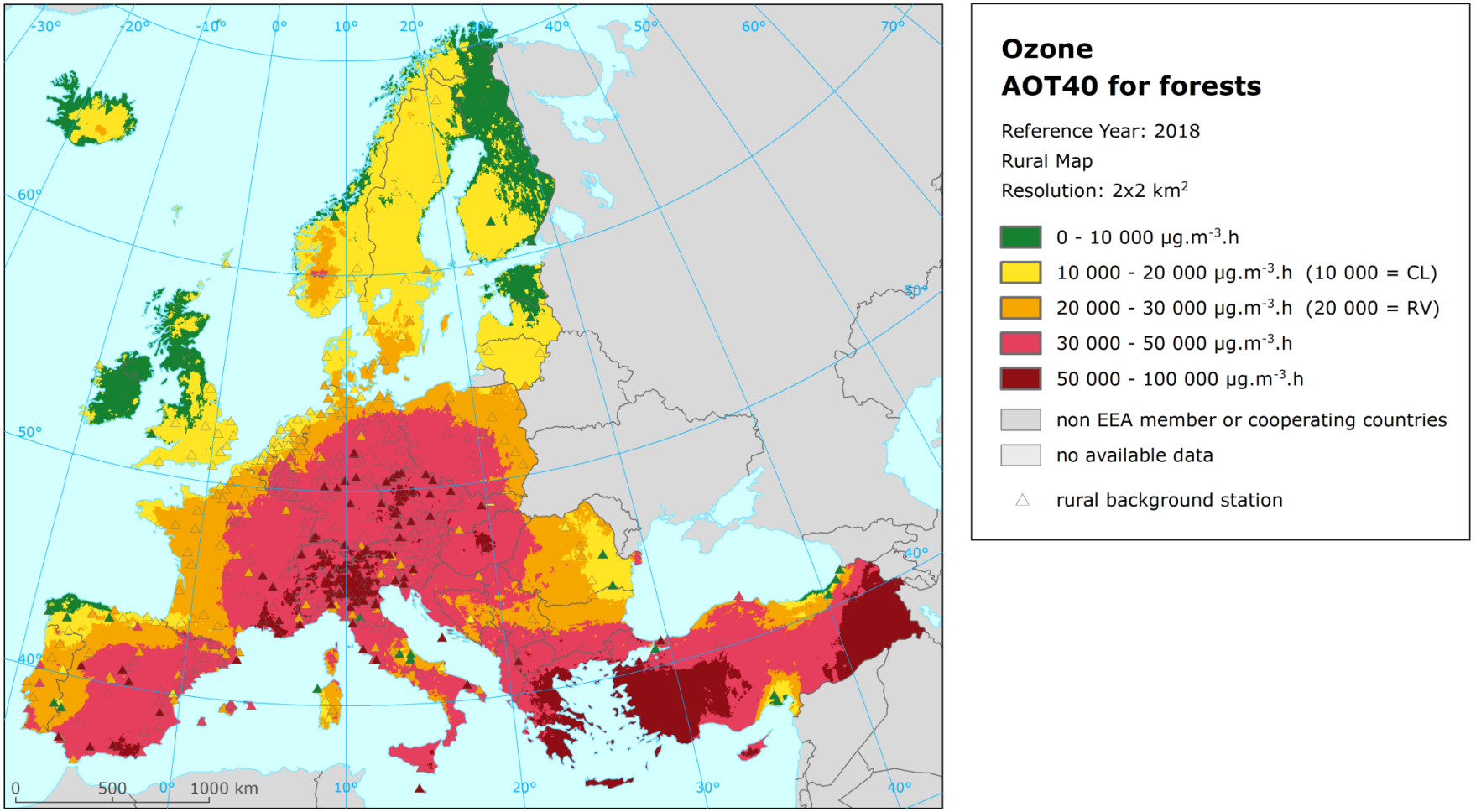

Map A5.9 Concentration map of NO_2 annual average including station points, 2018

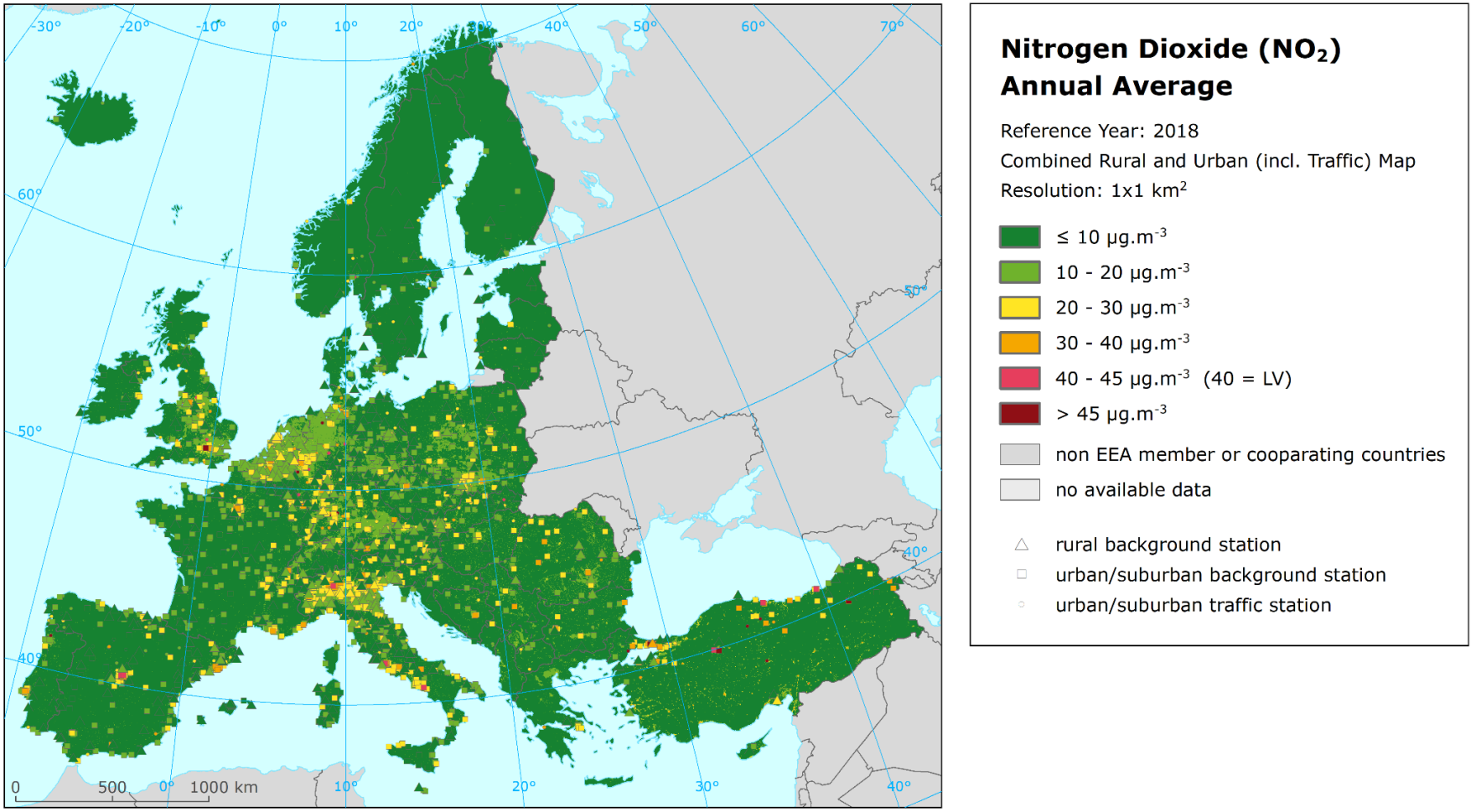

Map A5.10 Concentration map of NO_x annual average including station points, rural air quality, 2018

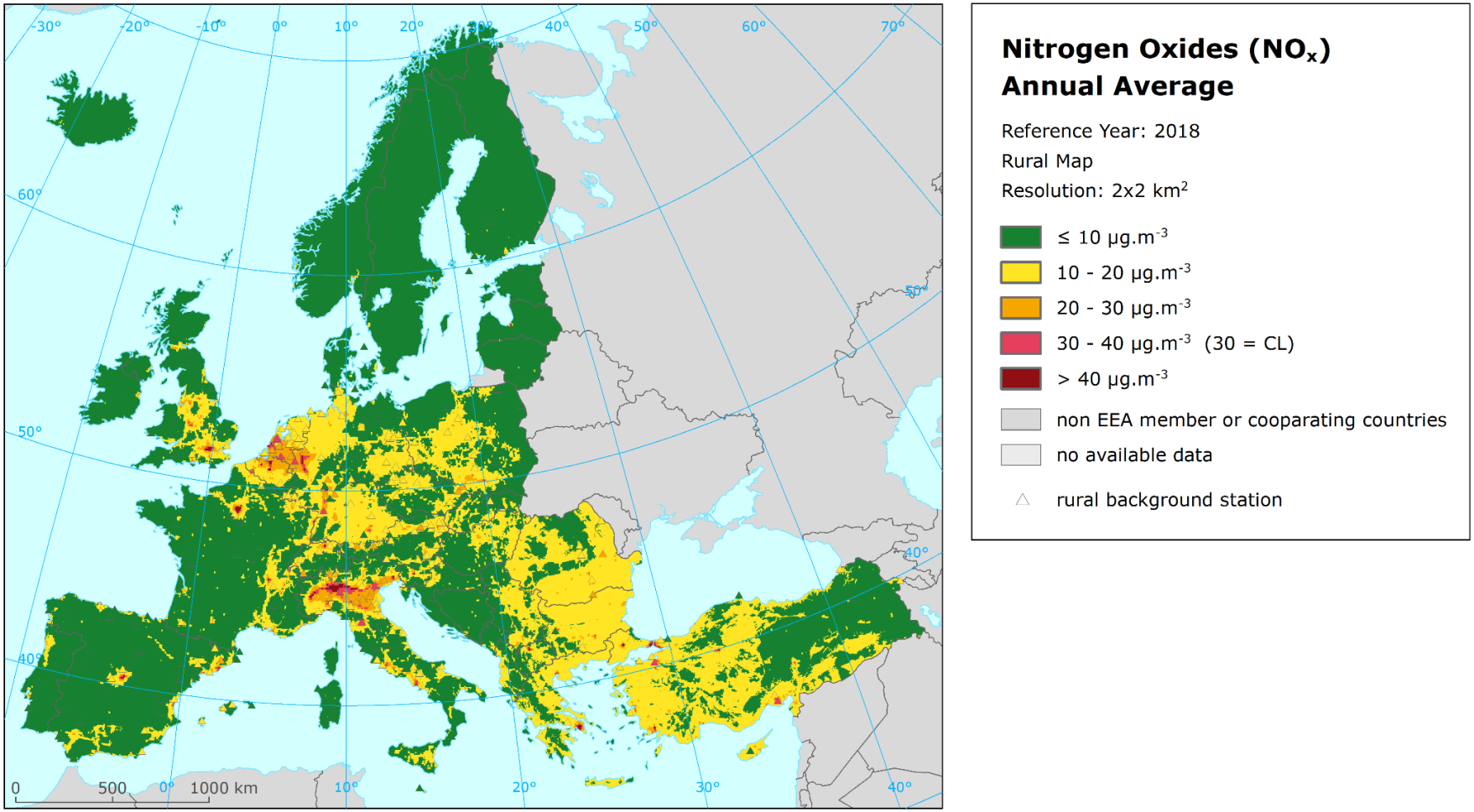

European Topic Centre on Air pollution,
transport, noise and industrial pollution
c/o NILU – Norwegian Institute for Air Research
P.O. Box 100, NO-2027 Kjeller, Norway
Tel.: +47 63 89 80 00
Email: etc.atni@nilu.no
Web : https://www.eionet.europa.eu/etcs/etc-atni

The European Topic Centre on Air pollution, transport, noise and industrial pollution (ETC/ATNI) is a consortium of European institutes under a framework partnership contract to the European Environment Agency.

European Environment Agency
European Topic Centre on Air pollution,
transport, noise and industrial pollution